

University of Jordan  
Faculty of Graduate Studies  
Graduate Department of Engineering,  
Mathematics and Physical Sciences

Theoretical Prediction of Fluid Flow  
and Convection Heat Transfer  
Coefficients Around Two-Dimensional  
Gas Turbine Blades

BY  
Amjad Isaaf Mansour Al-Sayeh

٢٤  
٢٤/٢

SUPERVISOR  
Dr. Mohammad Hamdan

Submitted in Partial Fulfillment of the Requirements for the Degree  
of Master of Science in Mechanical Engineering.

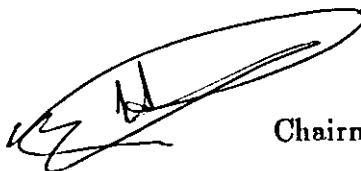
Amman, Jordan

September, 1992

عميد كلية الدراسات العليا

The Examining Committee considers this thesis satisfactory and acceptable for the award of the Degree of Master of Science in Mechanical Engineering.

Dr. Mohammad A. Hamdan

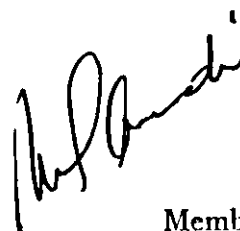


Chairman of Committee

Mechanical Engineering Department

University of Jordan

Prof. Dr. Mahmoud S. Audi

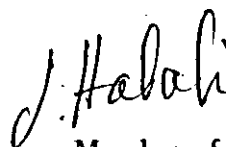


Member of Committee

Mechanical Engineering Department

University of Jordan

Dr. Sa'ad Habali



Member of Committee

Mechanical Engineering Department

University of Jordan

*To my father,  
to my mother,  
and to the other members of my family.*

# ACKNOWLEDGEMENTS

It is my pleasure to express my gratitude to all people who helped me in completing the present work. Special thanks are indebted to my supervisors Dr. M. A. Hamdan and Dr. B. Jubran, whom without their support, encouragement, guidance, and advice, my work could have been infinitely more difficult. Also I highly appreciate the great assistance given to me by the computer center staff at the Faculty of Engineering and Technology, University of Jordan.

I would like also to present my special thanks to Dr. D. A. Nealy (Chief of the Heat Transfer Section, Detroit Diesel Allison, General Motors Corporation), for his great help in supplying me with experimental data sets used in this study.

Finally, not to forget, the support and great care given to me by all my family members throughout my research.

# ABSTRACT

A two-dimensional boundary layer integral method for calculating laminar and turbulent convective heat transfer coefficients and boundary layer momentum thickness over the suction and pressure surfaces of solid turbine blades is described. This general method was evaluated using relevant experimental airfoil data available in the literature. Based on the findings of this evaluation, the method was modified for modeling the transition region (transition start, length, and path) found on the suction surface and the laminar heat transfer augmentation over the pressure surface due to free-stream turbulence effects. An effective viscosity formulation was included to model the complete behavior of the boundary layer on the pressure surface. This effective viscosity formulation permitted the boundary layer on the pressure surface to be treated as a laminar one but with the calculations being based on an effective viscosity formed by combining the dynamic (laminar) viscosity with the turbulence viscosity. On the other hand the suction surface is treated to have three separate boundary layer regions, namely, laminar, transitional, and fully turbulent ones.

Various single and/or combined model solutions ( transition start, length, and path models and turbulence viscosity models) were evaluated using experimental data in order to recommend the best combination. This evaluation process eventually led to the development of a specific method for gas turbine blade heat transfer prediction. Compar-

ing the obtained predicted data using the modified method with the experimental ones indicates a significant improvement in the predictive capability.

## ملخص

### التنبؤ النظري لجريان المائع ومعامل انتقال الحرارة حول الريشات الزعفرانية ثنائية الأبعاد

بناءً على فرضيات الأسياب الطبقي والمضطرب تم شرح طريقة تكاملية لطبقة متاخمة ثنائية الأبعاد من أجل حساب معامل انتقال الحرارة وشخانة كمية التحرك للطبقة المتاخمة فوق السطحين الماص (المحدب) والضاغط (المقعر) للريش الزعفرانية المصمته.

هذه الطريقة العامة تم تقييمها باستخدام النتائج المخبرية للريش الزعفرانية الموجودة في المراجع. بناءً على نتائج هذا التقييم، تم تعديل هذه الطريقة من أجل تمثيل المرحلة الإنتقالية المتواجدة على السطح الماص وظاهرة تعزيز الانتقال الحراري الانسيابي فوق السطح الضاغط (المقعر) بسبب عوامل التيار الطليق الاضطرابية.

لتمثيل السلوك الكامل للطبقة المتاخمة المتواجدة على السطح الضاغط (المقعر) تم اضافة صيغة جبرية فعالة لمعامل اللزوجة إلى هذه الطريقة التكاملية. هذه الصيغة الجبرية سمحت بمعاملة الطبقة المتاخمة المتواجدة على السطح الضاغط على أساس فرضية الأسياب الطبقي ولكن بحيث أن تتم الحسابات على أساس معامل اللزوجة الفعال المتكون من اضافة معامل اللزوجة الانسيابي إلى معامل اللزوجة الإضطرابي.

أما بالنسبة للطبقة المتاخمة المتواجدة فوق السطح الماص (المحدب)، فقد تم تمثيلها بثلاث مراحل مختلفة، هي، المرحلة الانسيابية، المرحلة الانتقالية والمرحلة الاضطرابية.

باستخدام النتائج المخبرية تم تقييم العديد من حلول النماذج النظرية (مجتمعة و/أو مفردة) والتي تستخدم لتمثيل المرحلة الانتقالية للطبقة المتاخمة المتواجدة على السطح الماص وظاهرة تعزيز الإنتقال الحراري فوق السطح الضاغط.

عملية التقييم هذه أدت في النهاية إلى اختيار أفضل تركيبه مجتمعه من النماذج النظرية وبالتالي إلى تطوير طريقة خاصة هدفها التوقع النظري لمعامل انتقال الحرارة حول الريش الزعنفية.

مقارنة النتائج النظرية لهذه الطريقة الخاصة (الطريقة التكاملية المعدلة) مع النتائج المخبرية يدل على تقدم واضح في قدرة التوقع النظري.



# NOMENCLATURE

$a$	coefficient in the velocity profile polynomial equation (3.6).
$b$	coefficient in the velocity profile polynomial equation (3.6).
$c$	coefficient in the velocity profile polynomial equation (3.6).
$C_f/2$	local friction coefficient, $\tau_o/(\rho_e U^2)$ .
$C_p$	specific heat of fluid (air) at constant pressure, $ft^2/(s^2 R)$ , $m^2/(s^2 K)$ .
$d$	coefficient in the velocity profile polynomial equation (3.6).
$D$	blade leading edge diameter, $ft, m$ .
$f$	stream function.
$h_x$ or $H$	local value of heat transfer coefficient, $Btu/(hr ft^2 R)$ , $W/(m^2 K)$ .
$H_{12}$	shape factor, $\delta_1/\delta_2$ .
$H_{32}$	shape factor, $\delta_3/\delta_2$ .
$k$	thermal conductivity of fluid (air), $Btu/(hr ft^2 R)$ , $W/(m^2 K)$ .
$K$	dimensionless velocity gradient shape factor based on boundary layer momentum thickness $\delta_2$ , $\frac{\delta_2^2}{\nu} \frac{dU}{dx}$ .
$l$	mixing-length or blade characteristic length (chord), $ft, m$ .
$M$	Mach number.
$Nu$	Nusselt number, $St.Pr.Re$
$P$ or $P_s$	thermodynamic static pressure, $psia, Pa$ .
$P_o$	total pressure of inlet free-stream, $psia, Pa$ .
$Pr$	Prandtl number, $\mu C_p/k$ .
$Pr_t$	turbulent Prandtl number, $\epsilon_M/\epsilon_H$ .
$\dot{q}''(x)$	local rate of heat transfer flux, $-k \left( \frac{\partial T}{\partial y} \right)_{y=0}$ , $Btu/(hr ft^2)$ , $W/(m^2)$ .
$r$	blade leading edge radius, $ft, m$ .
$Re$	Reynolds number.
$Re_{\delta_2}$	momentum thickness Reynolds number, $\delta_2 U/\nu_e$ .
$St$	Stanton number, $h_x/\rho_e C_p U$ .
$T$ or $T_s$	static temperature, $^{\circ}R, ^{\circ}K$ .
$T_o$	total temperature of inlet free-stream, $^{\circ}R, ^{\circ}K$ .
$TU, Tu$	longitudinal free-stream turbulence intensity, $\sqrt{w'^2}/U$ .

$u'$	fluctuation in $u$ component of velocity, $ft/s, m/s$ .
$u$	velocity component in the $x$ -direction, $ft/s, m/s$ .
$U$	boundary layer edge velocity, $ft/s, m/s$ .
$u_\tau$ or $u^*$	shear velocity, $\sqrt{\tau_o/\rho_o}$ , $ft/s, m/s$ .
$v'$	fluctuation in $v$ component of velocity, $ft/s, m/s$ .
$v$	velocity component in the $y$ -direction, $ft/s, m/s$ .
$x$	distance along blade surface, $ft, m$ .
$y$	distance normal to blade surface, $ft, m$ .

### Greek symbols

$\alpha$	thermal diffusivity of fluid (air), $k/(\rho C_p)$ , $ft^2/s, m^2/s$ .
$\gamma$	ratio of specific heats $C_p/C_v$ .
$\gamma_t$	intermittency function.
$\delta$	velocity boundary layer thickness, $ft, m$ .
$\delta_1$	boundary layer displacement thickness, $ft, m$ .
$\delta_2$	boundary layer momentum thickness, $ft, m$ .
$\delta_3$	boundary layer energy thickness, $ft, m$ .
$\delta_T$	thermal boundary layer thickness, $ft, m$ .
$\delta_{T,c}$	thermal boundary layer conduction thickness, $k/h_x$ , $ft, m$ .
$\delta_{T,en}$	thermal boundary layer enthalpy thickness, $ft, m$ .
$\Delta$	$\delta_T/\delta$ .
$\eta$	dimensionless distance from the blade wall, $y/\delta(x)$ .
$\eta_T$	dimensionless distance from the blade wall, $y/\delta_T(x)$ .
$\epsilon_H$	eddy diffusivity for heat, $ft^2/s, m^2/s$ .
$\epsilon_M$	eddy diffusivity for momentum, $ft^2/s, m^2/s$ .
$\kappa_1$	Von Karman constant.
$\lambda$	outer region length scale constant, mixing-length model.
$\Lambda$	dimensionless velocity (or pressure) gradient shape factor based on boundary layer thickness $\delta$ , $\frac{\delta^2}{\nu} \frac{dU}{dx} = -\frac{dP}{dx} \frac{\delta}{\rho U}$ .
$\mu$	dynamic viscosity of fluid, $Ib/(sft), Kg/(sm)$ .
$\mu_{TV}$	turbulence viscosity, $Ib/(sft), Kg/(sm)$ .
$\mu_{eff}$	combined dynamic and turbulence viscosity, $Ib/(sft), Kg/(sm)$ .
$\nu$	kinematic viscosity of fluid, $ft^2/s, m^2/s$ .
$\rho$	density of fluid, $Ib/ft^3, Kg/m^3$ .
$\tau$	laminar or turbulent shear stress, $Ib/(fts^2), Kg/(ms^2)$ .

Subscripts

<i>ad</i>	adiabatic condition.
<i>cr</i>	refers to critical sonic condition.
<i>D</i>	based on leading edge diameter.
<i>e</i>	edge of the boundary layer (free-stream).
<i>eff</i>	effective.
<i>g</i>	gas.
<i>o,w</i>	wall.
<i>s</i>	static.
<i>t</i>	turbulent.
<i>x</i>	based on surface distance.
$\infty$	blade row inlet free-stream value.

Superscripts

$\overline{(\quad)}$	time averaged quantity, or mean value.
$(\quad)'$	local value or derivative with respect to the independent variable $x$ .

# Contents

ACKNOWLEDGEMENTS . . . . .	iv
ABSTRACT . . . . .	v
NOMENCLATURE . . . . .	ix
<b>1 INTRODUCTION</b>	<b>1</b>
<b>2 BACKGROUND AND LITERATURE REVIEW</b>	<b>7</b>
2.1 Introduction . . . . .	7
2.2 Integral methods . . . . .	8
2.3 Finite-difference (differential) method . . . . .	16
2.4 Parameters affecting airfoil heat transfer . . . . .	20
<b>3 INTEGRAL METHOD FORMULATION</b>	<b>23</b>
3.1 Introduction . . . . .	23
3.2 The laminar region of the boundary layer (Velocity boundary layer) . . .	25
3.2.1 Solution of the differential equation for momentum thickness . . .	33
3.3 The laminar region of the boundary layer (Thermal boundary Layer) . .	40
3.3.1 Stagnation point heat transfer . . . . .	40
3.3.2 The laminar thermal boundary layer in front of the stagnation point	42
3.4 The turbulent region of the boundary layer . . . . .	46

3.4.1	Introduction . . . . .	46
3.4.2	Calculation of the momentum thickness $\delta_2(x)$ . . . . .	46
3.4.3	Calculation of the heat transfer coefficient . . . . .	52
<b>4</b>	<b>DEVELOPMENT OF A SPECIFIC METHOD FOR GAS TURBINE APPLICATIONS ( TRANSITION REGION MODELING AND TUR- BULENCE INTENSITY EFFECTS)</b>	<b>57</b>
4.1	Introduction . . . . .	57
4.2	Boundary conditions . . . . .	60
4.3	Modeling the boundary layer over the suction and pressure surfaces . . . .	62
4.4	Suction surface transition region modeling . . . . .	67
4.4.1	Transition origin (start) models . . . . .	68
4.4.2	Transition length models . . . . .	71
4.4.3	Transition path models (Intermittency) . . . . .	73
4.5	Turbulence viscosity ( $\mu_{TV}$ ) models . . . . .	75
4.6	Evaluation of transition region and turbulence viscosity models . . . . .	79
<b>5</b>	<b>DISCUSSION OF RESULTS</b>	<b>83</b>
5.1	Experimental data base . . . . .	83
5.2	Aerodynamic and temperature results . . . . .	85
5.3	Turbulence intensity results . . . . .	87
5.4	Transition start models results . . . . .	88
5.5	Heat transfer coefficients predictions . . . . .	90
5.6	Momentum thickness results . . . . .	92

	xiv
5.7 Other boundary layer parameters results . . . . .	95
<b>6 CONCLUSIONS AND RECOMMENDATIONS</b>	<b>97</b>
6.1 Conclusions . . . . .	97
6.2 Recommendations . . . . .	100
REFERENCES . . . . .	103
Figures . . . . .	110
<b>APPENDIX A</b>	<b>143</b>
Derivation of the momentum and energy integral equations for the boundary layer . . . . .	143
<b>APPENDIX B</b>	<b>147</b>
Literature figures . . . . .	147
<b>APPENDIX C</b>	<b>157</b>
Integral method Fortran program . . . . .	157
<b>APPENDIX D</b>	<b>173</b>
Experimental data base . . . . .	173
Static pressure distribution . . . . .	174
Heat transfer coefficient distribution . . . . .	175

# Chapter 1

## INTRODUCTION

The thermal design of modern high-pressure turbine nozzle guide vanes clearly represents one of the most difficult engineering tasks in the design of any modern aircraft gas turbine. Aerodynamic and thermal analysis procedures currently available to turbine designers have deficiencies that do not permit a priori designs that achieve design goals without expensive experimental development iterations.

In general, internal heat transfer correlations developed from simple bench/rig tests have proved reliable, and calculation of heat flow within the airfoil structure via finite element techniques is well in hand.

The external (gas-to-wall) heat transfer coefficient, however, still eludes satisfactory prediction because of a highly complex and interactive external flow field environment. In addition to the sharp gradients in the gas temperature distribution, the airfoil row is characterized by a flow field reflecting passage Mach Number ( $M$ ) variations from the low subsonic levels ( $M \leq 0.15$ ) to the transonic range ( $M \geq 1.0$ ).

The flow field is strongly influenced by viscous effects in the near wall region where, in turn, heat flow is alternately governed by molecular diffusion, laminar convective transport, turbulent shear transport, or combinations thereof.

Although the character of the boundary-layer over the greater radial extent of most airfoils is nominally two-dimensional (2-D), local boundary-layer behavior (and, hence, surface heat transfer rate) is strongly influenced by complex and interactive mechanisms summarized in Table (1.1).

Table (1.1): Basic mechanisms that influence gas-to-blade heat transfer.

Mechanism	Nature/Manifestation
Transitional Behavior	Transition from laminar/molecular diffusion transfer to turbulent shear transfer. Direct effect on heat transfer.
Free-stream turbulence	Temporal small-scale combustor or blade-passing induced stream velocity fluctuations. Influences production and diffusion of boundary-layer turbulence and boundary layer stability (transitional behavior).
Airfoil surface curvature	Influences boundary layer turbulence and dissipation. Affects boundary layer stability. May produce Goertler vortices (periodic large-scale disturbances along concave surface) with consequent strong effect on heat transfer.
Airfoil surface roughness	Directly influences boundary layer turbulence production and stability.
High mainstream velocity acceleration/deceleration	Direct influence on boundary layer thickness, profile shape, and stability. Controls turbulence production (deceleration) and dissipation (acceleration).
Flow separation and reattachment	Affects local character and thickness distribution of the boundary layer. Produces sharp local heat transfer rate increases.
Distributed surface injection	Strong influence on turbulence production in injection region. Directly affects near-wall temperature profile and downstream boundary layer profiles and thickness.
Shock/boundary layer interaction	Causes boundary layer separation and consequent effects.



Presently, a variety of prediction techniques are used to solve this complex problem with varying degrees of success. The simpler, well established correlative techniques have met with some success sufficient to provide initial design predictions [1]. However, only recently have the more powerful integral and finite difference solutions of the complete time-averaged boundary layer equations shown real promise [2-16].

Reinforced by carefully derived empirical turbulence modeling, the numerical techniques [5-16] have yielded reasonable predictions of the effects of strong acceleration / deceleration where the external flow field and state of the boundary layer are well defined. On the other hand, integral techniques [2-4] continue to show disagreement between predicted and measured heat transfer coefficient distributions on airfoils.

For non-film cooled airfoils, deviation of heat transfer predictions by integral methods from true or experimentally indicated levels can most probably be attributed to one or more of the following analytical deficiencies :

1. Lack of precision in the prediction of the inviscid flow field around the airfoil, particularly in the forward highly accelerated stagnation region .
2. Uncertainties regarding the surface location at which transition is initiated on the suction surface as well as the surface extent of the transition zone.
3. Uncertainties regarding the influence of free-stream turbulence on local heat transfer rates in the laminar region found over the pressure surface, as well as on initiation and extent of the transition region found on the suction surface.
4. Limited understanding of the role of airfoil surface curvature on turbulence production/dissipation and boundary layer stability.

Even if consideration is restricted to the nominally two-dimensional midspan region of the blade surface, the complex environment described above suggests the need for an improved design approach with sufficiently enlightened transition region and turbulence intensity modeling to accommodate the several interactive influences described previously.

A requirement is posed by the clear need to confirm, through realistic cascade experiments, that the physical details of the viscous flow field are in fact correctly modeled.

While a number of experimental turbine vane heat transfer studies have been reported over the past 35 years [17-21], the applicability of these data to modern low solidity, highly loaded vane rows is limited by conservatism in profile shape and/or Mach number range [17,19] or by incompleteness in availability of data [17,18,19,20,21].

The experimental studies cited above were not conducted under conditions that ensured coincident similarity of the principal independent aero-thermo parameters (Mach number, Reynolds number, wall-to-gas temperature ratio and turbulence intensity) to those existing in current generation core engines.

The objectives of this study are as follows :

1. To assess the capability of currently available integral method for predicting nonfilm-cooled airfoil surface heat transfer coefficient distribution in a two-dimensional flow field.
2. To incorporate several transition start, length and path models and turbulence viscosity models to this integral method.

3. To acquire additional airfoil heat transfer experimental data (From Literature) at simulated engine conditions and verify utilizing this acquired literature data that the incorporated models have achieved the desired results.

The results of an experimental study of aerodynamic (surface velocity) and heat transfer distributions over the surfaces of a highly loaded, low solidity modern turbine nozzle guide vane designs were kindly supplied by Dr. D.A. Nealy, Chief of the heat transfer section, Detroit Diesel Allison, General Motors Corporation [22].

The supplied experimental data set were conducted in moderate temperature, three vane cascades under steady-state conditions. The principal independent parameters values (Mach number  $M$ , Reynolds number  $Re$ , turbulence intensity  $Tu$ , and wall-to-gas temperature ratio  $T_w/T_g$ ) were consistent with actual engine operation.

The aerodynamic configurations of the data set emphasize fundamental differences in the character of the suction and pressure surfaces velocity distributions and the consequent effect on surface heat transfer. Thus this data set provide a data base covering a range of operating conditions and geometries for testing the predictive capability of the integral prediction method.

Chapter 2 briefly reviews some of the integral and finite-difference tools found in the literature for predicting non-film cooled airfoil surface heat transfer coefficient distribution.

In Chapter 3 the integral method used in this study is laid out and explained in detail. This integral method is capable to calculate the laminar and turbulent convective heat transfer coefficients and boundary layer momentum thickness over the surfaces of solid turbine blades .

In Chapter 4 several transition region models (transition start, length and path) and turbulence viscosity models are introduced in order to incorporate them with the integral method and recommend the best combination. Furthermore, since the suction and pressure surfaces have a fundamental differences in the character of the boundary layer developing on them, the author of this study has modeled the boundary layer found on these two surfaces by two different approaches, as follows:

1. On the suction surface of the blade, laminar, transitional, and turbulent flow regions do exist. The laminar and fully turbulent regions are computed as explained in Chapter 3, while the transition region is modeled using the transition start, length, and path models found in chapter 4.
2. On the pressure surface of the blade, the flow is characterized to be in transitional state from the leading to the trailing edge. However, modeling this transitional behaviour is different than modeling the transition region on the suction surface. An effective viscosity formulation was included to model this transitional behaviour. This formulation permitted the boundary layer on the pressure surface to be treated as a laminar one but with the calculations being based on an effective viscosity formed by combining the dynamic (laminar) viscosity to the turbulence viscosity.

In Chapter 5 various single and/or combined model solutions and results are discussed and evaluated using experimental data in order to recommend the best combination.

Finally, conclusions and recommendations are given in Chapter 6.

## Chapter 2

# BACKGROUND AND LITERATURE REVIEW

### 2.1 Introduction

One of the most critical inputs to heat transfer cooling design calculations for turbine airfoils is the prediction of the gas-side heat transfer coefficient distributions. Also, the heat fluxes form the boundary conditions in the conduction analysis necessary to predict the blade temperatures. For this reason, many research efforts have been aimed at improving understanding of the flow and heat transfer in the turbine components.

The blade temperatures may of course be obtained experimentally. Such a course of action is costly, and it is too time consuming to use in the iterative design and optimization process of turbine blades. An analytical method capable of giving accurate predictions of the surface heat transfer coefficients distributions over gas turbine blades would be a more appropriate assistance to engine designers and would also help to reduce the extent and cost of development testing required in an engine design.

The general approach used in the calculation of turbine airfoil heat transfer coefficients is based on two-dimensional boundary layer calculation methods using either finite difference or integral formulations.

All approximate integral methods have the common feature that, instead of satisfying the partial differential equations of boundary layer motion, they only satisfy a mean value taken over the equation of motion, as expressed physically by the momentum integral equation. In addition the boundary conditions at the wall and at the outer edge of the boundary layer are satisfied.

On the other hand, finite difference methods, sometimes called the field or differential methods satisfy the boundary layer equations at each node of the computational domain.

## 2.2 Integral methods

The large number of integral methods that are found in the literature are generally classified according to the type of flow (laminar or turbulent) they are applicable to, the number of motion equations and relations that are used to obtain a solution, and to the boundary layer they solve (velocity or thermal boundary layer).

A complete summary of the integral methods found in the literature is outlined by White [23].

Nealy [2], developed an integral method that solves a single ordinary differential equation (the integral form of the thermal energy equation). This method perhaps represents the simplest type of differential equation boundary layer methods, which might be used to determine heat transfer. The method is capable of solving both laminar and turbulent flows. For laminar flows, local similarity is assumed at each computational station, and therefore, the results obtained from exact solutions may be used. For turbulent flows, Nealy assumed that local equilibrium exists and the results of zero-pressure gradient (flat plate) are used to develop an expression for the turbulent Stanton number. Furthermore,

Nealy treats transition from laminar to turbulent flow as a single computational step process based on an arbitrary specification of occurrence. Because of these assumptions, Nealy's method have questionable range of application.

For the laminar velocity boundary layer, Pohlhausen [24] used the momentum integral equation together with a fourth order velocity profile to derive a non-linear first order differential equation describing the variation of the momentum thickness ( $\delta_2$ ) with surface distance ( $x$ ).

For the laminar thermal boundary layer, Squire [25] adopted a standard similar velocity and temperature distributions across the boundary layer (the Blasius distribution) and combined the momentum integral equation and the heat flux equation. The resulting equation is solved for the thermal boundary layer thickness (and hence the heat transfer coefficient) using the method of successive approximations. **414003**

Truckenbrodt [26] adopted Ludwig and Tillmann [27] and Rotta [28] investigations on the theoretical properties of turbulent flows, particularly of the wall shear stress and the energy loss in the boundary layer and developed a method for the calculation of the momentum thickness which is valid for both laminar and turbulent flows. The interesting point in Truckenbrodt method is that he followed a somewhat different path in that he made use of the energy integral equation and not of the momentum integral equation to solve for the momentum thickness. This energy integral equation is sometimes called the mechanical energy equation, which is merely the momentum equation multiplied by the velocity component  $u$ , that is, it changes forces into the rate of work done by those forces.

Gauntner and Sucec [3] described a method for calculating laminar, transitional and

turbulent convective heat transfer coefficients over the surfaces of turbine vanes. On the leading edge of the blade they used the heat transfer coefficient correlation for a cylinder in cross flow :

$$h = 1.14 Re_D^{0.5} Pr^{0.4} \frac{k}{D} \left[ 1 - \left( \frac{|\theta|}{90} \right)^3 \right] \quad 0^\circ < |\theta| < 80^\circ \quad (2.1)$$

In the laminar region, Gauntner and Sucec [3] corrected the flat plate correlation for heat transfer coefficient to account for pressure gradient, as follows:

$$h_x = \bar{F}_{lam} Re_x^{0.5} Pr^{1/3} \left( \frac{k}{x} \right) \quad (2.2)$$

Where:

$$\bar{F}_{lam} = Nu_x / Pr^{1/3} Re_x^{0.5}$$

$$\bar{F}_{lam} Pr^{1/3} = F_{lam}$$

The  $F_{lam}$  correction is evaluated as a function of the local Euler number  $\left( -\frac{dP}{dx} / \rho_e U^2 \right)$  and the local ratio of  $T_e/T_w$ . The values of  $F_{lam}$ , or  $Nu_x / Re_x^{0.5}$ , are approximated by solutions for wedge-type flow. As Gauntner and Sucec [3] indicates these wedge solutions may be used to approximate heat transfer coefficients along any arbitrary profile. The value of the Euler number at any position along the profile determines the corresponding wedge for which, at the same distance  $x$  from the stagnation point, the heat transfer on the wedge and the arbitrary profile are assumed to be equal.

The technique followed by Gauntner and Sucec [3] for predicting turbulent local convective heat transfer coefficients is based on the approximate integral solution of the energy equation given for the first time by Ambrok [4]. The solution of this thermal boundary layer equation takes into approximate account the effects of thermal history, free stream velocity variation, and free stream density variation.



Gauntner and Sucec arranged the energy integral equation into a form involving the local enthalpy thickness  $\delta_{T, en}$ .

$$\frac{d\delta_{T, en}}{dx} + \left[ \frac{1}{\rho_e} \frac{d\rho_e}{dx} + \frac{1}{U} \frac{dU}{dx} + \frac{1}{(T_w - T_e)} \frac{d(T_w - T_e)}{dx} \right] \delta_{T, en} = \frac{h_x}{\rho_e C_p U} = St_x \quad (2.3)$$

As Gauntner and Sucec suggested, if a relation could be found between  $St_x$  and  $\delta_{T, en}$ , equation (2.3) could be solved for  $\delta_{T, en}$  as a function of  $x$  and hence  $h_x$  as a function of  $x$ . The above authors used a flat plate turbulent constant property relation to relate  $St_x$  and  $\delta_{T, en}$ , as follows :

$$St_x = \frac{Nu_x}{Re_x Pr} = 0.0296 Pr^{-2/3} Re_x^{-0.2} \quad (2.4)$$

and,

$$St_x = B^{1/(1-m)} (1-m)^{-m/(1-m)} Re_{\delta_{T, en}}^{-m/(1-m)} \quad (2.5)$$

Where for turbulent flow  $B = 0.0296 Pr^{-2/3}$  and  $m = 0.2$ .

Furthermore, Gauntner and Sucec proposed that  $St_x$  in equation (2.3) is only function of  $Re_{\delta_{T, en}}$  but otherwise independent of body shape, surface temperature variation, free-stream velocity and density variation. The above authors then substituted equation (2.5) into equation (2.3) and the resulting expression was integrated. Their final result for turbulent flow is:

$$St_x = \frac{0.0296 Pr^{-2/3} (T_e - T_w)^{0.25} (T_e/T_w)^{0.25}}{\left\{ \int_{x_{tran, end}}^x \frac{\rho_e U (T_e - T_w)^{1.25}}{\mu_e} dx + \left[ \frac{0.8}{0.0296 Pr^{-2/3}} \left( \frac{\rho_e U \delta_{T, en}}{\mu_e} \right)_{x_{tran, end}} (T_e - T_w) \right]^{1.25} \right\}^{0.2}} \quad (2.6)$$

The factor  $(T_e/T_w)^{0.25}$  in the numerator of the right side of equation (2.6) is the temperature ratio correction for property variation across the boundary layer according to Crawford and Kays [29] for  $\frac{T_w}{T_e} < 1$ . The temperature dependent fluid properties are then evaluated at the local free-stream static temperature  $T_e$ .

For the transition region, Gauntner and Sucec uses the same methodology as in the turbulent region but instead of using equation (2.4), they used an empirical expression which is analogue to equation (2.4) and applicable in the transition region. This correlation is obtained from the experimental heat transfer results obtained by Ambrok [4] in the transition region along a flat plate.

$$Nu_x = 0.000386 Re_x^{10/9} \quad (2.7)$$

Assuming again the form of equation (2.5), with  $Pr = 0.7$ , the values  $B = 0.000435 Pr^{-2/3}$  and  $m = -1/9$  result. Gauntner and Sucec used these values to derive an expression for the transitional heat transfer coefficient which is similar to equation (2.6). That is,

$$St_x = \frac{0.000435 Pr^{-2/3} (T_e - T_w)^{-0.1} (T_e/T_w)^{0.25}}{\left\{ \int_{x_{tran}}^x \frac{\rho_e U (T_e - T_w)^{0.9}}{\mu_e} dx + \left[ \frac{1.111}{0.000435 Pr^{-2/3}} \left( \frac{\rho_e U \delta_{T,en}}{\mu_e} \right)_{x_{tran}} (T_e - T_w) \right]^{0.9} \right\}^{-0.111}} \quad (2.8)$$

To use equations (2.6) and (2.8) it is necessary to evaluate the quantity  $\left( \frac{\rho_e U \delta_{T,en}}{\mu_e} \right)$  at  $x_o$  (here  $x_o$  denotes either the start of transition  $x_{tran}$  or the end of transition  $x_{tran,end}$ ). Since  $\delta_{T,en}$  is continuous at  $x_o$  (between laminar and transitional regions and between transitional and turbulent regions) it is possible to evaluate  $\delta_{T,en}$  by rearranging equation (2.5), as follows :

$$\left( \frac{\rho_e U \delta_{T,en}}{\mu_e} \right)_{x_o} = \frac{B^{1/m}}{1-m} \left\{ \left( \frac{h_x}{\rho_e C_p U} \right)^{1-1/m} \right\}_{x_o} \quad (2.9)$$

At  $x_o$ , the values of  $m$ ,  $B$  and  $h_x$  are obtained from the laminar or transitional expressions. They are used in equations (2.8) and (2.6), respectively. For equation (2.6),  $B = 0.000435 Pr^{-2/3}$  and  $m = -1/9$ . Where as for equation (2.8),  $B = 0.332 Pr^{-2/3}$  and  $m = 0.5$  when  $\bar{F}_{lam} = 0.332$  in equation (2.2).

Gauntner and Sucec predicted the start of transition using Seyb criterion [30] and set

transition end at a momentum thickness Reynolds number  $Re_{\delta_2} = 360$ .

A method proposed by Head [31] makes use of a new idea. According to this, there ought to exist a functional relationship between the shape factor  $\left(\frac{\delta_2 - \delta_1}{\delta_2}\right)$  and the mass flow entrained by the boundary layer per unit length from the outside. Head used this relation together with the momentum integral equation and the Ludwig and Tillmann [27] coefficient of friction  $(C_f')$  law to solve for the three turbulent boundary layer unknowns,  $\delta_2$ ,  $H_{12} = \frac{\delta_2}{\delta_1}$ , and  $C_f'$ .

As it will be seen in the next chapter, the method used in this study to calculate the heat transfer coefficient around the laminar part of the blade profile involves first solving the momentum equation to establish the velocity field and then solving the energy equation. A still simpler approach, but one introducing a greater degree of approximation, involves a solution to either the momentum or the energy integral equation, but not both. Eckert [42] proposed a scheme based on the solution of the energy-integral equation alone. In this scheme, Eckert assumed that the rate of growth of any of the thermal boundary-layer thicknesses  $\delta_T$  is a function of local parameters alone, that is :

$$\frac{d\delta_T}{dx} = f\left(\delta_T, U, \frac{dU}{dx}, \nu, Pr\right)$$

As Eckert indicates, any of the thermal boundary-layer thicknesses might be used in the above equation, such as the conduction thickness  $\delta_{T,c}$ , where :

$$\delta_{T,c} = \frac{k(T_w - T_\infty)}{q_w} = \frac{k}{h_x}$$

By dimensional analysis, Eckert [42] shows that the variation of  $\delta_{T,c}$  can be expressed in non-dimensional form :

$$\frac{U}{\nu} \frac{d\delta_{T,c}^2}{dx} = f\left(\frac{\delta_{T,c}^2}{\nu} \frac{dU}{dx}, Pr\right) \quad (2.10)$$

The essence of Eckert method lies in the assumption that the function  $f$  for an arbitrary variation of free-stream velocity is the same as for the family of wedge flows. The latter (i.e. wedge flows solutions) are already evaluated using the similarity solutions.

Table (2.1), tabulates, for each particular value of  $m$  (where  $m = \frac{\gamma/\pi}{2-\gamma/\pi}$ ,  $\gamma = 0^\circ$  for flat plate,  $\gamma = 180^\circ$  for 2-D stagnation point) the corresponding wedge solution  $Nu_x Re_x^{-1/2}$  obtained from solving the boundary layer energy equation.

Table (2.1): Values of  $Nu_x Re_x^{-1/2}$  for various wedge flows, heat transfer to the laminar boundary layer ( $U(x) = Cx^m$ ),  $Pr = 0.7$ , [29].

m	-0.0753	0.0	0.111	0.333	1.0	4.0
$Nu_x Re_x^{-1/2}$	0.242	0.292	0.331	0.384	0.496	0.813

Thus,

$$Nu_x Re_x^{-1/2} = C_1$$

From which  $h_x \propto U^{1/2} x^{-1/2}$

Employing  $U(x) = Cx^m$  (wedge condition) and  $\delta_{T,c} = \frac{k}{h_x}$ , then the following expressions can be developed for the wedge solutions :

$$\frac{U}{\nu} \frac{d\delta_{T,c}^2}{dx} = \frac{1-m}{C_1^2} \quad (2.11)$$

and,

$$\frac{\delta_{T,c}^2}{\nu} \frac{dU}{dx} = \frac{m}{C_1^2} \quad (2.12)$$

Thus for  $Pr = 0.7$ , a plot of equation (2.10) can be prepared from the data in table (2.1), as shown in figure (2.1).

Eckert proposed to solve equation (2.10) numerically for any arbitrary free-stream velocity variation employing such a plot of the wedge solutions for the function  $f$ .

Such a numerical calculation would be tedious, but as seen from figure (2.1), a very good approximation is obtained by replacing the exact wedge solutions curve with a linear approximation which leads to a simpler integration procedure.

For  $Pr = 0.7$ , the following linear relation fits the wedge data exactly for the stagnation point case and for the case of a flat plate, it is a fair fit in between but begins to depart markedly for strongly decelerating flows, although boundary-layer transition limits the curve in this direction,

$$\frac{U}{\nu} \frac{d\delta_{T,c}^2}{dx} = 11.68 - 2.87 \frac{\delta_{T,c}^2}{\nu} \frac{dU}{dx} \quad (2.13)$$

Equation (2.13) may be integrated and thus reduced to :

$$\delta_{T,c}^2 = \frac{11.68\nu \int_0^x U^{1.87} dx}{U^{2.87}} \quad (2.14)$$

Equation (2.14) can now easily be evaluated for any desired variation of  $U$  with  $x$ , so the conduction thickness, and thus the local heat transfer rate can be readily calculated.

Thus with  $\delta_{T,c} = \frac{k}{h_x}$ , then equation (2.14) becomes :

$$h_x = \frac{k U^{1.435}}{\sqrt{11.68\nu^{1/2} [\int_0^x U^{1.87} dx]^{1/2}}} \quad (2.15)$$

Introducing the definition of the Prandtl number, i.e.  $Pr = \frac{\mu C_p}{k}$ , then,

$$h_x = \frac{\mu C_p U^{1.435}}{Pr \sqrt{11.68\nu^{1/2} [\int_0^x U^{1.87} dx]^{1/2}}} \quad (2.16)$$

For air,  $Pr = 0.7$ , then equation (2.16) becomes :

$$h_x = \frac{0.418 \mu C_p U^{1.435}}{\nu^{1/2} [\int_0^x U^{1.87} dx]^{1/2}} \quad (2.17)$$

Or using the definition of the Stanton number ( $St_x = \frac{h_x}{\rho C_p U}$ ), then,

$$St_x = \frac{0.418 \nu^{1/2} U^{0.435}}{[\int_0^x U^{1.87} dx]^{1/2}} \quad (2.18)$$

### 2.3 Finite-difference (differential) method

In this class of methods a grid, usually rectangular, is placed on the flow field, and the flow quantities are to be calculated only at the nodes of the grid. Algebraic equations at each node are obtained from the partial differential equations by approximating each derivative by an appropriate difference. The boundary conditions must also be incorporated to ensure that there are as many equations as unknowns. Obviously, there are a tremendous number of different algebraic formulations that can be used by the indicated procedures. The objective, however, is to ensure that the algebraic difference equations can be solved with reasonable efficiency and accuracy while representing acceptable approximations to the flow quantities. The above mentioned points have been studied in great detail and lead to the theory of stability and convergence of difference schemes.

The two-dimensional boundary layer problem is a parabolic phenomena, that is, when the differential equation is replaced by a finite difference one, the value of the dependent variable such as velocity, enthalpy or other transported entity at a nodal point is affected by the dependent variable values at lower  $x$  and same  $x$  nodes, but not by those at higher  $x$  nodes. Then the solution can be affected by a single down-stream sweep, using the well-known tri-diagonal matrix algorithm. Thus in two-dimensional boundary layers, down-stream cannot affect up-stream.

Several finite-difference methods and/or programs are found in literature. A complete survey of the finite-difference methods found in the literature is outlined by White [23].

Finite difference programs found in the literature differ from each other mainly by the numerical techniques used to convert the boundary layer partial differential equation to a finite difference one, the kinds of turbulence models used to obtain closure (i.e. defining the turbulent shear stress and turbulent heat flux) and by the choice of coordinate system and mesh sizes. When defining the shear stress, some methods used some sort of eddy-viscosity hypothesis (i.e. mixing-length formulations), while others use the turbulent kinetic energy equation. Since the turbulent kinetic energy equation contains three new variables (i.e. turbulent kinetic energy  $\frac{\alpha^2}{2}$ , dissipation  $\epsilon$ , and diffusion term  $\overline{v'p'}$ ), methods using this equation must search for further empirical correlations. Several methods found in [23] choose a relation between  $\tau$  and  $\frac{\alpha^2}{2}$  plus an empirical length-scale correlation for dissipation  $\epsilon$  and diffusion  $\overline{v'p'}$  terms.

Herring and Mellor [7] describes a finite-difference computer program which performs a numerical integration of the equations of motion for a compressible two-dimensional boundary layer. The basic numerical scheme used in their program is described as an implicit, Crank-Nicholson method resulting at each station in an ordinary differential equation. The ordinary differential equation is solved using a Gaussian elimination method to solve the characteristic matrix. Boundary layer calculations may be carried out for both laminar and turbulent flow for arbitrary Reynolds number and free stream Mach number distribution on planar or axisymmetric bodies with wall heating or cooling, wall suction or blowing and a rough or a smooth wall. Herring and Mellor [7] allow transition to be modeled by specifying the start and extent of transition as input.

Cebeci and Smith [12] developed a finite-difference program of the "mean field closure type", that is the fluctuation terms in the momentum and energy equations are specified

in the turbulence model in terms of mean flow parameters only. A full description of the program is given in Cebeci and Smith [12]. It is applicable to both laminar and turbulent compressible boundary layers in two-dimensional and axisymmetric flows. The continuity, momentum and energy (total enthalpy) equations, in mass averaged form, are solved in terms of a transformed system of coordinates specified by the Mangler, Levy-Lees transformation. The very efficient Keller's Box numerical method, described by Keller and Cebeci [13], is used. In this program, an eddy viscosity is calculated using Prandtl's mixing length. This eddy viscosity is then related to the Reynolds stresses and the mean velocity gradient. The fluctuations in total enthalpy is calculated from the mean total enthalpy gradient by applying Reynolds analogy in the form of a constant total turbulent Prandtl number (which allows the determination of a turbulent thermal conductivity). In the Cebeci and Smith [12] program the location of the transition point is specified as an external input by the user.

Patanker and Spalding [14,15,16] developed a finite-difference scheme and program they called Genmix IV. Their scheme is a general, implicit numerical marching procedure for the solution of parabolic partial differential equations with special reference to those of the boundary layer. The main new idea in this scheme lies in the choice of a grid which adjusts its width so as to conform to the thickness of the boundary layer in which significant property gradients are present. The non-dimensional stream function is employed as the independent variable across the layer.

Rodi and Scheuerer [32] incorporated the Patankar and Spalding program [14] with an extended version of the widely used  $k-\epsilon$  turbulence model of Jones and Launder [33]. Computationally, the method solves the same two governing partial differential equa-



tions (streamwise momentum and total enthalpy) plus two additional partial differential equations (turbulent kinetic energy,  $k$ , and isotropic dissipation rate,  $\epsilon$ , equations). The last two equations represent the turbulence model or closure assumption for defining the turbulent shear stress or viscosity. The turbulent heat flux is modeled using the assumption that the eddy diffusivity for heat is equal to the eddy viscosity (i.e. eddy diffusivity for momentum) divided by the turbulent prandtl number taken equal to 0.86. Rodi and Scheuerer used their method of calculation and applied it to various turbine blade situations for which Daniels and Browne [34] have carried out measurements.

The conclusions drawn from the predictions of Rodi and Scheuerer [32] is that the distribution of the heat transfer coefficient on the suction side of turbine blades is governed mainly by the onset of the laminar-turbulent transition. This process in turn is controlled by the local values of the pressure gradient and free-stream turbulence intensities. Surface curvature, variable fluid properties and surface roughness (if the blades are not well finished) exert only a negligible influence on the external heat transfer. Discrepancies between prediction and measurements on the suction side occur in the transitional region, where Rodi and Scheuerer method yields a somewhat faster transition than what is observed in the experiment.

On the pressure surface, Rodi and Scheuerer [32] assumed that transition usually starts very near the leading edge because of the high relative turbulence intensity on this side of the blade. After this early start, there is a balance between free-stream turbulence and pressure gradient effects, the former tending to promote and the latter to retard the transition to fully turbulent flow. According to Rodi and Scheuerer, due to the relaminarizing effect of the favourable pressure gradient on the pressure surface, the boundary

layer does not become fully turbulent on this surface.

## 2.4 Parameters affecting airfoil heat transfer

Some of the important geometric and flow field characteristics often associated with the accuracy of predicted heat transfer coefficients for solid surface turbine airfoils in a gas turbine environment include :

1. Laminar, transitional, and turbulent states.
2. Free-stream turbulence effects.
3. Effects of strong nonequilibrium conditions (favorable/adverse pressure gradients).
4. Surface-to-free-stream temperature ratio effects.
5. Surface curvature effects (convex/concave).
6. Body force effects.
7. Laminarization or reverse transition process effects.
8. Surface roughness effects.
9. Rotation effects.
10. Flow separation with and without reattachment.

The effects of mainstream turbulence on turbine airfoil heat transfer were studied by Lander [20] for a range of mainstream turbulence intensities of 6 to 22% on the suction surface of a vane. Similarly, Turner [19] and Kan [35] investigated the effects

of mainstream turbulence on turbine blade heat transfer in a stationary cascade and Brown and Burton [21] conducted similar studies in a wind tunnel with a curved surface simulating the suction surface of a turbine blade. The mainstream turbulence in the latter investigations ranged from 0.5 to 9%. The above experimental studies led to the following conclusions :

1. Mainstream turbulence influences the start of transition from a laminar to a turbulent boundary layer with increased turbulence promoting early transition.
2. Turbulence intensity has a marked effect on laminar boundary layers ( in particular on the pressure surface), increased turbulence results in an increased heat transfer coefficients in the laminar boundary layer region found on the pressure surface of turbine airfoils.
3. Mainstream turbulence level has little effect on the heat transfer coefficients in the turbulent boundary layer region.

It is well known that favourable pressure gradients suppress and that adverse pressure gradients amplify turbulence in a boundary layer as reported by Schubauer and Skramstad [36]. In addition it has been shown by various workers including Launder [37] and Patel and Head [38] that strong favourable pressure gradients can even relaminarize a fully turbulent boundary layer. Launder [37] suggests that when the pressure gradient parameter,  $\frac{\nu}{U^2} \frac{dU}{dx}$ , exceeds  $2 \times 10^{-6}$  laminarization effects will become significant. Furthermore, apart from the free-stream turbulence, the longitudinal pressure gradient exerts the largest effect on transition and hence on the distribution of the heat transfer coefficient.

The effect of streamwise surface curvature is to stabilize the boundary layer on the convex (suction) surface and to destabilize the boundary layer on a concave (pressure) surface, Schlichting [24]. The destabilizing effect of centrifugal forces on the concave wall induces an instability which results in Goertler vortices with axes in the same direction as the main stream flow. Shivaprasad and Ramaparian [39] conducted investigations on mildly curved surfaces (boundary layer thickness/ wall radius of curvature  $\cong 0.01$ ). Their results showed that turbulence intensities in the boundary layer are reduced on a convex wall and enhanced on a concave wall, and thus heat transfer on the concave wall is increased and that for the convex wall is decreased.

It is believed in this present work that a careful modeling of the distribution of the free-stream turbulence intensity along the blade surfaces automatically models the effects of surface curvature.

Rodi [32] shows that turbine blades has small ratio of boundary layer thickness to wall radius of curvature and thus centrifugal effects are negligible (i.e. surface curvature effects are small).

Johnston [40] reviewed the effects of rotation on boundary layers in turbomachinery rotors. He observed that rotation tends to stabilize the boundary layer on the suction side and destabilize the boundary layer on the pressure side of turbine blades. He also concluded that rotational effects on the heat transfer level in axial flow turbine blades are negligible except in separated flow regions.

## Chapter 3

# INTEGRAL METHOD FORMULATION

### 3.1 Introduction

The following method is used to calculate convection heat transfer coefficients and adiabatic wall temperatures along the blade profile. Static temperature and pressure are calculated outside the boundary layer from channel flow theory [41] using the following equations :

$$T_s = T_o \left[ 1 - \left( \frac{\gamma - 1}{\gamma + 1} \right) \left( \frac{U(x)}{U_{cr}} \right)^2 \right] \quad (3.1)$$

$$P_s = P_o \left( \frac{T_s}{T_o} \right)^{\frac{\gamma}{\gamma - 1}} \quad (3.2)$$

$$U_{cr} = \left[ \frac{2\gamma}{\gamma + 1} RT_o \right]^{1/2}$$

Where,  $U_{cr}$  is the critical speed of sound corresponding to the sonic state of a perfect gas ( $M = M_{cr} = 1$ ).

$C_p$ ,  $\mu$ ,  $Pr$  and  $\rho$  (characteristics of the fluid ) are entered as tables in the integral method Fortran program for the appropriate range of temperatures and pressures.

The calculation of convection heat-transfer coefficients and adiabatic wall temperatures is then carried out on the following assumptions :

1. On the suction side, the boundary layer is laminar from the stagnation point to the neighborhood of the point of minimum pressure. From this latter point on, the flow is transitional, then fully turbulent .
2. On the pressure side, the boundary layer is either laminar or transitional from the neighborhood of the stagnation point to the neighborhood of the trailing edge. (i.e. fully turbulent flow regime might occur near the trailing edge.)

The adiabatic wall temperatures are obtained from the following equations [24] :

For laminar boundary layer ;

$$T_{ad} = T_s + (T_o - T_s)Pr^{\frac{1}{2}} \quad (3.3)$$

and for turbulent boundary layer ;

$$T_{ad} = T_s + (T_o - T_s)Pr^{\frac{1}{3}} \quad (3.4)$$

On the leading edge and in the laminar region of the boundary layer, Pohlhausen [24] approximate integral method which is based on the momentum integral equation is used for the calculation of the velocity field. The laminar thermal boundary layer is calculated by Squire's method [25] for the calculation of heat transfer on a cylinder and on a flat plate with longitudinal pressure gradient. In the turbulent part of the boundary layer, the Von Karman formula for heat transfer in turbulent flows is used.

The theories of Schlichting [24] and Truckenbrodt [26] are used for the determination of the transition point and the computation of a two-dimensional turbulent boundary layer momentum thickness. Furthermore, the above mentioned theories were incorporated into a computer program by [41].

The above mentioned methods and theories will be described in the following sections.

### 3.2 The laminar region of the boundary layer (Velocity boundary layer)

Choosing a system of coordinates in which  $x$  denotes the arc measured along the wetted wall (blade surface) and  $y$  denotes the distance from the wall (figure (3.1)). The basic equation of the momentum theory is obtained by integrating the equation of motion with respect to  $y$  from  $y=0$  at the wall, to a certain distance  $H(x)$  which is assumed to be outside the boundary layer for all values of  $x$ .

With this notation the momentum integral equation has the following form :

$$U^2 \frac{d\delta_2}{dx} + (2\delta_2 + \delta_1)U \frac{dU}{dx} = \frac{\tau_o}{\rho} \quad (3.5)$$

The derivation of this momentum integral equation is outlined in Appendix A.

Equation (3.5) gives an ordinary differential equation for the boundary layer thickness, provided that a suitable form is assumed for the velocity profile. This allows the calculation of the momentum thickness ( $\delta_2$ ), the displacement thickness ( $\delta_1$ ) and the shearing stress at the wall ( $\tau_o$ ).

The assumed velocity profile has to take into account the no-slip condition at the wall, as well as the requirements of continuity at the point where this solution is joined to the potential solution. Furthermore, and in the presence of a pressure gradient, the velocity function must admit the existence of profiles with and without a point of inflexion corresponding to their occurrence in regions of negative and positive pressure gradients.

Finally, in order to be in a position to calculate the point of separation with the aid of this approximate method, the existence of a profile with zero velocity gradient at the wall,  $(\frac{\partial u}{\partial y})_{y=0} = 0$ , must also be possible.

Assuming a polynomial of the fourth degree for the velocity profile in terms of the

dimensionless distance from the wall  $\eta = \frac{y}{\delta(x)}$ , i.e.

$$\frac{u}{U} = f(\eta) = a\eta + b\eta^2 + c\eta^3 + d\eta^4 \quad (3.6)$$

in the range  $0 \leq \eta \leq 1$ , whereas for  $\eta > 1$  it is simply assumed that  $\frac{u}{U} = 1$ .

As noted before, the boundary layer should join the potential flow at the finite distance from the wall  $y = \delta(x)$ .

In order to determine the four free constants, a, b, c and d, the following four boundary conditions shall be prescribed :

$$y = 0, \quad u = 0, \quad \nu \frac{\partial^2 u}{\partial y^2} = \frac{1}{\rho} \frac{dP}{dx} = -U \frac{dU}{dx} \quad (3.7)$$

$$y = \delta, \quad u = U, \quad \frac{\partial u}{\partial y} = 0, \quad \frac{\partial^2 u}{\partial y^2} = 0 \quad (3.8)$$

These requirements are sufficient to determine the constants a, b, c and d, because the no-slip condition at the wall is implicit in equation (3.6). The second condition in equation (3.7) which is satisfied by the exact solution as seen from equation (A.1) in Appendix A is of particular importance. It determines the curvature of the velocity profile near the wall and makes sure that there is no point of inflexion in the velocity profile in regions of decreasing pressure. Furthermore, regions of increasing pressure contain points of inflexion as required by the exact solution (at point of inflexion  $\frac{\partial^2 u}{\partial y^2} = 0$ ).

Introducing the dimensionless quantity,

$$\Lambda = \frac{\delta^2}{\nu} \frac{dU}{dx} \quad (3.9)$$

and using the above boundary conditions then the following expressions may be obtained for the coefficients in equation (3.6),

$$a = 2 + \frac{\Lambda}{6} ; \quad b = -\frac{\Lambda}{2} ; \quad c = -2 + \frac{\Lambda}{2} ; \quad d = 1 - \frac{\Lambda}{6} ;$$



and hence for the velocity profile :

$$\frac{u}{U} = F(\eta) + \Lambda G(\eta) = (2\eta - 2\eta^3 + \eta^4) + \frac{\Lambda}{6}(\eta - 3\eta^2 + 3\eta^3 - \eta^4) \quad (3.10)$$

Where;

$$F(\eta) = 2\eta - 2\eta^3 + \eta^4 = 1 - (1 - \eta)^3(1 + \eta) \quad (3.11)$$

$$G(\eta) = \frac{1}{6}(\eta - 3\eta^2 + 3\eta^3 - \eta^4) = \frac{1}{6}\eta(1 - \eta)^3 \quad (3.12)$$

It is easily recognized that the velocity profiles expressed in terms of  $\eta = \frac{y}{\delta(x)}$ , constitute a one-parameter family of curves, the dimensionless quantity  $\Lambda$  being a shape factor.

The dimensionless quantity  $\Lambda$  which may also be written as,

$$\Lambda = \frac{\delta^2}{\nu} \frac{dU}{dx} = -\frac{dP}{dx} \frac{\delta}{\mu U / \delta}$$

can be interpreted physically as the ratio of pressure forces to viscous forces.

In order to obtain a quantity to which real physical significance can be ascribed, it would be necessary to replace  $\delta$  in the above definition by a linear quantity which itself possesses physical significance, such as the momentum thickness  $\delta_2$ . This will be done later in this section.

Velocity profiles for various values of  $\Lambda$  are shown in figure (3.2). The profile which corresponds to  $\Lambda = 0$ , is obtained when  $\frac{dU}{dx} = 0$ , i.e. for the boundary layer with no pressure gradient (flat plate at zero incidence). The profile at separation with  $(\frac{\partial u}{\partial y})_{y=0} = 0$  (i.e. with  $\alpha = 0$ ), occurs for  $\Lambda = -12$ .

It will be shown later that the profile at the stagnation point corresponds to  $\Lambda = 7.052$ .

For  $\Lambda > 12$ , values of  $\frac{u}{U} > 1$  occur in the boundary layer, but this must be excluded in

steady flow. Since beyond the point of separation the present calculation based, as it is, on the boundary-layer concept, loses significance, the shape factor is seen to be restricted to the range  $-12 \leq \Lambda \leq +12$ .

Before proceeding to calculate the boundary layer thickness  $\delta(x)$  from the momentum theorem, it is now convenient to calculate the momentum thickness  $\delta_2$ , the displacement thickness  $\delta_1$ , and the viscous shearing stress at the wall  $\tau_o$ , in terms of the boundary layer thickness  $\delta(x)$ .

The displacement thickness  $\delta_1$ , and the momentum thickness  $\delta_2$ , of the boundary layer are defined by :

$$\delta_1 U = \int_{y=0}^{\infty} (U - u) dy \quad (3.13)$$

and,

$$\delta_2 U^2 = \int_{y=0}^{\infty} u(U - u) dy \quad (3.14)$$

Using equations (3.13) and (3.14), together with the approximate velocity profile equation (3.10), then the following equations may be obtained,

$$\frac{\delta_1}{\delta} = \int_{\eta=0}^1 [1 - F(\eta) - \Lambda G(\eta)] d\eta \quad (3.15)$$

$$\frac{\delta_2}{\delta} = \int_{\eta=0}^1 [F(\eta) + \Lambda G(\eta)][1 - F(\eta) - \Lambda G(\eta)] d\eta \quad (3.16)$$

Computing the definite integrals with the aid of the values of  $F(\eta)$  and  $G(\eta)$  from equations (3.11) and (3.12), then

$$\frac{\delta_1}{\delta} = \frac{3}{10} - \frac{\Lambda}{120} \quad ; \quad \frac{\delta_2}{\delta} = \frac{1}{63} \left( \frac{37}{5} - \frac{\Lambda}{15} - \frac{\Lambda^2}{144} \right) \quad (3.17)$$

Similarly, the viscous stress at the wall,  $\tau_o = \mu \left( \frac{\partial u}{\partial y} \right)_{y=0}$  is given by ;

$$\frac{\tau_o \delta}{\mu U} = 2 + \frac{\Lambda}{6} \quad (3.18)$$

In order to determine the still-unknown shape factor  $\Lambda(x)$  and, hence, the function  $\delta(x)$  from equation (3.9), it is now necessary to refer to the momentum integral equation (3.5), which may be expressed in the following dimensionless form when multiplied by  $(\frac{\delta_2}{\nu U})$ :

$$\frac{U\delta_2\delta_2'}{\nu} + (2 + \frac{\delta_1}{\delta_2})\frac{U'\delta_2^2}{\nu} = \frac{\tau_o\delta_2}{\mu U} \quad (3.19)$$

in which the boundary-layer thickness  $\delta$  does not appear explicitly. This feature is the corner stone of the momentum integral equation method. It is, therefore, natural to begin with the calculation of  $\delta_2$  from equation (3.19) and then to deduce  $\delta$  from it with the aid of equation (3.17). For this purpose, it is convenient to introduce a second shape factor,

$$K = \frac{\delta_2^2}{\nu} \frac{dU}{dx} \quad (3.20)$$

which is connected with the momentum thickness in the same way as the first shape factor  $\Lambda$  was connected with the boundary-layer thickness  $\delta$  in equation (3.9).

In addition, the following is defined,

$$Z = \frac{\delta_2^2}{\nu} \quad (3.21)$$

so that;

$$K = Z \frac{dU}{dx} \quad (3.22)$$

It is seen from equations (3.9), (3.20), and (3.17) that the shape factors  $\Lambda$  and  $K$  satisfy the universal relation :

$$K = \left( \frac{37}{315} - \frac{1}{945}\Lambda - \frac{1}{9072}\Lambda^2 \right)^2 \Lambda \quad (3.23)$$

Denoting<sup>1</sup> ;

$$H_{12} = \frac{\delta_1}{\delta_2} = \frac{\frac{3}{10} - \frac{1}{120}\Lambda}{\frac{37}{315} - \frac{1}{945}\Lambda - \frac{1}{9072}\Lambda^2} = f_1(K) \quad (3.24)$$

and,

$$\frac{\tau_o \delta_2}{\mu U} = (2 + \frac{1}{6}\Lambda)(\frac{37}{315} - \frac{1}{945}\Lambda - \frac{1}{9072}\Lambda^2) = f_2(K) \quad (3.25)$$

and substituting  $K$ ,  $Z$ ,  $f_1(K)$  and  $f_2(K)$  from equations (3.20), (3.21), (3.24) and (3.25), respectively, into the momentum equation (3.19) together with  $\frac{\delta_2 \delta_2'}{\nu} = \frac{1}{2} \frac{dZ}{dx}$ , then the following relation may be obtained :

$$\frac{1}{2}U \frac{dZ}{dx} + [2 + f_1(K)]K = f_2(K) \quad (3.26)$$

Finally, introducing the additional abbreviation :

$$F(K) = 2f_2(K) - 4K - 2K f_1(K) \quad (3.27)$$

or, written out fully,

$$F(K) = 2(\frac{37}{315} - \frac{1}{945}\Lambda - \frac{1}{9072}\Lambda^2)[2 - \frac{116}{315}\Lambda + (\frac{2}{945} + \frac{1}{120})\Lambda^2 + \frac{2}{9072}\Lambda^3] \quad (3.28)$$

where the relation between  $\Lambda$  and  $K$  was given in equation (3.23). With all these abbreviations and substitutions, the momentum integral equation (3.26) can now be rewritten in the very condensed form :

$$\frac{dZ}{dx} = \frac{F(K)}{U} \quad ; \quad K = ZU' \quad (3.29)$$

This is a non-linear differential equation of the first order for  $Z = \frac{\delta_2^2}{\nu}$  as a function of the current length coordinate  $x$ .

<sup>1</sup>The quantity  $H_{12} = \frac{\delta_1}{\delta_2}$  is also regarded as a shape factor ; it is of particular importance for the turbulent boundary layer. Its value for laminar boundary layers ranges from about 2.3 to 3.5 ; and from about 1.3 to 2.2 in the case of turbulent boundary layers.

Table (3.1): Functions for the approximate calculation of laminar boundary layers.

$\Lambda$	$K$	$F(K)$	$f_1(K) = H_{12} = \delta_1/\delta_2$	$f_2(K) = \tau_o\delta_2/\mu U$
12	0.0948	-0.00948	2.250	0.356
11	0.0941	-0.00912	2.253	0.355
10	0.0919	-0.00800	2.260	0.351
9	0.0882	-0.00608	2.273	0.347
8	0.0831	-0.00335	2.289	0.340
7.8	0.0819	-0.00271	2.293	0.338
7.6	0.0807	-0.00203	2.297	0.337
7.4	0.0794	-0.00132	2.301	0.335
7.2	0.0781	-0.00051	2.305	0.333
7.052	0.0770	0.0	2.308	0.332
7.0	0.0767	0.0021	2.309	0.331
6.8	0.0752	0.0102	2.314	0.330
6.6	0.0737	0.0186	2.318	0.328
6.4	0.0721	0.0274	2.323	0.326
6.2	0.0706	0.0363	2.328	0.324
6.0	0.0689	0.0459	2.333	0.321
5.0	0.0599	0.0979	2.361	0.310
4.0	0.0497	0.1579	2.392	0.297
3.0	0.0385	0.2255	2.427	0.283
2.0	0.0264	0.3004	2.466	0.268
1.0	0.0135	0.3820	2.508	0.252
0.0	0.0	0.4698	2.554	0.235
-1.0	-0.0140	0.5633	2.604	0.217
-2.0	-0.0284	0.6609	2.647	0.199
-3.0	-0.0429	0.7640	2.716	0.179
-4.0	-0.0575	0.8698	2.779	0.160
-5.0	-0.072	0.9780	2.847	0.140
-6.0	-0.0862	1.0877	2.921	0.120
-7.0	-0.0999	1.1981	2.999	0.100
-8.0	-0.1130	1.3080	3.085	0.079
-9.0	-0.1254	1.4167	3.176	0.059
-10.0	-0.1369	1.5229	3.276	0.039
-11.0	-0.1474	1.6257	3.383	0.019
-12.0	-0.1567	1.7241	3.500	0.0

### 3.2.1 Solution of the differential equation for momentum thickness

Concerning the solution of equation (3.29) it is possible to make the following remarks: The calculation should begin at the stagnation point  $x = 0$ , where  $U = 0$  and  $\frac{dU}{dx}$  is finite and different from zero. From equation (3.29), it is seen that the initial slope of the integral curve ( $\frac{dZ}{dx}$ ) would become infinite at the stagnation point were it not for the fact that  $F(K)$  vanishes there simultaneously. Thus the function  $F(K)$  is seen to have a physically meaningful initial value. The zero value of  $F(K)$  occurs for values of  $\Lambda$  for which the second bracketed term on the right-hand side of equation (3.28) vanishes. Thus,

$$F(K) = 0 \text{ for } K = K_o = 0.077 \text{ ; or for } \Lambda = \Lambda_o = 7.052$$

Hence  $\Lambda = 7.052$  is the value of the first shape factor at the stagnation point, as already mentioned.

In this manner the initial slope of the integral curve at the stagnation point is seen to be of the indefinite form  $\frac{0}{0}$  (singular point of equation (3.29)), but its value can be computed by using L'Hospital rule, thus:

$$Z_o = \frac{K_o}{U'_o} = \frac{0.077}{U'_o} \text{ ; } \left(\frac{dZ}{dx}\right)_o = \frac{(dF(K)/dK)_o U''_o}{(1 - dF(K)/dK)_o U'^2_o} \quad (3.30)$$

Where the subscript  $o$  refers to the stagnation point.

With these initial values, equation (3.29) can be graphically integrated. The calculation begins with the values  $\Lambda_o = 7.052$  and  $K_o = 0.077$  at the leading-edge stagnation point, and becomes completed upon reaching the point of separation where  $\Lambda = -12$  and  $K = -0.1567$  (if transition did not occur). The velocity function  $U(x)$ , together with its first derivative  $\frac{dU}{dx}$ , is given by the potential-flow solution. The value of  $\frac{d^2U}{dx^2}$  is only

required at the leading edge for the initial slope of the integral curve.

Computational procedure may be summarized as follows :

1. The potential flow function  $U(x)$ , together with its derivative  $\frac{dU}{dx}$ , are given in terms of the arc length.
2. Graphical integration of equation (3.29) gives both  $Z(x)$  and the second shape factor  $K(x)$  so that the momentum thickness  $\delta_2(x)$  can be calculated from equation (3.20), and the position of the point of separation may be found subsequently.
3. The variation of the first shape factor  $\Lambda(x)$  is obtained from equation (3.23) and table (3.1).
4. The displacement thickness  $\delta_1$  and the shearing stress at the wall  $\tau_0$  are found from equations (3.24) and (3.25) , respectively, together with the values in table (3.1).
5. The boundary-layer thickness  $\delta(x)$  is obtained from equation (3.17).
6. Finally, the velocity distribution is found from equation (3.10).

Integration of equation (3.29) as indicated above requires the use of both the above mentioned equations together with table (3.1) to obtain the solution. Thus this procedure is characterized to be a very tedious and time consuming one. Also, this procedure can not be employed in a computer program. Instead equation (3.29) can be reduced to a simple quadrature by the introduction of a further approximation without any appreciable loss of accuracy.

On the suction surface of most turbine blades, the first  $\sim 30\%$  of the surface length is characterized to have a laminar boundary layer with positive values of the shape factor

$K = \frac{\delta_2^2}{\nu} \frac{dU}{dx}$  (i.e. accelerating flow) up to the transition point. Furthermore, the pressure surface of most turbine blades is characterized to have an accelerating flow (i.e. positive values of  $K$ ) from the leading to the trailing edges.

As seen in figure (3.3), for positive values of  $K$ , the auxiliary function  $F(K)$  can be approximated quite closely by the straight line.

$$F(K) = a - bK$$

with  $a = 0.47$  and  $b = 6$  (intercept and slope of the line). Thus this approximation is justified for most turbine blades.

With this approximation equation (3.29) reduces to,

$$U \frac{dZ}{dx} = a - bK$$

Substituting the original values of  $Z$  and  $K$  in the above equation, then :

$$\frac{d}{dx} \left( \frac{U \delta_2^2}{\nu} \right) = a - (b-1) \frac{U \delta_2^2}{\nu} \frac{1}{U} \frac{dU}{dx}$$

This differential equation for  $\frac{U \delta_2^2}{\nu}$  can be integrated explicitly to yield,

$$\frac{U \delta_2^2}{\nu} = \frac{a}{U^{b-1}} \int_{x=0}^x U^{b-1} dx$$

or, using the numerical values of  $a$  and  $b$  given earlier, then

$$\frac{U \delta_2^2}{\nu} = \frac{0.47}{U^5} \int_{x=0}^x U^5 dx$$

or,

$$\delta_2^2 = \frac{0.47 \nu}{U^6} \int_{x=0}^x U^5 dx \quad (3.31)$$

Thus the solution of equation (3.29) is seen to reduce to a simple quadrature. The only input to the program is the variation of the free stream velocity  $U(x)$ . Velocity derivatives



$(\frac{dU}{dx}$  and  $\frac{d^2U}{dx^2})$  are being calculated using Subroutine VLOCT as shown in Appendix C.

With the momentum thickness  $\delta_2$  being calculated, the computational procedure is carried out as follows :

1. The potential flow function  $U(x)$  is given in terms of the arc length. Velocity derivatives  $(\frac{dU}{dx}$  and  $\frac{d^2U}{dx^2})$  are being calculated using Subroutine VLOCT.
2. Boundary layer momentum thickness  $\delta_2(x)$  is calculated using equation (3.31).
3. The second shape factor  $K(x)$  is found from equation (3.20)
4. The boundary layer thickness  $\delta(x)$  is calculated from equation (3.17), that is;

$$\frac{\delta_2}{\delta} = \frac{1}{63} \left( \frac{37}{5} - \frac{\Lambda}{15} - \frac{\Lambda^2}{144} \right) = \left( \frac{37}{315} - \frac{\Lambda}{945} - \frac{\Lambda^2}{9072} \right)$$

but since at this step the shape factor  $\Lambda$  is still unknown, it is necessary to neglect the terms  $\frac{\Lambda}{945}$  and  $\frac{\Lambda^2}{9072}$  compared to the  $\frac{37}{315}$  term in the above equation. With this assumption, the boundary layer thickness is calculated from,

$$\frac{\delta_2}{\delta} = \frac{37}{315}$$

5. The shape factor  $\Lambda$  is calculated from equation (3.9), that is,

$$\Lambda = \frac{\delta^2}{\nu} \frac{dU}{dx}$$

6. The displacement thickness  $\delta_1$  and the shearing stress at the wall  $\tau_w$  are found from equations (3.17) and (3.18), respectively, that is;

$$\frac{\delta_1}{\delta} = \frac{3}{10} - \frac{\Lambda}{120} \quad ; \quad \frac{\tau_w \delta}{\mu U} = 2 + \frac{\Lambda}{6}$$

7. Finally, the velocity distribution is found from equation (3.10).

The pressure gradient in the external flow has a great influence on the stability of the boundary layer, and hence on transition, in the sense that a favourable pressure gradient stabilizes the flow and an adverse pressure gradient renders it less stable.

It is known from the theory of laminar boundary layers, that generally speaking, the curvature of the wall has little influence on the development of the boundary layer on a cylindrical body of arbitrary shape (eg. turbine blade), this is true as long as the radius of curvature of the wall is much larger than the boundary-layer thickness, which amounts to saying that the effect of the centrifugal force may be neglected when analyzing the formation of a boundary layer on such bodies. Hence, the boundary layer is seen to develop in the same way as on a flat wall, but under the influence of that pressure gradient which is determined by the potential flow past the body (i.e. turbine blade). The same applies to the determination of the limit of stability of the boundary layer with a pressure gradient different from zero.

The approximate method described earlier is convenient for the calculation of laminar velocity profiles and it is, therefore, useful to investigate the stability of the associated velocity profiles.

The shape of the velocity profiles is determined by the dimensionless shape factor :

$$\Lambda = \frac{\delta^2}{\nu} \frac{dU}{dx}$$

The family of velocity profiles was shown in figure (3.2).

At the point of minimum pressure,  $\Lambda = 0$ , and for  $\Lambda > 0$  the pressure decreases, while for  $\Lambda < 0$  the pressure increases. The velocity profiles for  $\Lambda < 0$  each possess a point of inflexion.

Schlichting and Ulrich [24] carried out stability calculations for this family of velocity

profiles. A family of neutral stability curves defined by the shape factor  $\Lambda$  and representing the variation of  $\delta_1$  with the Reynolds number  $\frac{U\delta_1}{\nu}$  is shown in figure (3.4). Both branches of the curves of neutral stability for all velocity profiles with a decreasing pressure ( $\Lambda > 0$ ) tend to zero as  $Re = \frac{U\delta_1}{\nu} \rightarrow \infty$ .

On the other hand the upper branches of curves corresponding to profiles with adverse pressure gradient ( $\Lambda < 0$ ) tend to an asymptote which differs from zero, so that even for  $Re_{\delta_1} \rightarrow \infty$  there exists a finite region of wavelengths at which disturbances are always amplified .

The point on these curves (figure (3.4)) at which the Reynolds number  $Re_{\delta_1}$  has its smallest value is defined as the limit of stability for the laminar flow of interest. This  $Re_{\delta_1}$  is called the critical Reynolds number  $Re_{\delta_1,cr}$ .

It follows that  $Re_{\delta_1,cr}$  can be plotted as a function of  $\Lambda$  (figure (3.5)), and hence, of the surface distance  $x$ . The intercept of this curve with that representing the variation of the local Reynolds number  $\frac{U\delta_1}{\nu}$  with  $x$  will yield the point of instability.

Thus the determination of the position of the point of transition for prescribed blade shapes becomes very easy if use is made of the results contained in figures (3.4-3.5).

As stated earlier, the calculations starts with the evaluation of the laminar boundary layer from the potential velocity distribution  $U(x)$ , which is regarded as known, by the use of the approximate method outlined previously. Such a calculation furnishes values of the shape factor  $\Lambda$  and the displacement thickness  $\delta_1$  in terms of the length of arc  $x$ , measured from the stagnation point.

On proceeding along the laminar boundary layer from the stagnation point in a downstream direction at an assumed constant body Reynolds number  $\frac{U_{\infty}l}{\nu}$  ( $l$ : Blade chord ),

it is noticed that, at the beginning, the limit of stability  $(\frac{U\delta_1}{\nu})_{crit}$  is very high owing to the sharp pressure decrease (i.e. near stagnation point).

On the other hand the boundary layer is thin and consequently the local Reynolds number  $\frac{U\delta_1}{\nu}$  is certain to be smaller than the critical value  $(\frac{U\delta_1}{\nu})_{crit}$  and the boundary layer is stable. Further downstream the rate of pressure decrease becomes smaller and is followed by a pressure increase beyond the point of minimum pressure so that the local limit of stability  $(\frac{U\delta_1}{\nu})_{crit}$  decreases in the downstream direction, whereas the boundary-layer thickness and, with it, the local Reynolds number  $(\frac{U\delta_1}{\nu})$  increases.

As stated previously, at a certain point the two become equal :

$$\frac{U\delta_1}{\nu} = (\frac{U\delta_1}{\nu})_{crit} \quad (\text{Point of instability})$$

and from this point onwards the boundary layer is unstable.

The location of this point, evidently, depends on the blade chord Reynolds number  $(\frac{U_{\infty}l}{\nu})$  because the local boundary-layer thickness is influenced by it.

As a rough guide in approximate calculations it is possible to deduce the rule that the point of transition almost coincides with the point of minimum pressure of the potential flow in the range of Reynolds numbers from  $10^6$  to  $10^7$  [24]. At very large Reynolds numbers the point of transition may lie a very short distance in front of that position (i.e. minimum pressure point) and it may move a small distance behind it at small Reynolds numbers, particularly when the pressure gradient, whether positive or negative, is small. On the other hand, it should be noted that the point of transition always lies in front of the point of laminar separation [24] irrespective of the value of the Reynolds number. Furthermore, since the point of minimum pressure almost coincides with the point of instability [24], then, for typical gas turbine applications, it can be assumed, that the

point of instability coincides with the point of minimum pressure and that the point of transition follows shortly afterwards. The precise distance between the point of transition and the point of instability depends on the rate of amplification of the unstable disturbances and on the intensity of turbulence in the free stream. In turn, the rate of amplification is strongly influenced by the pressure gradient.

Further discussion on transition region models (i.e. transition start, length, and path) is presented in the next chapter.

### 3.3 The laminar region of the boundary layer (Thermal boundary Layer)

#### 3.3.1 Stagnation point heat transfer

Starting with the class of velocity boundary layers on wedges and assuming that the external flow is of the form  $U(x) = u_1 x^m$ , where  $u_1$  is a constant, and the wall-temperature distribution also satisfies a power law, say one of the form,

$$T_w(x) - T_\infty = T_1 x^n$$

where  $T_1$  is a constant and walls of constant temperature are included as the case  $n = 0$ . It is shown in [24], that 2-D wedge flows are described by the following momentum and energy equations.

$$f''' + \frac{m+1}{2} f f'' + m(1 - f'^2) = 0 \quad (3.32)$$

and ;

$$\theta'' + \frac{m+1}{2} Pr f \theta' - n Pr f' \theta = -Pr E x^{2m-n} f''^2 \quad (3.33)$$

where : ( ' ) denotes the derivative with respect to  $\xi$ , and ;

$$\frac{u}{U} = f' = \frac{df}{d\xi}, \quad \xi = y \sqrt{\frac{U(x)}{\nu x}}, \quad \theta = \frac{T - T_\infty}{T_w - T_\infty}$$

and the solution must satisfy the boundary conditions :

$$\xi = 0 , f = f' = 0 , \theta = 1$$

$$\xi = \infty , f' = 1 , \theta = 0$$

Here  $E = \frac{u_1^2}{c_p T_1}$  represents the Eckert number.

When the effect of dissipative heat is neglected in equation (3.33), the following simpler energy equation is obtained :

$$\theta'' + \frac{m+1}{2} Pr f \theta' - n Pr f' \theta = 0 \quad (3.34)$$

whose solutions for different values of the parameters  $m, n, Pr$  have been published by a number of authors [42,43].

Eckert [42] solved equation (3.34) and demonstrated that for  $n = 0$ , the local Nusselt number is given by :

$$\frac{Nu_x}{\sqrt{Re_x}} = F(m, Pr) = \left\{ \int_0^\infty \exp \left[ -Pr \sqrt{\frac{m+1}{2}} \int_0^\xi f(\xi) d\xi \right] d\xi \right\}^{-1} \quad (3.35)$$

Where  $Nu_x = -\sqrt{Re_x} \theta'(0)$ .

In the neighbourhood of the stagnation point, where the velocity distribution is represented by  $U(x) = u_1 x$  with  $m = 1$ , the Nusselt number defined in equation (3.35) can be represented by the following equation :

$$\frac{Nu_x}{\sqrt{Re_x}} = F(Pr, 1) = A(Pr) \quad (3.36)$$

on condition that energy dissipation is neglected .

The constant  $A$  as function of  $Pr$  has been tabulated by Squire [25], as shown in table (3.2).

Table (3.2): The constant  $A$  in the equation for the calculation of the coefficient of heat transfer in the neighbourhood of stagnation point, after Squire [25].

Pr	0.6	0.7	0.8	0.9	1.0	1.1	7.0	10.0	15.0
A	0.466	0.495	0.521	0.546	0.570	0.592	1.18	1.34	1.54

The above table is entered as subroutine PRAN in the Integral method Fortran program.

For the leading edge of the blade, putting  $U(x) = U_\infty \sin(\frac{x}{r})$  so that  $u_1 = \frac{4U_\infty}{D}$ , where  $D$  is the diameter of the blade leading edge, then equation (3.36) becomes :

$$\frac{Nu_x}{\sqrt{Re_x}} = \frac{hx}{k} \sqrt{\frac{D\nu}{4U_\infty x^2}} = \frac{1}{2} \frac{hD}{k} \sqrt{\frac{\nu}{U_\infty D}} = \frac{1}{2} \frac{Nu_D}{\sqrt{Re_D}} = A(Pr) \quad (3.37)$$

Thus,

$$Nu_D = 2A(Pr)\sqrt{Re_D}$$

From the above equation, the heat transfer coefficient at the stagnation point is :

$$h = \frac{2A\sqrt{Re_D}k}{D} = \frac{2A\sqrt{Re_D}C_p\mu}{DPr}$$

### 3.3.2 The laminar thermal boundary layer in front of the stagnation point

For steady, two-dimensional boundary-layer compressible flow of a perfect gas, the energy equation is given by:

$$\rho C_p \left( u \frac{\partial T}{\partial x} + v \frac{\partial T}{\partial y} \right) = k \frac{\partial^2 T}{\partial y^2} + \mu \left( \frac{\partial u}{\partial y} \right)^2 + u \frac{dP}{dx} \quad (3.38)$$

For the following approximate integral method of solution it is necessary to neglect the effects of compressibility and frictional heat in the above energy equation.

In doing this, it is possible to integrate the energy equation from  $y = 0$  to  $y = \infty$ , and so to obtain the heat-flux equation :

$$\frac{d}{dx} \int_0^{\infty} [u(T - T_{\infty})] dy = -\alpha \left( \frac{\partial T}{\partial y} \right)_{y=0} \quad (3.39)$$

where  $\alpha = \frac{k}{\rho C_p}$  is the thermal diffusivity of the fluid.

The above equation is sometimes called the energy-integral equation which is quite analogous to the momentum-integral equation (3.5) for the velocity boundary layer.

From among the numerous procedures used for the solution of the heat flux equation (3.39), the method of Squire [25] is used in this study.

In order to evaluate the integral on the left-hand side of equation (3.39), the variables  $\eta = \frac{y}{\delta}$  for the velocity boundary layer and  $\eta_T = \frac{y}{\delta_T}$  for the thermal boundary layer are introduced, where  $\delta_T$  is the thermal boundary-layer thickness. Furthermore, their ratio is denoted by  $\Delta = \frac{\delta_T}{\delta}$ .

Squire [25] assumed that the velocity and temperature distributions have the following forms :

$$\frac{u}{U(x)} = [2\eta - 2\eta^3 + \eta^4] = F(\eta) \quad (3.40)$$

$$\frac{T - T_{\infty}}{T_w - T_{\infty}} = [1 - 2\eta_T + 2\eta_T^3 - \eta_T^4] = L(\eta_T) \quad (3.41)$$

The velocity distribution used here corresponds to equation (3.11) used before, and the form of the temperature distribution function was so selected by Squire in order to ensure identical velocity and temperature distributions for  $\delta_T = \delta$ , as required by the Reynolds analogy.

On substituting equations (3.40) and (3.41) into equation (3.39), the following equation



is obtained :

$$\frac{d}{dx} \{ \delta_T U H(\Delta) \} = \frac{2\alpha}{\delta_T} \quad (3.42)$$

Where  $H(\Delta)$  is a universal function of  $\Delta = \frac{\delta_T}{\delta}$  which turns out to be given by :

$$H = \int_0^\infty F(\delta) L(\delta_T) d\delta_T \quad (3.43)$$

Performing the indicated integrations, in the above equation, then :

$$\begin{aligned} H(\Delta) &= \frac{2}{15}\Delta - \frac{3}{140}\Delta^3 + \frac{1}{180}\Delta^4 && \text{for } \Delta < 1 \\ H(\Delta) &= \frac{3}{10} - \frac{3}{10}\frac{1}{\Delta} + \frac{2}{15}\frac{1}{\Delta^2} - \frac{3}{140}\frac{1}{\Delta^4} + \frac{1}{180}\frac{1}{\Delta^6} && \text{for } \Delta > 1 \end{aligned} \quad (3.44)$$

The last equation for  $H(\Delta)$  (i.e. equation (3.44) with  $\Delta > 1$ ) is to be used in the present calculations, since it is known that air (or more precisely, combustion gases) has  $Pr$  value around 0.7, thus  $\delta_T > \delta$  and  $\Delta > 1$ .

The integration of equation (3.42) yields :

$$(\delta_T U H)^2 = 4\alpha \int_0^x U H dx \quad (3.45)$$

The velocity boundary-layer thickness  $\delta$  can be evaluated with the aid of equation (3.31) and equation (3.17), thus :

$$\delta^2 = 34 \frac{\nu}{U^3} \int_0^x U^5 dx \quad (3.46)$$

Upon dividing equation (3.45) by equation (3.46), the following equation is obtained :

$$\Delta^2 H(\Delta) = \frac{4}{34} \frac{1}{Pr} \frac{U^4 \int_0^x U H dx}{H \int_0^x U^5 dx} \quad (3.47)$$

Since  $H(\Delta)$  is a known function of  $\Delta$ , and the velocity distribution  $U(x)$  outside the boundary layer is known, the preceding equation can be used to determine  $\Delta(x)$  and hence  $\delta_T(x)$ . The calculation is best performed by successive approximations, starting

with the initial assumption that  $\Delta \equiv \text{constant}$  (i.e. omitting  $H$  from the right-hand side of equation (3.47)), so that ;

$$\Delta^2 H(\Delta) = \frac{4}{34} \frac{1}{Pr} \frac{U^4 \int_0^x U dx}{\int_0^x U^5 dx} \quad (3.48)$$

The obtained values of  $H$  and  $\Delta$  from equation (3.48) and equation (3.44) are substituted back into the right-hand side of equation (3.47) which together with equation (3.44) yield an improved value of  $\Delta$ . In general, two steps in the iteration are found to be sufficient. In this successive approximations solution scheme, Subroutine DTFRMX is used to iteratively solve for the unknown  $\Delta$ .

Using equation (3.41), the local rate of heat transfer flux becomes :

$$\dot{q}''(x) = -k \left( \frac{\partial T}{\partial y} \right)_o = 2(T_w - T_\infty) \frac{k}{\delta_T} \quad (3.49)$$

and hence the local Nusselt number referred to a characteristic length  $l$  is :

$$Nu_x = \frac{\dot{q}''(x) l}{T_w - T_\infty k} = 2 \frac{l}{\delta_T} \quad (3.50)$$

and the heat transfer coefficient is:

$$h(x) = \frac{\dot{q}''(x)}{T_w - T_\infty} = 2 \frac{k}{\delta_T(x)} = 2 \frac{c_p \mu}{Pr \delta_T(x)} \quad (3.51)$$

The steps taken to evaluate the thermal boundary layer, and in particular, to determine the variation of the heat transfer coefficient along the laminar part of the boundary layer found over the blade surfaces of prescribed shape (i.e.  $U(x)$  distribution is known) are thus as follows :

1. Evaluate  $\Delta(x)$  from equations (3.47) and (3.48).
2. Evaluate  $\delta(x)$  from equation (3.46).

3. Steps **1** and **2** give  $\delta_T(x)$ , since  $\delta_T(x) = \Delta(x) \cdot \delta(x)$ .

4. Finally, the heat transfer coefficient  $h(x)$  follows from equation (3.51).

## 3.4 The turbulent region of the boundary layer

### 3.4.1 Introduction

In the present section discussion will be given to the behaviour of a turbulent boundary layer in the presence of a positive or negative pressure gradient along the wall. The existence of a negative and, in particular, of a positive pressure gradient exerts a strong influence on the formation of the boundary layer just as was the case with the laminar part of the boundary layer.

At the present time this very complicated phenomena is far from being understood completely but there are in existence several semi-empirical methods of calculation which lead to comparatively satisfactory results.

All approximate (Integral) methods for the calculation of turbulent boundary layers are based on the integral forms of the momentum and/or energy equations. Since, however, no general expressions for the shear and dissipation in turbulent flow can be deduced by purely theoretical considerations, it is necessary to make additional suitable assumptions, these can only be obtained from the results of systematic measurements and, consequently, the calculation of turbulent boundary layers by approximate methods is semi-empirical.

### 3.4.2 Calculation of the momentum thickness $\delta_2(x)$

In calculating the momentum thickness  $\delta_2$ , Truckenbrodt [26] followed a somewhat different path in that he made use of the energy-integral equation and not the momentum-

integral equation.

As seen from equation (A.12), the energy-integral equation may be written as :

$$\frac{1}{U^3} \frac{d}{dx} (U^3 \delta_3) = 2 \frac{d+t}{\rho U^3} \quad (3.52)$$

where:  $\frac{d+t}{\rho U^3} = \int_0^\infty \frac{\tau}{\rho U^2} \frac{\partial}{\partial y} \left( \frac{u}{U} \right) dy$  (shear-stress work)

and  $\delta_3$  denotes the energy thickness as defined in equation (A.10).

The quantity :

$$\frac{d+t}{\rho U^3} = \int_0^\delta \frac{\tau}{\rho U^2} \frac{\partial}{\partial y} \left( \frac{u}{U} \right) dy \quad (3.53)$$

represents the dimensionless friction work performed in the boundary layer by the shearing stresses  $\tau$ . The quantity  $d$  is the portion of this friction work which is transformed in to heat (dissipation) and  $t$  is the energy of the turbulent motion.

For calculation of the turbulence energy  $t$ , Rotta [28] indicates an approximation formula. With the aid of this formula, Truckenbrodt [26] showed that the turbulence energy  $t$  is negligibly small compared to the dissipation, this fact has already been pointed out by Rotta [28]. Therefore, for further calculations the following is assumed :

$$\frac{t}{\rho U^3} = 0.0 \quad (3.54)$$

Ludwig and Tillmann [27], as well as Rotta [28], dealt in detail with the determination of the wall-shear stress in case of turbulent boundary layers with pressure gradient. Ludwig and Tillmann indicated that for the range of the momentum thickness Reynolds numbers  $1 \times 10^3 < \frac{U \delta_2}{\nu} < 4 \times 10^4$ , wall shear stress is given by the following empirical formula :

$$\frac{\tau_0}{\rho U^2} = 0.123 \times 10^{-0.678 H_{12}} \times \left( \frac{U \delta_2}{\nu} \right)^{-0.268} \quad (3.55)$$

where  $H_{12} = \delta_1 / \delta_2$

Rotta [28] proposed for the wall-shear stress the following experimentally deduced relation

$$\frac{U}{u^*} = \frac{1}{\kappa_1} \ln \left( H_{12} \frac{U \delta_2}{\nu} \right) + B \quad (3.56)$$

where  $u^* = \sqrt{\frac{\tau_w}{\rho}}$  signifies the shear velocity.

Thus :

$$\frac{\tau_w}{\rho U^2} = \left( \frac{u^*}{U} \right)^2 \quad (3.57)$$

is valid. In equation (3.56),  $\frac{1}{\kappa_1} = 2.5$  and  $B = B(I_1)$  is a function of the quantity  $I_1 = \frac{H_{12}-1}{H_{12}} \frac{U}{u^*}$ . The function  $B$  was evaluated and graphically represented by Rotta.

Rotta calculated the wall shear-stress values for various values of  $H_{12}$  and plotted them against the Reynolds number  $\frac{U \delta_2}{\nu}$  in figure (3.6). The agreement between the data of Ludwig-Tillmann and Rotta is quite satisfactory. This implies that the Ludwig-Tillmann empirical formula for the wall shear stress could be used in the turbulent part of the boundary layer.

Rotta [28] also dealt with the calculation of the shear-stress work (i.e. dissipation and turbulence energy). He found out that the dissipation term may be given by :

$$\frac{d}{\rho U^3} = \left( \frac{u^*}{U} \right)^3 \left[ \frac{1}{\kappa_1} \ln \left( H_{12} \frac{U \delta_2}{\nu} \right) + G \right] \quad (3.58)$$

The function appearing here,  $G = G(I_1)$ , has been evaluated by Rotta.

Using equation (3.56), one may write equation (3.58) as :

$$\frac{d}{\rho U^3} = \left( \frac{u^*}{U} \right)^2 \left[ 1 + \frac{u^*}{U} (G - B) \right] \quad (3.59)$$

since  $\frac{u^*}{U} = f \left( \frac{U \delta_2}{\nu}, H_{12} \right)$ ,  $G = G(I_1)$ ,  $B = B(I_1)$  and  $I_1 = \frac{H_{12}-1}{H_{12}} \frac{U}{u^*}$ , the dissipation term may also be represented as a function of the Reynolds number  $\frac{U \delta_2}{\nu}$  and of the shape factor  $H_{12}$ , this is shown in figure (3.7). It is found that the differences in the dissipation values for different values of  $H_{12}$  are only slight.

From figure (3.7), it turns out that the dissipation curves are almost independent of  $H_{12}$  and it may be assumed that the dissipation term may be approximated by :

$$\frac{d}{\rho U^3} = \frac{\beta_t(H_{12})}{\left(\frac{U\delta_2}{\nu}\right)^{\frac{1}{n}}} \quad (3.60)$$

Rotta indicated that the dependence of the value of  $\beta_t$  on  $H_{12}$  is only slight, so that it may be assumed that  $\beta_t$  has the constant value of  $0.56 \times 10^{-2}$  recommended by Rotta.

Thus, the dissipation in the turbulent boundary layer becomes :

$$\frac{d}{\rho U^3} = \frac{0.56 \times 10^{-2}}{\left(\frac{U\delta_2}{\nu}\right)^{\frac{1}{n}}} \quad (3.61)$$

combining the above dissipation equation with equation (3.54) for the turbulent energy (i.e.  $\frac{t}{\rho U^3} = 0.0$ ), then the shear-stress work (i.e. friction work performed in the boundary layer by the shearing stresses  $\tau$ ) becomes :

$$\frac{d+t}{\rho U^3} = \frac{\beta_t(H_{12})}{\left(\frac{U\delta_2}{\nu}\right)^{\frac{1}{n}}} = \frac{0.56 \times 10^{-2}}{\left(\frac{U\delta_2}{\nu}\right)^{\frac{1}{n}}} \quad (3.62)$$

As mentioned earlier, the momentum thickness shall be determined from the energy-integral equation (3.52). Substituting the expression for frictional work from equation (3.62) into the energy-integral equation (3.52), then,

$$\frac{1}{U^3} \frac{d}{dx} (U^3 \delta_3) = 2 \frac{\beta_t(H_{12})}{\left(\frac{U\delta_2}{\nu}\right)^{\frac{1}{n}}} = \frac{1.12 \times 10^{-2}}{\left(\frac{U\delta_2}{\nu}\right)^{\frac{1}{n}}} \quad (3.63)$$

or using the definition of  $H_{32} = \frac{\delta_3}{\delta_2}$ ,

$$\frac{1}{U^3} \frac{d}{dx} (U^3 \delta_2 H_{32}) = \frac{1.12 \times 10^{-2}}{\left(\frac{U\delta_2}{\nu}\right)^{\frac{1}{n}}} \quad (3.64)$$

Truckenbrodt [26] assumed a mean value of the shape factor  $H_{32}$  and integrated equation (3.64) to yield ;

$$\delta_2 \left(\frac{U\delta_2}{\nu}\right)^{\frac{1}{n}} = \frac{C_1 + A \int_{x=\pi_2}^x U^{3+\frac{2}{n}} dx}{U^{3+\frac{2}{n}}} \quad (3.65)$$

where the constant  $C_1$  accounts for the laminar part of the boundary layer that precedes the turbulent boundary layer. Detailed derivation of equation (3.65) is given in Truckenbrodt paper [26].

The constant  $A$  in equation (3.65) can be expressed with the aid of the total coefficient of turbulent skin friction,  $C_f$ , for a flat plate at zero incidence which is known to depend on the Reynolds number  $\frac{U_\infty l}{\nu}$  (where  $l$  is the characteristic length and  $U_\infty$  is the upstream inlet velocity).

The skin-friction drag  $D(x)$  of a flat plate of length  $x$  and width  $b$  on one side satisfies the following relation :

$$D(x) = b \int_0^x \tau_o(x') dx' = b \rho \int_{y=0}^{\delta(x)} u(U_\infty - u) dy \quad (3.66)$$

Introducing the momentum thickness  $\delta_2$  for a flat plate defined by  $\delta_2 U_\infty^2 = \int_0^\delta u(U_\infty - u) dy$ , into equation (3.66), then,

$$D(x) = b \rho U_\infty^2 \delta_2(x) \quad (3.67)$$

From equations (3.66) and (3.67) , the local shear stress can be written as :

$$\frac{1}{b} \frac{dD}{dx} = \tau_o(x) = \rho U_\infty^2 \frac{d\delta_2}{dx} \quad (3.68)$$

Introducing the well known dimensionless coefficients for the local and total skin friction :

$$C'_f = \frac{\tau_o}{\frac{1}{2} \rho U_\infty^2} \quad \text{and} \quad C_f = \frac{D}{\frac{1}{2} \rho U_\infty^2 b l} \quad (3.69)$$

Substituting equations (3.68) and (3.67) into equation (3.69), then

$$C'_f = 2 \frac{d\delta_2}{dx} \quad \text{and} \quad C_f = 2 \frac{\delta_2(l)}{l} \quad (3.70)$$

where  $( ' )$  denotes the local value.

Returning back to the determination of the constant  $A$  in equation (3.65), and assuming

for a while, that the turbulent boundary layer start from the leading edge, then according to equation (3.70), the total skin friction over the entire characteristic length is  $C_f = 2\frac{\delta_2(l)}{l}$ , with  $C_1 = 0$ ,  $x_t = 0$ ,  $x = l$  and  $U = U_\infty$ , thus equation (3.65) yields :

$$\left(\frac{C_f}{2}\right)^{\frac{n+1}{n}} \left(\frac{U_\infty l}{\nu}\right)^{\frac{1}{n}} = A \quad (3.71)$$

Using equation (3.71) the momentum thickness from equation (3.65) becomes :

$$\frac{\delta_2(x)}{l} = \left(\frac{U}{U_\infty}\right)^{-3} \left\{ C_1^* + \left(\frac{C_f}{2}\right)^{\frac{n+1}{n}} \int_{x_t/l}^{x/l} \left(\frac{U}{U_\infty}\right)^{3+\frac{2}{n}} d\left(\frac{x}{l}\right) \right\}^{\frac{n}{n+1}} \quad (3.72)$$

A very good value of the local coefficient of skin friction could have been obtained from the Ludwig-Tillmann empirical formula (i.e. equation (3.55)) but unfortunately Truckenbrodt's method does not solve for the variation of the shape factor  $H_{12}$  along the blade profile. Instead,  $\frac{1}{2}C_f'$  was obtained from,

$$\frac{1}{2}C_f' = \frac{\tau_o}{\rho U_\infty^2} = \frac{\Omega}{\left(\frac{U_\infty \delta_2}{\nu}\right)^{\frac{1}{n}}} \quad (3.73)$$

The resistance equation (3.73) has been derived by Prandtl [26], for the velocity distribution in the turbulent boundary layer on a flat plate given by  $\frac{u}{U} = \left(\frac{y}{\delta}\right)^{\frac{1}{n}}$ .

The shear stress at the blade wall is assumed to be of the same form as that for the flat plate at zero incidence, i.e. equation (3.73), except that instead of the constant external velocity  $U_\infty$ , the variable velocity  $U(x)$  is substituted.

The quantities  $\Omega$  and  $n$  still depend to a certain extent on the Reynolds number. For typical turbulent flows encountered on turbine blades, Truckenbrodt [26] gives the values :  $\Omega = 0.0128$ , and  $n = 4$ , thus equation (3.73) becomes :

$$\frac{1}{2}C_f' = \frac{\tau_o}{\rho U^2} = \frac{0.0128}{\left(\frac{U \delta_2}{\nu}\right)^{\frac{1}{4}}} \quad (3.74)$$



Also, in accordance with the Appendix of [26], Truckenbrodt gives the following formula for the calculation of the constant  $A$  in equation (3.71) :

$$A = \left[ \frac{n+1}{n} \right] \Omega$$

inserting the numerical values of  $\Omega$  and  $n$ , then

$$A = \left[ \frac{4+1}{4} \right] \times 0.0128 = 0.016$$

thus equation (3.71) becomes :

$$\left( \frac{C_f}{2} \right)^{\frac{n+1}{n}} = \frac{0.016}{\left( \frac{U_{\infty} l}{\nu} \right)^{\frac{1}{4}}} \quad (3.75)$$

The value of  $\left( \frac{C_f}{2} \right)^{\frac{n+1}{n}}$  obtained from equation (3.75), is now substituted into equation (3.72).

Thus the momentum thickness  $\delta_2(x)$ , can be found from equation (3.72) by simple quadrature process.

The constant  $C_1^*$  in equation (3.72) takes into account the laminar portion of the boundary layer, and  $x_t$  denotes the position of the point of transition.

$C_1^*$  value is found to be:

$$C_1^* = \left[ \frac{1}{2} C_{f_t} \left( \int_0^{x_t/l} \left( \frac{U}{U_{\infty}} \right)^6 d \left( \frac{x}{l} \right) \right)^{\frac{1}{2}} \right]^{\left( \frac{n+1}{n} \right)} \quad (3.76)$$

Where  $C_{f_t}$  denotes the laminar total coefficient of skin friction for a flat plate at zero incidence at a Reynolds number  $Re_{x=l} = \frac{U_{\infty} l}{\nu}$ . (i.e.  $C_{f_t} = \frac{1.328}{\sqrt{U_{\infty} l}}$ , laminar exact Blasius solution ) and  $n = 4$ .

### 3.4.3 Calculation of the heat transfer coefficient

The occurrence of a fluctuating motion in a turbulent flow causes momentum to be exchanged vigorously between the layers of different velocities. It also causes an increase

in the transfer of heat when temperature gradients are present. For this reason, there exists an intimate connexion between heat and momentum transfer in general. In particular, we must expect the existence of a relation between the heat flux and the shear stress at the wall itself.

The existence of such an analogy between heat and momentum transfer was first discovered by Reynolds (i.e. Reynolds analogy). This analogy enables us to make statements concerning the transfer of heat from the known laws of drag in turbulent boundary layer. The exchange coefficients for momentum and heat ( $\epsilon_M$  and  $\epsilon_H$ ) both have the dimension of viscosity, so that in addition of the molecular Prandtl number  $Pr = \frac{\mu C_p}{k}$ , it is convenient to introduce a corresponding, dimensionless, turbulent Prandtl number :

$$Pr_t = \frac{\epsilon_M}{\epsilon_H} \quad (3.77)$$

As it is known already, the velocity and temperature profiles are identical in the case of laminar flow past a flat plate at zero incidence on condition that frictional heat is neglected and that the Prandtl number is equal to unity. The same can be asserted in relation to turbulent flow, on condition that  $Pr_t = 1$  as well as  $Pr = 1$ . This implies physically that it is assumed that the same mechanism causes the exchange of momentum and heat. Reynolds assumed that the velocity and temperature profiles are identical and therefore the following equation is valid :

$$q(x) = \frac{k}{\mu} \frac{T_w - T_\infty}{T_w} \tau_o(x) \quad (3.78)$$

Furthermore, Reynolds rearranged the preceding equation to the following form :

$$Nu_x = \frac{1}{2} Re_x C_f' \quad (\text{Reynolds, } Pr_t = Pr = 1) \quad (3.79)$$

The principal difficulty in studying turbulent boundary layers and turbulent heat transfer problems stems from the fact that the eddy or exchange coefficients  $\epsilon_M$  and  $\epsilon_H$  are not properties of the fluid, unlike the viscosity  $\mu$  or the thermal conductivity  $k$ , but that they depend on the distance from the wall inside the boundary layer. At a sufficiently large distance from the wall they assume values which are many times greater than the molecular coefficients  $\mu$  and  $k$ , so much so, in fact, that in most cases the latter can be neglected with respect to the former. By contrast, in the immediate neighbourhood of the wall, i.e. in the laminar sub-layer, the eddy coefficients vanish, because in this sub-layer turbulent fluctuations and hence turbulent mixing are no longer possible. Nevertheless, the rate of heat transfer between the stream and the wall depends precisely on the phenomena in the laminar sub-layer and so on the molecular coefficients  $\mu$  and  $k$ .

It is fortunate that equation (3.79) remains valid throughout, regardless of the existence of a laminar sub-layer, because when  $Pr = 1$ , the velocity and temperature distribution in the laminar sub-layer remain identical. By contrast, the Prandtl number in the laminar sub-layer can differ appreciably from unity, as in the present case (i.e. flow of air over turbine blades), when this is the case, equation (3.79) loses its validity.

Extensions of the Reynolds analogy to cases when  $Pr \neq 1$  have been formulated by many authors, among them L. Prandtl [24] and Th. Von Karman [44].

Prandtl assumed that  $Pr_t = 1$  and divided the boundary layer into two zones: the laminar sub-layer in which the eddy coefficients vanish, and the turbulent external boundary layer, in which the molecular coefficients  $\mu$  and  $k$  can be neglected. Under these assumptions he derived the following extension of the Reynolds analogy:

$$Nu_x = \frac{\frac{1}{2} C_f' Re_x Pr}{1 + (u_t/U)(Pr - 1)} \quad (\text{Prandtl, } Pr_t = 1) \quad (3.80)$$

where  $\frac{u_t}{U}$  is the ratio of the mean velocity at the outer edge of the laminar sub-layer to that in the free stream.

Prandtl used for this ratio the following formula:

$$\frac{u_t}{U} = 5\sqrt{\tau/\rho U^2} = 5\sqrt{\frac{1}{2}C_f'} \quad (3.81)$$

Thus equation (3.80) becomes:

$$Nu_x = \frac{\frac{1}{2}C_f' Re_x Pr}{1 + 5\sqrt{\frac{1}{2}C_f'} (Pr - 1)} \quad (Prandtl, Pr_t = 1) \quad (3.82)$$

In deriving the Prandtl equation (3.82), it was supposed that the boundary layer could be sharply divided into a turbulent layer and a laminar sub-layer. In actual fact one region merges into the other in a continuous way and it is possible to notice the existence of an intermediate, or buffer layer in which the magnitudes of the molecular and turbulent exchange are comparable.

Von Karman [44] subdivided the boundary layer into three zones and derived a similar formula for the relation between the coefficient of heat transfer and skin friction. This relation is given by:

$$Nu_x = \frac{\frac{1}{2}C_f' Re_x Pr}{1 + 5\sqrt{\frac{1}{2}C_f'} \left\{ (Pr - 1) + \ln \left[ 1 + \frac{5}{9} (Pr - 1) \right] \right\}} \quad (VonKarman, Pr_t = 1) \quad (3.83)$$

Where  $\frac{1}{2}C_f'$  is obtained from equation (3.74).

The extended analogy relation (i.e. equation (3.83)) between the rate of heat transfer in turbulent flow is of great practical importance because its application to flows past flat plates. It can be used for arbitrary turbulent flows (temperature gradients) and thus enjoy much more general applicability. The relation has been confirmed by numerous measurements [24].

Thus, equation (3.83) shall be used to determine the heat transfer coefficient distribution over the turbulent part of the boundary layer found on the blade surfaces. .

## Chapter 4

# DEVELOPMENT OF A SPECIFIC METHOD FOR GAS TURBINE APPLICATIONS ( TRANSITION REGION MODELING AND TURBULENCE INTENSITY EFFECTS)

### 4.1 Introduction

The overall objective of the present study has been to define and/or develop a suitable analytical technique for predicting local gas-to-blade heat transfer coefficients for nonfilm-cooled airfoils operating in a gas turbine environment.

Although any computational method which does not solve the full Navier-Stokes and energy equations cannot be expected to be universally valid over the entire range of circumstances governed by these equations, there are solutions from reduced sets of these equations that are valid for a subset of problems. In particular the boundary layer equations physically satisfy most of the theoretical assumptions used to formulate the reduced set of equations. It is implied in this work that the flow field immediately adjacent to the solid surface of an airfoil at typical gas turbine geometry conditions can be analytically

modeled using the boundary layer equations.

In the previous chapter, an integral boundary layer method was defined and laid out in detail. This method is capable to solve the laminar and turbulent regions of the boundary layer present over the blade profile. What is lacking in the above method are ways to incorporate the effects of transition start, path, and length and turbulence intensity on the prediction of the heat transfer coefficient.

The previously defined integral method predicts the start of transition near the minimum pressure point (i.e. where the point of instability is defined by  $\frac{U\delta_x}{\nu} = \left\{ \frac{U\delta_x}{\nu} \right\}_{crit}$ ). This transition start model although contains the effect of pressure gradient, it lacks the effects of turbulence intensity on the start of transition. Furthermore, nothing up till now is mentioned about how to model the transition path and length, and how to predict the boundary layer parameters including the heat transfer coefficient in the transition region.

In a latter section of this chapter, several transition region models (start, path and length models) extracted from the literature are introduced which are used in an evaluation task against available airfoil heat transfer experimental data in order to test their capability to model the transition region found over the suction surface of modern gas turbine blades.

The turbulence intensity level has an effect on the transition region start, path, and length as it will be seen latter in this chapter. Other than this effect, the turbulence intensity has a very important effect on the heat transfer level in the laminar region of the boundary layer.

In a general laminar boundary layer analysis (such as the integral method previously defined), it is generally assumed that the external stream (potential flow region) is also

laminar. However, in a typical gas turbine environment, the external stream carries with it a certain degree of turbulence which means that at every point in the stream the velocity fluctuates, changing its magnitude and direction.

Several studies found in the literature [19,20,21] concluded that an increase in the intensity of turbulence of the free-stream must produce two essentially important and different effects. First, an increase in turbulence intensity causes earlier transition region start and hence an increase in the rate of heat transfer which is a characteristic of a turbulent flow as compared with a laminar flow. Secondly, in the presence of a laminar boundary layer, increasing the turbulence intensity in the free-stream has the effect of increasing the heat transfer level.

As seen from Turner's experimental results [19] shown in figure (4.1), the pressure surface, which has a favourable pressure gradient from the leading to the trailing edge (see figure (4.2)) has no observed sudden transition from a purely laminar to a purely turbulent flow, but a systematic increase in pressure surface heat transfer levels is observed as turbulence intensity was increased. Figure (4.1) also shows that the laminar flat plate prediction agrees well with the 0.45% turbulence intensity heat transfer experimental curve. On the other hand, higher turbulence intensity heat transfer experimental curves (i.e. 2.2% and 5.9%) lies between the laminar and fully turbulent flat plate prediction curves. These observations show the necessity to include the effect of turbulence intensity on laminar heat transfer prediction by the previously laid out integral method.

Latter in this chapter the effect of turbulence intensity will be included by modifying the laminar (dynamic) viscosity  $\mu$  to include a turbulence viscosity  $\mu_{TU}$  term which will account for the effect of turbulence intensity on the boundary layer prediction over the



pressure surface.

Turner's suction surface experimental results shown in figure (4.1) indicates that increasing the inlet turbulence intensity from 0.45% to 2.2% produced little or no effect in the local heat transfer level over the first 70% of the surface (i.e. where laminar flow exist), but a further increase in turbulence to 5.9% produced a significant increase in the local heat transfer most probably due to the movement of the point of transition upstream toward the leading edge.

The above observations indicate the need for two different approaches for modeling the suction and pressure surfaces of the blade. Before introducing these two different approaches, a word about the boundary conditions needed to drive the integral method program should be given. This is done in the following section.

## 4.2 Boundary conditions

Any given boundary layer code is only as good as the experiment or the inviscid blade-to-blade code which are used to predict the boundary layer edge velocity conditions. Therefore, any discussion of the development of a suitable airfoil heat transfer prediction scheme should begin with a discussion of the manner in which boundary conditions are specified.

In general, boundary conditions become very important when strong nonequilibrium streamwise pressure gradients are present. This is because streamwise pressure gradient terms appear explicitly in the boundary layer equations and become dominant terms when the flow is strongly accelerated or decelerated.

The specified boundary conditions near the leading edge are usually considered par-

ticularly important aspects of the boundary layer problem because the boundary layer equations themselves have rather strong "upstream memory" properties (boundary layer equations are parabolic in nature, thus upstream boundary conditions inaccuracy affects downstream predictions). Therefore the boundary layer solutions can be made less sensitive to near stagnation point boundary condition errors by starting the boundary layer solutions far enough downstream of the blade leading edge where it is difficult to accurately specify the boundary conditions because of the complex flow that exist there and the small thickness of the boundary layer.

This, of course, cannot be done for airfoil boundary layer computations because the entire airfoil surface makes up the computational domain and, therefore, is of interest. Thus, near stagnation point boundary conditions are critical to airfoil heat transfer problems, because computations are usually started near the leading edge stagnation point, which is of critical importance to the designer.

For the airfoil boundary layer computations performed within this study, boundary conditions were obtained from literature, in which they were generated by both experiment and the two-dimensional inviscid blade-to-blade solutions (potential flow solution) computed using the time dependent Euler equation solver of Delaney [45]. The Delaney method uses a body-centered coordinate system , which allows detailed resolution of the leading edge and/or stagnation region. Accurate resolution of the stagnation region flow field is essential to establish accurate boundary conditions in the leading edge region.

### 4.3 Modeling the boundary layer over the suction and pressure surfaces

Since the suction and pressure surfaces of modern gas turbine blades have fundamental differences in the character of the boundary layer developing on them due to different boundary layer edge velocity distributions, the author of this study has modeled the boundary layer found on these two surfaces by two different approaches, as follows:

#### Suction surface

On this surface of the blade, laminar, transitional, and turbulent flow regions do exist. The laminar and fully turbulent regions are computed as explained in Chapter 3, while the transition region is modeled using the transition start, length, and path models. Through the transition region, the boundary layer parameters (heat transfer coefficient  $h$ , momentum thickness  $\delta_2$ , momentum thickness Reynolds number  $Re_{\delta_2}$ , and boundary layer thickness  $\delta$ ) are calculated using the following equations :

$$h = (1 - \gamma_t)h_{laminar} + \gamma_t h_{turbulent} \quad (4.1)$$

$$\delta_2 = (1 - \gamma_t)\delta_{2,laminar} + \gamma_t \delta_{2,turbulent} \quad (4.2)$$

$$Re_{\delta_2} = (1 - \gamma_t)Re_{\delta_2,laminar} + \gamma_t Re_{\delta_2,turbulent} \quad (4.3)$$

$$\delta = (1 - \gamma_t)\delta_{laminar} + \gamma_t \delta_{turbulent} \quad (4.4)$$

where  $h_{laminar}$ ,  $\delta_{2,laminar}$ ,  $Re_{\delta_2,laminar}$  and  $\delta_{laminar}$  are computed based on laminar flow assumption from the blade leading edge to the trailing edge. Likewise  $h_{turbulent}$ ,  $\delta_{2,turbulent}$ ,  $Re_{\delta_2,turbulent}$  and  $\delta_{turbulent}$  values are computed based on turbulent flow assumption from the blade leading edge to the trailing edge.

The term  $\gamma_t$  appearing in equations (4.1-4.4) is commonly referred to as intermittency function. Its purpose is to "turn-on" or "turn-off" the terms it multiplies in a specified manner. Thus, as it is seen the transition process from laminar to turbulent flow is modeled through  $\gamma_t$ .

The physical meaning of  $\gamma_t$  is that fraction of time a local fluid spot spends in turbulent mode of motion. According to Emmons [46], turbulent spots originate randomly over a restricted area at some location downstream of the instability point, then grow independently as they move downstream, progressively overlapping and eventually covering the whole blade surface. By definition, the transition zone extends from the origin of the turbulent spots to where the blade is fully covered with turbulent flow. It follows that over the transition zone the flow is alternately laminar and turbulent. This alternance behavior is expressed using  $\gamma_t$ , that is :

$$\gamma_t = \begin{cases} 0 & \text{laminar-zone} \\ 0 < \gamma_t < 1 & \text{transition-zone} \\ 1 & \text{turbulent-zone} \end{cases} \quad (4.5)$$

specification of the actual functional form of the intermittency function,  $\gamma_t$ , is the result of transition origin, path, and length modeling . These models will be given latter in this chapter.

### Pressure surface

On this surface of the blade, the flow is characterized to be in transitional state from the leading to the trailing edge. However, modeling this transitional behaviour is different from modeling the transition region on the suction surface. To model this transitional behaviour, the following effective viscosity formulation is included to accommodate explicit

modeling of free-stream turbulence effects which cause this transitional behaviour.

$$\mu_{eff} = \mu + \mu_{TV} \quad (4.6)$$

Thus, the pressure surface transitional behaviour due to free-stream turbulence effects is accounted for by introducing an additional term,  $\mu_{TV}$ , referred to here as the "turbulence viscosity". With this formulation the boundary layer on the pressure surface is treated to be a laminar one but with the calculations being based on an effective viscosity formed by combining the dynamic (laminar) viscosity to the turbulence viscosity as given in equation (4.6).

In closing this section, it should be stated that the effective viscosity equation (4.6) together with equations (4.1-4.4) contains new terms ( $\gamma_t$  and  $\mu_{TV}$ ) which are not modeled previously in the integral method program, implying that no attempt was made to explicitly represent and model the transition region and free-stream turbulence phenomena. These points are not made to disparage the original program but rather to support statements that extensions to the general integral method are necessary for developing a suitable airfoil heat transfer prediction scheme.

In the next sections several of the various models suggested for defining the terms ( $\gamma_t$  and  $\mu_{TV}$ ) are discussed together with their potential for implementation into a gas turbine airfoil heat transfer prediction method.

The types of models extracted from the literature fall within one of the following four categories :

- Transition origin models.
- Transition length models.

- Transition path models (intermittency).
- "Turbulence" viscosity ( $\mu_{TU}$ ) models.

Taken together, models in the first three categories give a complete definition of the transition process on the suction surface and mathematically define the intermittency term,  $\gamma_t$ . Models in the fourth category define the turbulence viscosity term  $\mu_{TU}$ . Before listing the models tested, it is useful to first define some of the nomenclature used in the analytical definitions given for these models. A number of the models are functions of free-stream turbulence. A distinction is made between upstream level of free-stream turbulence intensity,  $TU_\infty$ , local boundary layer outer edge level,  $TU_e$ , and average level,  $\overline{TU}$ . The definitions of these three types of turbulence intensity level follows Dunham [47], who developed a transition origin model using  $\overline{TU}$ .

$TU_\infty$  is defined as the assumed isotropic free-stream turbulence intensity that would correspond to the uniform flow field approaching a cascade of airfoils. This would represent, for example, an experimentally reported upstream value.  $TU_e$  is the local boundary layer edge value and it is defined here ( as suggested by Dunham, [47] ) using the following equation :

$$TU_e = \begin{cases} TU_\infty & \text{for } a_1 > 1 \\ a_1[TU_\infty] & \text{for } 0 \leq a_1 \leq 1 \end{cases} \quad (4.7)$$

where:

$$a_1 = \sqrt{\frac{1}{2a_3} \left( 1 + \frac{a_2}{a_3^3} \right)}$$

$$a_2 = \begin{cases} \frac{\tan^{-1} \sqrt{a_3^{-3} - 1}}{\sqrt{a_3^{-3} - 1}} & \text{when } a_3 < 1 \\ \frac{\ln \left[ a_3^{1.5} \left( 1 + \sqrt{1 - a_3^{-3}} \right) \right]}{\sqrt{1 - a_3^{-3}}} & \text{when } a_3 > 1 \end{cases}$$

$$a_3 = \frac{(\rho u)_e}{(\rho U)_\infty} = \frac{\rho_e U}{\rho_\infty U_\infty}$$

In computations,  $TU_e$ , is constrained, as implied by equation (4.7), to be less than or equal to  $TU_\infty$ . Also, Dunham [47] originally defined  $a_3 = \frac{u_e}{U_\infty} = \frac{U}{U_\infty}$ , (velocity ratio) but in this study the density-velocity ratio is used (to include the effect of compressibility). The average  $\overline{TU}$  is defined as follows :

$$\overline{TU} = \frac{(TU_\infty + TU_e)}{2} \quad (4.8)$$

Models written as functions of either of the three types of turbulence intensities defined above assume that actual values are given in decimal equivalent (i.e. 10% $TU$  is 0.10, not 10.0).

The various Reynolds number definitions given in what follows are all based on the use of local boundary layer edge velocity with the first subscript indicating length scale basis and the second identifying how the Reynolds number is used :

$Re_{\delta_2,tran}$	momentum thickness Reynolds number where transition begins (transition origin criterion).
$Re_{\delta_2,end}$	momentum thickness Reynolds number where transition ends (transition length criterion).
$Re_{x,tran}$	surface distance Reynolds number where transition begins (transition origin criterion).
$Re_{x,end}$	surface distance Reynolds number where transition ends (transition length criterion).
$Re_L$	transition zone length Reynolds number.

For zero-pressure gradient flows, the last three definitions are related by the following equation,

$$Re_{x,end} = Re_{x,tran} + Re_L \quad (4.9)$$

For the airfoil problem, the above equation is approximately valid. Also,  $L$ , as used here, corresponds to the physical length of the transition zone defined as follows :

$$L = (x|_{\gamma_t=0.99} - x|_{\gamma_t=0.0}) \quad (4.10)$$

Or, alternately,  $L$ , is the distance from the transition origin to where transition is 99% complete. The definition of  $\gamma_t$  used in equation (4.10) is represented by equation (4.5). Some of the transition length and path (Intermittency) models found in the literature are based on other definitions of transition zone length. For instance, Dhawan and Narasimha [48] define the transition zone length,  $d$ , as :

$$d = (x|_{\gamma_t=0.75} - x|_{\gamma_t=0.25}) \quad (4.11)$$

which defines the physical transition zone length as the distance between the points where transition is 25% and 75% complete.

Dunham [47] related  $L$  given by equation (4.10) to  $d$  given by equation (4.11) using the following relation,

$$L = 3.36d \quad (4.12)$$

The procedure used in this work was to convert all transition zone length definitions to the equivalent of equation (4.10).

#### 4.4 Suction surface transition region modeling

An important characteristic of a laminar boundary layer, is that under certain conditions the flow is unstable in the presence of small disturbances, and a transition to a fundamentally different kind of flow, a turbulent flow, can occur. The viscous forces, largely responsible for the characteristics of a laminar flow, have the effect of restoring a laminar flow to its previous state when it is subjected to an external disturbance. On the other hand, inertia forces associated with local transient velocity changes have quite the opposite effect. Inertia forces tend to be destabilizing and thus amplify local disturbances. The Reynolds number is a ratio of inertia to viscous forces, and thus one might



well expect that the stability of a laminar flow is in considerable part associated with the value of the Reynolds number, stable laminar flows being associated with low values of the Reynolds number.

In laminar boundary layer, disturbances to the flow will either decay or grow, if the disturbances continue to grow, there will be a region down-stream where transition occurs, beyond which fully turbulent flow will eventually be established. The onset of transition depends to a large extent upon whether the prevailing boundary conditions have a stabilizing or a destabilizing effect on the flow. Smooth blade surfaces and favorable pressure gradients (acceleration) can cause a stabilizing effect, while rough surfaces, adverse pressure gradients, and free-stream turbulence can cause a destabilizing effect on the boundary layer.

To be able to model the transition region found on the suction surface, it is necessary to define three important points :

1. Point where transition begins (i.e. end of laminar region)
2. Point where transition ends (i.e. transition length)
3. Transition path (i.e. intermittency function  $\gamma_t$  distribution in the transition region)

The models used in this study to define the above mentioned points are listed below.

#### 4.4.1 Transition origin (start) models

Five analytical models for the prediction of transition origin were tested against available experimental data, the goal being to select the best model that predicts the start of transition on the suction surface. These five models are analytically summarized below,

along with brief comments when appropriate. A full discussion of each model will not be given here for the purpose of brevity.

1. Schlichting [24]

This model is represented by :

$$\frac{U\delta_1}{\nu} = \left\{ \frac{U\delta_1}{\nu} \right\}_{crit} \quad (4.13)$$

This transition start model was explained in detail in chapter 3. The above equality is valid at the point of instability. Thus when using this model, it is assumed that the point of transition coincides with the point of instability.

The quantity  $\left\{ \frac{U\delta_1}{\nu} \right\}_{crit}$  is a function of the shape factor  $\Lambda$  as seen from figure (3.5). This figure is used to create Subroutine CRITCL which tabulates the values of  $\left\{ \frac{U\delta_1}{\nu} \right\}_{crit}$  as function of  $\Lambda$ . Thus, at each  $x$  station along the blade surface where the shape factor  $\Lambda$  is being calculated, the quantity  $\left\{ \frac{U\delta_1}{\nu} \right\}_{crit}$  is found by calling Subroutine CRITCL. Furthermore, since the Reynolds number  $Re_{\delta_1} = \frac{U\delta_1}{\nu}$  is also being calculated at each  $x$  station, then transition is initiated when the equality (4.13) is satisfied.

2. Van Driest and Blumer [49]

This model is represented by :

$$\sqrt{Re_{x,tran}} = \frac{-1 + \sqrt{1 + 132500 TU_{\infty}^2}}{39.2 TU_{\infty}^2} \quad (4.14)$$

This is a flat plate type model, which specifies transition origin as a function of free-stream turbulence only. Selection of this flat plate model was intended to demonstrate the use of zero-pressure gradient correlations for nonequilibrium applications.

Transition is predicted when the computed value for the Reynolds number from the above model becomes equal to the surface Reynolds number  $Re_x = \frac{U_e}{\nu}$  computed along the blade surface.

### 3. Seyb [30]

This model is represented by :

$$Re_{\delta_1,tran} = \frac{1000}{1.2 + 70 TU_e} + 10 \left[ \frac{K + 0.09}{0.0106 + 3.6 TU_e} \right]^{2.62} \quad (4.15)$$

where  $K$  is the velocity gradient parameter,  $K = \frac{\delta_1^2}{\nu} \frac{dU}{dx}$ , and  $TU_e = \frac{u'_e}{u_e} = \frac{u'_e}{U}$  (i.e. local boundary layer edge free-stream turbulence level found from equation (4.7)). This model is based on the airfoil measurements of Goldstein and Mager [50], Crabtree [51], and Hodge [18] such that, over the investigated range  $-0.1 < K < 0.1$  the transition value of  $Re_{\delta_1}$  is insensitive to increases in  $TU_e$  above 0.04 and to reductions below 0.015.

Thus, this model was tested in this study using the upper and lower limits for  $TU_e$  (i.e. 0.04 and 0.015 respectively) as suggested by Brown and Burton [21], i.e.,

$$TU_e = \begin{cases} 0.015 & \text{if } TU_e < 0.015 \\ TU_e & \text{if } 0.015 \leq TU_e \leq 0.04 \\ 0.04 & \text{if } TU_e > 0.04 \end{cases} \quad (4.16)$$

Seyb's model for transition origin is a function of both free-stream turbulence intensity,  $TU_e$ , and pressure gradient,  $K$ .

### 4. Dunham [47]

This model is represented by :

$$Re_{\delta_2,tran} = \left[ 0.27 + 0.73 \exp(-80 \overline{TU}) \right] \times \left[ 550 + 680 (1 - E)^{-1} \right] \quad (4.17)$$

where :

$$E = \begin{cases} (21 K - 100 \overline{TU}) & \text{if } (21 K - 100 \overline{TU}) \leq 0.75 \\ 0.75 & \text{if } (21 K - 100 \overline{TU}) > 0.75 \end{cases}$$

This model, like Seyb's predicts transition origin as a function of both free-stream turbulence intensity (average value, defined by equation (4.8)) and pressure gradient parameter  $K$ .

#### 5. Abu-Ghannam and Shaw [52]

This model is given by :

$$Re_{\delta_2,tran} = 163 + \exp [E(K) (1 - \overline{TU}/0.0691)] \quad (4.18)$$

where :

$$E(K) = \begin{cases} 6.91 + 12.75 K + 63.64 K^2 & \text{if } K < 0.0 \\ 6.91 + 2.48 K - 12.27 K^2 & \text{if } K > 0.0 \end{cases}$$

The development of this model was based on extensive experimental data taken by the above authors, where both pressure gradient and free-stream turbulence level were varied. In form, equation (4.18) is similar to the transition origin model of Hall and Gibbings [53] but more generalized.

Each of the last three models will predict transition start when the computed value for the Reynolds number  $Re_{\delta_2,tran}$  from equations (4.15), (4.17) or (4.18) equals the surface Reynolds number  $Re_{\delta_2} = \frac{U\delta_2}{\nu}$  computed along the blade surface.

### 4.4.2 Transition length models

Following are descriptions of the two transition zone length or endpoint models tested.

The common feature of these two models is that the transition zone length is defined

in terms of an appropriate transition origin Reynolds number. This implies that the accuracy of these length models depends on the accuracy of the transition origin model used.

1. Dhawan and Narasimha [48]

This model is given by :

$$Re_d = 5 Re_{x,tran}^{0.8} \quad (4.19)$$

Where :

$$d = (x|_{\gamma_i=0.75} - x|_{\gamma_i=0.25})$$

This model defines the actual zone length Reynolds number based on 25% to 75% intermittency. As discussed earlier, for ease of implementation into a computer program and/or systematizing definition, the models were all used in a modified form, where the characteristic length scale,  $L$ , was defined as 0–99% intermittency as in equation (4.10) (also referred to as the total transition length). Therefore, based on the total length and using equation (4.12) (i.e.  $L = 3.36 d$ ), the Dhawan and Narasimha model becomes :

$$Re_L = 16.8 Re_{x,tran}^{0.8}, \quad L \equiv \text{Equation}(4.10) \quad (4.20)$$

and,

$$Re_{x,end} = Re_{x,tran} + Re_L$$

where as defined before,  $Re_{x,end}$  is the surface distance Reynolds number, which defines the end of the transition zone.

## 2. Debruge [54]

This model is given by :

$$Re_d = 0.005 Re_{x,tran}^{1.28} , d \equiv Equation(4.11) \quad (4.21)$$

Again this model was used in the following modified form (using  $L = 3.36 d$ ),

$$Re_L = 0.0168 Re_{x,tran}^{1.28} , L \equiv Equation(4.10) \quad (4.22)$$

and,

$$Re_{x,end} = Re_{x,tran} + Re_L$$

Equations (4.20) and (4.22) are shown in figure (4.3) together with the experimental transition measurements of Brown and Burton [21] and Martin [55]. The Brown and Burton measurements are scattered around the modified Dhawan and Narasimha length model line, while Martin measurements fall somewhat below this line, but well above that of Debruge length model, i.e. equation (4.22).

Figure (4.4) showing  $Re_{x,end}$  as a function of  $Re_{x,tran}$  includes Abu-Ghannam and Shaw [52] experimental results for zero and non-zero pressure gradients as well as the above mentioned data of Brown and Burton [21] and Martin [55]. Equation (4.20) is also plotted and agrees well with the results for both zero and non-zero pressure gradients.

### 4.4.3 Transition path models (Intermittency)

The two models used to define the intermittency function  $\gamma_i$  are listed below. Again, these models were redefined, where necessary, in terms of the total transition zone length,  $L$ , given by equation (4.10).

### 1. Dhawan and Narasimha [48]

Dhawan and Narasimha measured the intermittency factor during transition by photographing the hot-wire signal as it appeared on the screen of an oscilloscope. The intermittency factor was then deduced by dividing the time that the signal showed bursts of turbulence by the total sampling time. The intermittency function relation of Dhawan and Narasimha is :

$$\gamma_t = 1 - \exp \left[ -0.412 \left( \frac{x - x_{tran}}{d} \right)^2 \right] \quad (4.23)$$

Where :

$d \equiv \text{Equation}(4.11)$

$x$  and  $x_{tran}$  correspond to local physical location along the surface and physical location of the transition origin point, respectively.

Redefining equation (4.23) in terms of  $L$  using equation (4.12) yields,

$$\gamma_t = 1 - \exp \left[ -4.65 \left( \frac{x - x_{tran}}{L} \right)^2 \right] \quad (4.24)$$

Where :  $L \equiv \text{Equation}(4.10) \iff (x_{end} - x_{tran})$

or equation (4.24) can be written as :

$$\gamma_t = 1 - \exp \left[ -4.65 \Upsilon^2 \right] \quad (4.25)$$

Where :  $\Upsilon = \left( \frac{x - x_{tran}}{x_{end} - x_{tran}} \right)$

### 2. Abu-Ghannam and Shaw [52]

Abu-Ghannam and Shaw deduced their intermittency function relation from the amplitude density function of the hot-wire signal which was digitally measured using the amplitude probability analysis system, and which is defined as the percentage of time the signal lies within a small window. Signals inside the window

represented laminar flow and those outside the window represented turbulent flow. Abu-Ghannam and Shaw used their experimental results together with numerous other measurements with different pressure gradients and turbulence intensity levels to derive the following relationship for the intermittency function.

$$\gamma_t = 1. - \exp(-4.65 \Upsilon^3) \quad (4.26)$$

Where :  $\Upsilon = \left( \frac{Re_x - Re_{x,tran}}{Re_{x,end} - Re_{x,tran}} \right)$

This model differs from the previous one in that Reynolds numbers are used in place of physical surface distances and the non-dimensional quantity  $\Upsilon$  is raised to a cubic power.

Equation (4.26) together with equation (4.25) are plotted in figure (4.5). From the experimental data shown in this figure it can be concluded that the pressure gradient has no effect on the  $\gamma_t$  distribution.

In concluding this presentation of the intermittency models, it should be noted that, as defined,  $\gamma_t$ , assumes that transition origin and length information are known. Therefore it can be concluded that the above intermittency representations are only as accurate as the models developed for transition origin and length.

## 4.5 Turbulence viscosity ( $\mu_{TU}$ ) models

In this study it became apparent that the pressure surface experimental heat transfer data would be very difficult to be predicted assuming fully laminar, fully turbulent, or a laminar-transition-turbulent flow character. In fact, the pressure surface experimental heat transfer data lies in between the fully laminar and the fully turbulent flow predictions (measurements are greater than laminar predictions and lower than turbulent ones).



These observations forced the modeling effort toward development of a model that would give better pressure surface predictions. As a first step, the concept of a natural transition (like that on the suction surface) occurring on the pressure surface was eliminated. It was argued that if transition models of the type given in the previous section for the suction surface are considered reasonable for predicting natural transition on the pressure surface, then the pressure surface was not undergoing natural transition because no transition model tested produced satisfactory pressure surface predictions.

As mentioned earlier in this chapter, the flow over the entire pressure surface is modeled to be laminar but with the calculations being based on the effective viscosity formulation given by equation (4.6). Thus, dropping the concept of natural transition on the pressure surface simplifies modeling this surface but forces the turbulence viscosity ( $\mu_{TV}$ ) term in equation (4.6) to model all the turbulent phenomena.

Two turbulence viscosity models extracted from the literature are given below as part of the effective viscosity definition given by equation (4.6). These turbulence viscosity models are used to account for the effects of free-stream turbulence on augmenting the laminar heat transfer values over the pressure surface.

The idea behind  $\mu_{TV}$  formulation is that the characteristic velocity that should be used to define the velocity scale depends on free-stream turbulence intensity. To further explain the concept of  $\mu_{TV}$ , reference is made to Spalding [56] for modeling both the turbulent viscosity ( $\mu_t$ ) and the turbulence viscosity ( $\mu_{TV}$ ), as follows :

$$\mu_{TV}, \mu_t = \rho \cdot (\text{Length Scale}) \cdot (\text{Velocity Scale}) \quad (4.27)$$

Spalding suggested that the difference between turbulent ( $\mu_t$ ) and turbulence ( $\mu_{TV}$ ) viscosities is in the assumed velocity scale. Furthermore, Spalding suggested that the proper

velocity scale to be used to define  $(\mu_t)$  is given by:

$$\text{Velocity Scale} = (\text{Length Scale}) \cdot \left| \frac{\partial u}{\partial y} \right| \quad (4.28)$$

and that for  $(\mu_{TV})$  is given by:

$$\text{Velocity Scale} = (\text{Free Stream Turbulence Intensity}) \cdot U \quad (4.29)$$

Thus,  $(\mu_t)$  and  $(\mu_{TV})$  definitions become,

$$\mu_t = \rho \cdot (\text{Length Scale})^2 \cdot \left| \frac{\partial u}{\partial y} \right| \quad (4.30)$$

$$\mu_{TV} = \rho \cdot (\text{Length Scale}) \cdot (\text{Free Stream Turbulence Intensity}) \cdot (U) \quad (4.31)$$

On the basis of equation (4.31) several workers have developed empirically deduced turbulence viscosity models. Two of these models are given below.

1. Smith and Kuethe [57]

This model is represented by:

$$\mu_{TV} = 0.0164 \rho \delta TU_{\infty} U_{\infty} \quad (4.32)$$

In this model, the boundary layer thickness  $\delta$ , is the length scale, and  $TU_{\infty} U_{\infty}$  is the velocity scale. This model was actually developed for predicting the effects of free-stream turbulence on stagnation region heat transfer to cylinders in cross flow and was included in this study to test its validity in airfoil surface boundary layer computations.

2. Hylton et.al [58]

This model is represented by:

$$\mu_{TV} = (T_1 + T_2) \rho \ell TU_e U_{\infty} \quad (4.33)$$

Where :

$$l \equiv \lambda \delta$$

$$\lambda \equiv 0.085$$

$$TU_e \equiv \text{Equation (4.7)}$$

$$T_1 = 0.167$$

$$T_2 = \left( \frac{Re_1 Re_{\delta_2}}{Re_2 44} \right)^3$$

$$\frac{Re_1}{Re_2} = \frac{(\rho_\infty U_\infty / \mu_\infty)_{inlet}}{(\rho_\infty U_\infty / \mu_\infty)_{exit}}$$

$$Re_{\delta_2} = \frac{U \delta_2}{\nu_e}$$

In the above model, use of the local value of free-stream turbulence intensity,  $TU_e$ , in defining velocity scale partially accounts for the effects of curvature implicitly. Note that  $T_2$  is function of the inlet-to-exit unit Reynolds number ( unity length scale) ratio ( $Re_1/Re_2$ ). Here inlet and exit refer to nominally uniform upstream and downstream flow conditions for the blade row.

The function of the term ( $T_1 + T_2$ ) is to model the complete surface distance from the stagnation point to the trailing edge.  $T_1$  term models the leading edge stagnation region while  $T_2$  models the rest of the blade surface. The definition of  $T_2$  as indicated above represents a somewhat tuned function and demonstrates that the momentum thickness  $\delta_2$  is actually used as a length scale in defining a local momentum thickness Reynolds number. Thus, when the local boundary layer edge velocity  $U$  is small (i.e. near the leading edge in the stagnation region),  $T_2$  is relatively small. Therefore, in the region near the stagnation point where  $U$  (and likewise  $Re_{\delta_2}$ ) is small and  $TU_e = TU_\infty$ , equation (4.33) reduces to a similar model

like that of equation (4.32), i.e. cylinders in cross flow model. This reduction in the influence of  $T_2$  in the leading edge region is further accelerated because, as defined,  $T_2 \propto (Re_{\delta_2}/44)^3$ .

Further downstream, the momentum thickness increases inducing higher values of  $T_2$  which will counterpart the reduction in  $TU_e$ . Therefore,  $T_1$  and  $T_2$  may be viewed relatively as low and high Reynolds number functions.

Hylton et.al [58] derived this model using extensive airfoil experimental data ( in particular laminar pressure surface data) and as it will be seen latter, this model is expected to yield the best results.

## 4.6 Evaluation of transition region and turbulence viscosity models

The several models discussed in the previous sections for defining transition origin, length, and path (intermittency) and turbulence viscosity were added as modifications to the integral method computer program, and an evaluation task was initiated. The evaluation activity involved definition of combinations of models, generation of solution, and comparisons with experimental data. The procedure used to evaluate the literature models given in the previous sections is briefly discussed below.

The computational scheme used to evaluate the models is given below in the order in which solutions were computed and were compared with a given set of experimental data for determining the "best" combinations.

## Suction surface

- Step No. 0 Choose experimental data (i.e. heat transfer coefficient distribution along the blade) taken at known operating condition (i.e. blade row inlet operating conditions and boundary layer edge velocity conditions distributions).
- Step No. 1 For a base-line, compute laminar and turbulent solutions using the integral method outlined in chapter 3 without any of the present chapter models. Compare with experimental data.
- Step No. 2 Determine "best" transition origin model. That is, compute solutions using different origin model each time with no length or path (intermittency) models. Compare with experimental data. Choose "best" model.
- Step No. 3 Determine "best" transition length model. That is, compute solutions using a different length model each time but with a common "best" (step no. 2) origin model and common path (intermittency) model. Compare with experimental data. Choose "best" model.
- Step No. 4 Determine "best" transition path (intermittency,  $\gamma_t$ ) model. That is, compute solutions using a different path model each time but with the same "best" (step no. 2) origin model and "best" (step no. 3) length model. Compare with experimental data. Choose "best" model.
- Step No. 5 If available choose a different set of experimental data (i.e. heat transfer coefficient distribution along the blade) taken at another known operating condition (i.e. blade row inlet operating conditions and boundary layer edge velocity conditions distributions). Compute one solution using "best" combination of models from step 4. Compare with experimental data.
- Step No. 6 Repeat step 5 until comparison for some experimental data set is unacceptable (in this case, use this data set and return to step 1) or all experimental data sets have been predicted. In this case, step no. 4 models are the best for all experimental data included and evaluation terminates.

The order in which the transition models is determined in steps 2, 3, and 4 is important because the models evaluated in the higher number steps are functions of results obtained from models in previous steps. For example, path (intermittency,  $\gamma_t$ ) models

are functions of transition origin and length variables previously determined.

### Pressure surface

- Step No. 0 Choose experimental data (i.e. heat transfer coefficient distribution along the blade) taken at known operating condition (i.e. blade row inlet operating conditions and boundary layer edge velocity conditions distributions).
- Step No. 1 For a base-line, compute laminar and turbulent solutions using the integral method outlined in chapter 3 without any of the present chapter models. Compare with experimental data.
- Step No. 2 Determine "best" turbulence viscosity ( $\mu_{TV}$ ) model. That is, compute solutions using different  $\mu_{TV}$  models each time but with no transition (i.e. the flow is artificially considered to remain laminar all over the blade with no transition and turbulent modeling. Therefore, this step is a direct test of the ability of the  $\mu_{TV}$  models to model all the turbulent phenomena). Compare with experimental data. Choose "best" model.

## Chapter 5

# DISCUSSION OF RESULTS

### 5.1 Experimental data base

In order to assess the predictive capability of the present integral method and models, all the following items should be available :

1. Boundary layer edge velocity (pressure) distribution along the blade surfaces.
2. Blade geometry.
3. Blade row inlet and outlet conditions.
4. Corresponding (to the above conditions) experimental heat transfer coefficient distribution along blade suction and pressure surfaces.

The results of an experimental study of aerodynamic (surface velocity) and heat transfer distributions over the surfaces of a turbine nozzle guide vane were kindly supplied by Dr. D. A. Nealy, Chief of the heat transfer section, Detroit Diesel Allison, General Motors Corporation [22].

Figure (5.1) shows the blade surface velocity distribution computed by Nealy [22] using the two-dimensional inviscid blade-to-blade time dependent Euler equation solver of Delaney [45]. This inviscid code uses the experimental static pressure distribution shown

in figure (5.2) to yield the velocity distribution.

The geometric information of the blade tested in this study is as follows :

$$\text{Leading Edge Diameter} = 2.336\text{cm} = 0.92\text{in} = 0.0767\text{ft}$$

$$\text{Trailing Edge Diameter} = 0.346\text{cm} = 0.136\text{in} = 0.01133\text{ft}$$

$$\text{Blade Height} = 7.62\text{cm} = 3\text{in}$$

$$\text{Suction Surface Arc Length} = 17.782\text{cm} = 7.001\text{in} = 0.5834\text{ft}$$

$$\text{Pressure Surface Arc Length} = 13.723\text{cm} = 5.403\text{in} = 0.4503\text{ft}$$

$$\text{True Chord} = 14.493\text{cm} = 5.706\text{in} = 0.4755\text{ft}$$

$$\text{Axial Chord} = 7.816\text{cm} = 3.077\text{in} = 0.2564\text{ft}$$

The three vane cascade inlet and outlet conditions are as follows :

$$\text{Cascade inlet total pressure} \equiv P_o = 35.58\text{psia}$$

$$\text{Cascade inlet total temperature} \equiv T_o = 795^\circ\text{K} = 1431^\circ\text{R}$$

$$\text{Cascade or vane row inlet Mach number} \equiv M_1 = 0.17$$

$$\text{Upstream or vane row inlet Reynolds number} \equiv Re_1 = 0.39 \times 10^6$$

$$\text{Downstream or vane row exit Mach number} \equiv M_2 = 0.92$$

$$\text{Downstream or vane row exit Reynolds number} \equiv Re_2 = 1.51 \times 10^6$$

$$\text{Vane row inlet free-stream turbulence intensity} \equiv TU_\infty = 6.55\%$$

$$\text{Average wall-to-gas temperature ratio} \equiv T_w/T_g = 0.81$$



## 5.2 Aerodynamic and temperature results

The blade velocity distribution shown in figure (5.1) indicates the fundamental aerodynamic difference between the suction and pressure surfaces. The first 25% of the suction surface length is characterized to have a strong favorable pressure gradient (accelerating flow) followed by an adverse pressure gradient region and finally a moderate favorable pressure gradient region. On the other hand, the pressure surface is characterized to have a favorable pressure gradient from the leading to the trailing edges. Later, it will be shown that these pressure gradient types will strongly affect the shape, level and distribution of the heat transfer coefficient as well as the boundary layer momentum thickness. Furthermore, the boundary layer on the suction surface is expected to undergo transition near the minimum pressure point ( maximum velocity) where the pressure gradient changes from favorable to adverse. On the other hand, the boundary layer on the pressure surface is expected to remain laminar all over the surface length.

Figure (5.2) shows the experimental static pressure distribution along the blade surfaces together with the predicted distribution by channel flow theory (i.e. equations (3.1-3.2)). Perfect prediction is obtained on the pressure surface, while on the suction surface, deviation between prediction and experiment starts near the point of minimum pressure (expected transition point), but still the trend of the theoretical curve is exactly the same as the experimental one and the accuracy of the predicted values of static pressure are acceptable. The importance of these predictions of static pressure is that they are used together with the boundary layer edge temperature predictions shown in figure (5.3) to call subroutine PROPER and thus obtain the properties of air ( $C_p$ ,  $\mu$ ,  $Pr$  and  $\rho$ ) at each x station along the blade surfaces.

Figure (5.3) shows the experimental blade wall temperature distribution together with the predicted distribution of both the boundary layer edge temperature and the adiabatic wall temperature. On the suction surface, the gas temperature (i.e. boundary layer edge temperature) starts to decrease from the leading edge up to the point of minimum pressure. This behavior is expected since in this region very high acceleration exist and thus thermal energy is being converted to kinetic energy. Further downstream and beyond the minimum pressure point, the gas temperature starts to increase due to the deceleration effect of the flow. This increase is then followed by a decrease in the gas temperature but at a slower rate than that found in the leading edge region. On the other hand the gas temperature distribution along the pressure surface was found to remain almost constant along the first 50% of the surface and then to experience a slow decrease due to the moderate acceleration over the entire surface distance.

The suction and pressure surfaces experimental blade wall temperature is seen to remain almost constant although it starts to increase near the blade trailing edge. The reason for this increase is due to the presence of small size cooling tubes which run inside the blade body along its height. Finally, and as it is known, the driving force for heat transfer at each  $x$  station along the blade is the difference between the gas and blade wall temperatures.

Also shown in figure (5.3) is the adiabatic wall temperature distribution. For an adiabatic wall, the temperature distribution across the boundary layer is given by [24]:

$$T(y) = T_e + \frac{1}{2C_p}(U^2 - u^2) \quad (5.1)$$

Where  $T_e$  denotes the temperature at the outer edge of the boundary layer. Consequently the adiabatic wall temperature  $T = T_{ad}$  for  $u = 0$  is given by:

$$T_{ad} = T_e + \frac{U^2}{2C_p} \quad (5.2)$$

Thus, the quantity,  $T_{ad} - T_e = \frac{U^2}{2C_p}$ , represents the temperature increase of an adiabatic wall which is due to frictional heat. The distribution of the quantity  $(T_{ad} - T_e)$  is shown in figure (5.3).

This adiabatic wall temperature results from two situations:

1. The increase in temperature of the fluid as it is brought to rest at the surface while the kinetic energy of the flow is converted to thermal energy.
2. The heating effect due to viscous dissipation.

### 5.3 Turbulence intensity results

Figure (5.4) shows the variation of the local boundary layer outer edge free stream turbulence intensity,  $TU_e$ , calculated from equation (4.7). Also shown in this figure are the constant blade row inlet turbulence intensity,  $TU_\infty$ , and the average value  $\overline{TU}$ . The difference between the suction and pressure surfaces distribution of,  $TU_e$ , is quite evident. On the suction surface and as a consequence of the rapid acceleration near the stagnation point,  $TU_e$  is decreased to about 40% of its inlet value in a very short surface length and remains constant thereafter. This distribution is quite typical for suction surfaces and points to the importance of using local values of turbulence intensity (i.e.  $TU_e$ ), especially for transition calculations, rather than a characteristic reference value (i.e.  $TU_\infty$ ). On the other hand,  $TU_e$  remains constant (and equal to  $TU_\infty$ ) over the first 35% of the

pressure surface length and then decreases gradually to a value equal to 40% of its inlet value at the end of the surface. Thus, it could be concluded that the pressure surface has higher values of turbulence intensity than the suction surface.

## 5.4 Transition start models results

This section tends to illustrate how each transition start model predicted transition.

Figure (5.5) shows the distribution of the surface Reynolds number ( $Re_x$ ) along the blade surfaces. Also shown in this figure is the distribution of the Van Driest and Blumer model for ( $Re_{x,tran}$ ) computed from equation (4.14). This model indicated very early transition on both surfaces due to its dependence on the inlet free stream turbulence intensity,  $TU_\infty$ , rather than  $TU_e$ . The value of ( $Re_{x,tran}$ ) computed from this model is (18481.7).

Figure (5.6) shows the distribution of the momentum thickness Reynolds number ( $Re_{\delta_2}$ ) based on laminar flow assumption. Also shown in this figure is the distribution of the Seyb, Dunham, and Abu-Ghannam and shaw models for ( $Re_{\delta_2,tran}$ ) computed from equations (4.15), (4.17) and (4.18) respectively. Each model indicates transition when its  $Re_{\delta_2,tran}$  curve intersects the  $Re_{\delta_2}$  curve. Thus, it is noticed that Seyb model indicated transition only at the suction surface, while Dunham, and Abu-Ghannam and shaw models predicted transition on both the suction and pressure surfaces. Furthermore, Dunham, and Abu-Ghannam and shaw models indicated late transition on the pressure surface.

Figure (5.7) shows the computed distribution of the shape factor parameter  $K = \frac{\delta_2^2}{\nu} \frac{dU}{dx}$  along the blade surfaces. In this figure,  $K$  values based on laminar flow assumption is shown for both the suction and pressure surfaces. Furthermore,  $K$  values based on

laminar flow assumption but with computations being based on the effective viscosity formulation (i.e.  $\mu_{eff} = \mu + \mu_{TV}$ ) is also shown for the pressure surface. It is interesting to note that, for the pressure surface, the same values of  $K$  is obtained whether the flow is being treated as laminar or as laminar but with  $\mu$  replaced by  $\mu_{eff} = \mu + \mu_{TV}$ . This fact is due to the unchange in the magnitude of the quantity  $(\delta_2^2/\nu)$  whether computations is being based on  $\mu$  or  $(\mu_{eff} = \mu + \mu_{TV})$ . The tormented shape of the  $K$  parameter distribution is attributed to the dependence of  $K$  on  $\frac{dU}{dx}$  which undergoes abrupt changes along the blade surfaces and especially on the suction one. Furthermore, the values of the  $K$  factor shown in figure (5.7) are used in the transition start models (equations (4.15), (4.17) and (4.18)) to compute the  $Re_{\delta_2,trans}$  distribution shown in figure (5.6).

Figure (5.8) shows the distribution of the shape factor  $K$  based on laminar, turbulent and transition at a point flow assumptions. The suction surface transition at a point solution is based on Schlichting transition start model, equation (4.13), which is considered to be the best model tested in this study as it will be shown later.

Figure (5.9) shows the calculated distribution of the boundary layer displacement thickness,  $\delta_1$ . These calculated values of  $\delta_1$  are used to calculate the distribution of the displacement thickness Reynolds number,  $Re_{\delta_1}$ , shown in figure (5.10). The importance of figure (5.10) is that it furnishes the left hand side of Schlichting transition start model given by equation (4.13).

Figure (5.11) shows the calculated variation of the first shape factor  $\Lambda = \frac{\delta_1^2}{\nu} \frac{dU}{dx}$ . These calculated values of  $\Lambda$  are then used to call subroutine CRITCL to obtain the corresponding distribution of the critical displacement thickness Reynolds number  $\left\{ \frac{U\delta_1}{\nu} \right\}_{crit}$  shown plotted in figure (5.12). Thus, the right hand side of Schlichting transition start model is

now calculated. As it may be seen from figures (5.10) and (5.12), for the suction surface and for small  $x/arc$  values,  $Re_{\delta_1}$  is small and  $Re_{\delta_1,crit} = \left\{ \frac{U\delta_1}{\nu} \right\}_{crit}$  is large. As  $x/arc$  becomes larger, this relationship is inverted and consequently  $Re_{\delta_1,crit}$  decreases while  $Re_{\delta_1}$  increases. Eventually, these two quantities ( $Re_{\delta_1}$  and  $Re_{\delta_1,crit}$ ) become equal and yield the transition point on the suction surface as computed from Schlichting model. On the other hand, the  $Re_{\delta_1,crit}$  values over the pressure surface is always greater than the  $Re_{\delta_1}$  values, and thus no transition is predicted on the pressure surface using Schlichting model.

## 5.5 Heat transfer coefficients predictions

The heat transfer prediction results obtained through the evaluation procedure outlined in section (4.6) are shown in figures (5.13) through (5.17).

Figure (5.13) shows the experimentally determined heat transfer coefficient distribution for the set of operating conditions outlined in section (5.1) together with suction and pressure surfaces evaluation process step No. 1, outlined in section (4.6). As seen from this figure, the pressure surface experimental data lies in between the fully laminar and fully turbulent predictions. Furthermore, the laminar prediction, although underpredict the experimental data, has the same trend.

Figure (5.13) also includes the pressure surface evaluation process step No.2 (i.e. modified solution results using turbulence viscosity models). Both turbulence viscosity models gave excellent representation of the experimental data. The model of Hylton et al. is selected as the best one since it gave better results in the last 50% of the surface length where the results of the model of Smith and Kuethe starts to deviate from experiment.

On the suction surface, figure (5.13), shows that the laminar solution agrees well with experimental data up to the experimentally determined transition point. The change in the curvature of the laminar solution (from concave up to concave down) is due to the high flow acceleration in this portion of the surface length.

The determination of the best transition origin model (suction surface step No. 2) is shown in figures (5.14) and (5.15). Note that the laminar solution is repeated for comparison purposes. For these solutions, no length or path models are used (transition region is treated as a point). As seen from figure (5.14), both Dunham and Abu-Ghannam and shaw models predicted transition on the suction surface with good accuracy, however, these two models are not selected as best since they have predicted transition on the pressure surface.

Figure (5.15) shows that the model of Van Driest and Blumer predicted early transition on both the suction and pressure surfaces, thus its solution curve looks like the fully turbulent flow assumption one shown earlier in figure (5.13). Also shown in figure (5.15) are the results of Schlichting and Seyb models. These two models are considered to be the best since they have predicted transition only on the suction surface and with very good accuracy. Furthermore, and as seen from figure (5.15), Schlichting model is selected to be more accurate than Seyb's and thus it is considered to be the fixed transition start model for the solutions shown in figures (5.16) and (5.17).

The determination of best transition length model (suction surface step No. 3) is illustrated in figure (5.16). For these solutions, the fixed transition origin model was that of Schlichting (as determined above), and the fixed (but not yet determined to be best) path ( $\gamma_t$ ) model was that of Abu-Ghannam and Shaw. The length model of Dhawan and

Narasimha was selected to be the best, since Debruge model underestimated the length of transition (transition was predicted to end more rapidly than the measurements indicated). Also, in this figure, the solution based on transition at a point assumption using Schlichting transition origin model is repeated for comparison purposes (i.e. whether transition is at a point or a region).

The determination of best path ( $\gamma_t$ ) model (i.e. suction surface step No. 4) is shown in figure (5.17). In these solutions, fixed transition origin model was that of Schlichting. Furthermore, although the Dhawan and Narasimha length model was selected to be better than that due to Debruge, solutions based on Debruge length model is also shown in this figure. Thus, four combinations of solutions are presented (i.e. combinations using two length and two path models). From this figure, it was concluded that the Dhawan and Narasimha path model when combined with Dhawan and Narasimha length model (solid curve) gave better predictions than that obtained using Abu-Ghannam and shaw path model combined with Dhawan and Narasimha length model. Thus, the Dhawan and Narasimha path model is selected to be the best.

Figure (5.18) shows the distribution of the intermittency factor ( $\gamma_t$ ) from the point where Schlichting transition origin model indicated transition. These distributions are used in equation (4.1) to yield the solutions shown in figure (5.17).

## 5.6 Momentum thickness results

The predicted momentum thickness results corresponding to the operating conditions outlined in section (5.1) and which is obtained through the evaluation procedure outlined in section (4.6) are shown in figures (5.19) through (5.22). Before going through these



figures, it should be noted that the procedure is now a computational one rather than being an evaluation one, since no experimental data are available for the momentum thickness parameter (i.e. the experimental data base supplied by Dr. Nealy [22] does not include momentum thickness experimental data). Thus, discussion is only given to the theoretical prediction curves with brief comments on the expected experimental trends.

Figure (5.19) shows the pressure surface computational process step No.1 and 2. For this surface, it is expected that the experimental data trend will lie in between the fully laminar and fully turbulent flow prediction results. With this assumption, the turbulence viscosity models solutions will overestimate the expected experimental trend for the first 40% of the surface length while giving good predictions for the rest of the surface length. Furthermore, from the suction and pressure surfaces fully laminar and fully turbulent flow predictions given in figures (5.19) and (5.20) the following observations are noted:

1. The suction and pressure surfaces have quite different shapes of the momentum thickness distribution. This fact is due to the different surface curvature between the suction and pressure surfaces. The convex curvature of the suction surface enhance the growth of the boundary layer momentum thickness while the concave curvature of the pressure surface retards the growth of the boundary layer after a short enhancement in the leading edge region. Of course, these surface curvature effects are translated or sensed by the computer program using the input velocity boundary conditions distribution shown in figure (5.1). Thus, as mentioned earlier, in section (5.2), the velocity boundary conditions (or the pressure gradient distribution) have indeed the strongest effect on the shape and the level (as seen below) of the momentum thickness distribution.

2. The suction and pressure surfaces have quite different levels of the momentum thickness distribution. The boundary layer over the suction surface is being characterized to be thick while that over the pressure surface is characterized to be thin. This fact is illustrated in figure (5.19) where the suction surface laminar solution of the momentum thickness has the same order of magnitude as the turbulent solution of the momentum thickness for the pressure surface. This observation is also clear by comparing the laminar and/or turbulent momentum thickness solutions of the suction and pressure surfaces found in figure (5.20).

Figures (5.20) and (5.21) shows the suction surface computational process step No. 1 and 2 (i.e. step No. 1: fully laminar and fully turbulent solutions, step No. 2: transition at a point solutions). The fully laminar and fully turbulent flow predictions for the pressure surface are repeated for comparison purposes with suction surface results. Again for these solutions, like heat transfer results, no length or path models are used (i.e. transition region is treated as a point). Once again, and referring to figure (5.20), the transition origin models of Dunham, and Abu-Ghannam and Shaw are not selected because they have predicted transition on the pressure surface. Furthermore, the solutions based on Van Driest and Blumer transition origin model are not shown because this model indicated very early transition on both surfaces, thus its solution curves will not differ from the fully turbulent ones.

In figure (5.21) the solutions based on the best transition origin models (i.e. Schlichting and Seyb models) determined in section (5.5) (i.e. from heat transfer results and measurements) are shown. Although, experimental values of momentum thickness are not available to judge the performance of these two models, it is expected that they

will give good representation of reality. This claim is most probably true, since when defining the transition point of the flow using any available boundary layer parameter measurements together with the above mentioned models, then the result (i.e. predicted transition point) should be valid for all other boundary layer parameters.

Figure (5.22) shows the suction surface computational step No. 3 and 4. In these solutions, fixed transition origin model was that of Schlichting. Furthermore, although the Dhawan and Narasimha length and path models (solid curve) were selected (from heat transfer experimental results) to be the best length and path models, solutions based on the two length and two path models used in this study are presented (i.e. four combinations of solutions). Furthermore, it is noticed that the momentum thickness solutions based on these four combinations of models are closer to each other than those corresponding to heat transfer shown in figure (5. 17), thus it could be concluded that momentum thickness predictions results are less sensitive to the choice of the length and path models.

Finally, it is believed that while the transition length and path models were found necessary to model the suction surface heat transfer coefficient distribution during transition (i.e. to model transition as a region), the transition at a point assumption (i.e. transition region is considered a point) may be enough as far as the momentum thickness predictions are concerned.

## 5.7 Other boundary layer parameters results

Figure (5.23) shows the calculated distribution of the boundary layer thickness, ( $\delta$ ). These calculated values of  $\delta$  are used to calculate the distribution of the first shape

factor,  $\Lambda = \frac{\delta^2}{\nu} \frac{dU}{dx}$ , previously shown in figure (5.11). Unfortunately, the integral method of solution outlined in chapter 3 is not capable to solve for the fully turbulent value of the boundary layer thickness,  $\delta$ . Thus, computational process for this parameter is terminated.

Similarly, figure (5.24), shows the calculated variation of the thermal boundary layer thickness distribution ( $\delta_T$ ). These distributions are used in equation (3.51) to obtain the heat transfer coefficient distributions based on laminar flow assumption and/or laminar flow assumption but with computations being based on ( $\mu_{eff}$ ). Furthermore, comparing the relative values of  $\delta$  and  $\delta_T$  from figures (5.23) and (5.24), it is clear that the thermal boundary layer always contains inside it the velocity boundary layer (i.e.  $\delta_T > \delta$ ), which is the case for air with  $Pr = \frac{\delta}{\delta_T} < 1$ .

Finally, the momentum thickness Reynolds number prediction results are shown in figures (5.25) through (5.27) with the same computational steps as that used for the momentum thickness. No further discussion shall be given to these figures, since almost the same comments and observations of the momentum thickness results are applicable to these figures.

## Chapter 6

# CONCLUSIONS AND RECOMMENDATIONS

### 6.1 Conclusions

The followings are the important results of the present investigation :

1. The general unmodified integral boundary layer method outlined in chapter three, although capable to solve both fully laminar and fully turbulent flows, is inadequate for direct application to the gas turbine airfoil heat transfer prediction problem. The reasons supporting this conclusion were related to the lack in this integral method to model the transition region on the suction surface and the laminar heat transfer augmentation on the pressure surface due to free stream turbulence intensity effects.
2. The specification of accurate free-stream velocity (pressure) boundary conditions for boundary layer methods is essential for two important reasons: First, boundary layer integral method solutions are very sensitive to the pressure gradient characteristics of a gas turbine airfoil (eg. transition start is mainly dependent on the pressure gradient distribution). Secondly, resolution of the inviscid flow field in the vicinity of the stagnation point is essential in determining accurate stagnation point heat transfer level.

3. Airfoil stagnation point heat transfer prediction method, which implicitly assumes the behaviour of cylinders in cross flow are quite satisfactory for direct use in a gas turbine blade cascade prediction method.
4. In general, commonly available transition process models (origin, length and path (intermittency)) were found to be adequate for providing a consistent representation of the experimental data over the suction surface.
5. Transition origin models gave reasonable results over the suction surface where natural transition appears to be a valid concept. However, transition origin predictions were inconclusive over the pressure surface where the concept of natural transition appears questionable. For the suction surface, Schlichting transition start model gave the best predictions followed by that of Seyb. These two models are considered to be the best because they gave quite satisfactory results on the suction surface and no transition on the pressure surface.
6. Extended regions of boundary layer transition do exist on suction surfaces of turbine blades in cascade. Thus, transition at a point assumption will reflect low quality predictions. The assumption of an abrupt transition from laminar to turbulent flow regime leads to overcooling precisely in the area where the heat transfer coefficient is actually the lowest. This situation, of course, induces high stresses in the blade.
7. The free stream velocity distribution, which is a direct result of the blade shape, is the most significant parameter affecting the start and length of transition and the general level of heat transfer.

8. For the suction surface, it was concluded that the moderate levels of turbulence intensity present in the boundary layer prior to transition do not have a great influence on both the start and the development of the transition process initiated by an adverse pressure gradient.
9. On the suction surface, heat transfer coefficient predictions in the fully turbulent region predicts higher values than the experimental data. On the other hand, the predictions in the laminar region agrees very well with experiment.
10. The distribution of the heat transfer coefficient on the suction side of turbine blades is governed mainly by the onset of the laminar-turbulent transition. This process in turn is controlled by the local value of the pressure gradient.
11. On the pressure surface, transition usually starts very near the leading edge because of the high relative turbulence intensity on this side of the blade. After this start, there is a balance between the free-stream turbulence and the favourable pressure gradient effects, the former tends to promote and the latter to retard the transition to fully turbulent flow. Due to the relaminarizing effect of the pressure gradient, the boundary layer does not become fully turbulent on the pressure surface.
12. Transition length models, which are functions of transition origin models, lead to generally satisfactory predictions on the suction surface. Debruge transition length model underestimated the length of transition (i.e. transition was predicted to complete more rapidly than the measurements indicated) while the Dhawan and Narasimha length model gave more satisfactory predictions of the transition zone length.

13. Transition path (intermittency) models, which are functions of both fixed origin and length models, lead to generally satisfactory predictions. When Schlichting transition origin model and Dhawan and Narasimha transition length model are used as the best (and fixed) transition origin and length models, the path (intermittency) model of Abu-Ghannam and Shaw underpredicted the level of heat transfer, while the Dhawan and Narasimha path model gave more satisfactory predictions.
14. Turbulence viscosity models were found to be adequate to predict the influence of free-stream turbulence on a nominally laminar boundary layer developing over the pressure surface.
15. Blade curvature has a marked effect on the distribution of the free-stream turbulence intensity along the blade surfaces. Suction (convex) surface is characterized to have a very rapid decay in the level of free stream turbulence intensity, while pressure (concave) surface has a slower decay.
16. Suction surface is characterized to have a thicker boundary layer than the pressure surface. Thus drag forces are larger on the suction surface than on the pressure surface.

## 6.2 Recommendations

The followings are recommended for future work :

1. Additional heat transfer and momentum thickness experimental data taken at known operating conditions are required to confirm the validity of the present integral method and models (i.e. transition and turbulence viscosity models). These



experiments need not be limited to airfoil geometries but should reflect the pressure gradient and free-stream turbulence intensity characteristics of the gas turbine environment.

2. On the suction surface, the largest deviation between predicted and experimentally determined values of the heat transfer coefficient occurred in the fully turbulent region. This deviation is most probably attributed to the relaminarizing effect of the favorable pressure gradient present in this region. Thus it is recommended to extend the Von Karman formula for heat transfer in turbulent flows to account for this phenomena. Such an extension might be achieved by using the relation between heat transfer and skin friction for turbulent flows with pressure gradients derived by Gerhart and Thomas [59].

$$St = \frac{h}{\rho U C_p} = \frac{C_f}{2} Pr^{-1/2} \left[ \frac{1 + \left(1 - \frac{4T}{(C_f/2)^2}\right)^{1/2}}{2} \right]$$

Where  $T = (\nu/U^2) \frac{dU}{dx}$ .

The above formula was derived by the so called surface renewal and penetration model, which is based on the assumption that macroscopic elements of fluid (i.e. eddies) intermittently move from the turbulent core to the close vicinity of the wall, thus renewing it.

# Bibliography

- [1] A. Brown and B. W. Martin, "Heat Transfer to Turbine Blades with Special Reference to the Effects of Mainstream Turbulence," ASME Paper No. 79-GT-26, March 1979.
- [2] D. A. Nealy, "Some Effects of Variable Surface Temperature on Heat Transfer to a Partially Porous Flat Plate," Trans. ASME, Journal of Engineering for Power, October 1973, pp. 317-325.
- [3] D. J. Gauntner and J. Sucec, "Method for Calculating Convective Heat Transfer Coefficients Over Turbine Vane Surfaces," NASA TP-1134, 1978.
- [4] G. S. Ambrok, "Approximate Solution of Equations for the Thermal Boundary Layer with Variations in Boundary Layer Structure," Sov. Phys.- Tech. Phys., Vol. 2, No. 9, 1957, pp. 1979-1986. (English Translation).
- [5] H. McDonald and R. W. Fish, "Practical Calculations of Transitional Boundary Layers," International Journal of Heat and Mass Transfer, Vol. 16, No. 9, 1972.
- [6] J. J. Herring and G. L. Mellor, "A Computer Program to Calculate Incompressible Laminar and Turbulent Boundary Layer Behavior," NASA CR 1564 , 1970.

- [7] J. J. Herring and G. L. Mellor, "Computer Program for Calculating Laminar and Turbulent Boundary Layer Development in Compressible Flow," NASA CR 2068, 1972.
- [8] T. Cebeci, A. M. O. Smith, and L. C. Wang, "Finite Difference Method for Calculating Compressible Laminar and Turbulent Boundary Layers," Douglas Aircraft Co. Report DAC 67131, 1969.
- [9] M. E. Crawford and W. M. Kays, "STAN5: A Program for Numerical Computation of Two-Dimensional Internal and External Boundary Layer Flows," NASA CR 2742, 1976.
- [10] W. M. Kays, "STAN7: A Program for Numerical Computation of Two-Dimensional Internal and External Boundary Layer Flows," Personal Communications.
- [11] A. E. Forest, "Engineering Predictions of Transitional Boundary Layers," AGARD-CP-224, 1977.
- [12] T. Cebeci and A. M. O. Smith, Analysis of Turbulent Boundary Layers, Academic Press, 1974.
- [13] H. B. Keller and T. Cebeci, "Accurate Numerical Methods for Boundary Layer Flows, II: Two dimensional Flow," AIAA Journal, Vol. 10, 1972, pp. 1193-1199.
- [14] S. V. Patankar and D. B. Spalding, Heat and Mass Transfer in Boundary Layers, Second Edition, International Textbook Company Ltd., London, 1970.
- [15] S. V. Patankar and D. B. Spalding, Heat and Mass Transfer in Boundary Layers, First Edition, Morgan-Grampian, London, 1967.

- [16] S. V. Patankar and D. B. Spalding, "A Finite-Difference Procedure for Solving the Equations of the Two-Dimensional Boundary Layer," *International Journal of Heat and Mass Transfer*, Vol. 10, 1967, pp. 1389- 1411.
- [17] D. G. Wilson and J. A. Pope, "Convective Heat Transfer to Gas Turbine Blade Surfaces," *Proc. Inst. of Mechanical Engineers*, Vol. 168, 1954, pp. 861-876.
- [18] R. I. Hodge, "A Turbine Nozzle Cascade for Cooling Studies," *Aeronautical Research Council*, CP 492-493, 1960, pp. 1-39.
- [19] A. B. Turner, "Local Heat Transfer Measurements On a Gas Turbine Blade," *Journal of Mechanical Engineering Science*, Vol. 13, 1971, pp. 1-12.
- [20] R. D. Lander, "An Evaluation of the Effect of Free-Stream Turbulence on the Heat Transfer to Turbine Airfoils," Report AFAPL-TR-69-70 , Sept. 1969.
- [21] A. Brown and R. C. Burton, "The Effects of Free-Stream Turbulence Intensity and Velocity Distribution on Heat Transfer to Curved Surfaces," *Tran. ASME, Journal of Engineering for Power*, Vol. 100, 1978, pp . 159-168.
- [22] D. A. Nealy, Personal Communications.
- [23] F. M. White, Viscous Fluid Flow, McGraw-Hill, Inc., New York, 1974.
- [24] H. Schlichting, Boundary Layer Theory, McGraw-Hill Book Co., 6th Edition, 1968.
- [25] H. B. Squires, "Heat Transfer Calculation for Aerofoils," *Aeronautical Research Council*, R and M 1986, 1942, pp. 1-20.

- [26] E. Truckenbrodt, "A Method of Quadrature for Calculating the Laminar and Turbulent Boundary Layer in Case of Plane and Rotationally Symmetrical Flow," NACA TM 1379, 1955, pp. 1-40.
- [27] H. Ludwig and W. Tillmann, *Ing.-Arch.*, Vol. 17, 1949, pp. 288- 299.
- [28] J. Rotta, "Turbulent boundary layers in incompressible flow," *Progress in Aeronautical Sciences*, Vol. 2, 1962, pp. 1-219.
- [29] M. E. Crawford and W. M. Kays, Convective Heat and Mass Transfer, Second Edition, McGraw-Hill, 1980.
- [30] N. J. Seyb, "The Role of Boundary Layers in Axial Flow Turbomachines and the Prediction of Their Effects," AGARD-AG-164, 1972, pp. 241-259.
- [31] M. R. Head, "Entrainment in the turbulent boundary layer," Aeronautical Research Council, R and M 3152, 1958.
- [32] W. Rodi and G. Scheuerer, "Calculation of Heat Transfer to Convection-Cooled Gas Turbine Blades," *Trans. ASME, Journal of Engineering for Gas Turbines and Power*, Vol. 107, 1985, pp. 620-627.
- [33] W. P. Jones and B. E. Launder, "The Calculation of Low-Reynolds Number Phenomena with a Two-Equation Model of Turbulence," *Int. J. Heat Mass Transfer*, Vol. 16, 1973, pp. 1119-1130.
- [34] L. C. Daniels and W. B. Browne, "Short Duration Measurements of Heat Transfer Rate to a Gas Turbine Rotor Blade," *Int. J. Heat Mass Transfer*, Vol. 24, 1981, pp. 871-879.

- [35] S. Kan, K. Miwa, T. Morishita, Y. Munakata, and M. Nomura, "Heat Transfer of a Turbine Blade," Paper No. JSME-30, Tokyo Joint International Gas Turbine Conference and Products Show, Tokyo, Japan, Oct. 1971.
- [36] G. B. Schubauer and H. K. Skramstad, "Laminar Boundary Layer Oscillations and Transition on a Flat Plate," NACA Rept. No. 909, 1949.
- [37] B. E. Launder, "Laminarization of a Turbulent Boundary Layer in a Severe Acceleration," Trans. ASME, Journal of Applied Mechanics, Vol. 86, No. 4, 1964.
- [38] V. C. Patel and M. R. Head, "Reversion of Turbulent to Laminar Flow," Journal of Fluid Mechanics, Vol. 34, Part 2, 1968, p. 707.
- [39] B. G. Shivaprasad and B. R. Ramaparian, "Turbulence Measurements in Boundary Layers Along Mildly Curved Surfaces," Trans. ASME, Journal of Fluids Engineering, Vol. 100, 1978, pp. 37-46.
- [40] J. P. Johnston, "The Effects of Rotation on Boundary Layers in Turbomachine Rotors," ID 1939-D, May 1970, Stanford University.
- [41] L. L. Debruge and W. H. Mitchel, "Determination of Convection Heat Transfer Coefficients Around a Turbine Airfoil," Report AFAPL-TR-68-143, April 1969.
- [42] E. R. G. Eckert, VDI-Forschungsh, Vol. 416, 1942, pp. 1-24.
- [43] I. Imai, "On the heat transfer to constant property laminar boundary layer with power function free stream velocity and wall temperature distribution," Quart. Appl. Math., Vol. 16, 1958, pp. 33-45.

- [44] Th. Von Karman, "The Analogy Between Fluid Friction and Heat Transfer," Trans. ASME, Vol. 61, 1939, pp. 705-710.
- [45] R. A. Delaney, "Time-Marching Analysis of Steady Transonic Flow in Turbomachinery Cascades Using the Hopscotch Method," ASME Paper No. 82- GT-152, 1982.
- [46] H. W. Emmons, "The Laminar Turbulent Transition in a Boundary-Layer, Part 1," Journal of the Aeronautical Sciences, Vol.18, 1951 , pp. 490-498.
- [47] J. Dunham, "Predictions of Boundary Layer Transition on Turbomachinery Blades," AGARD-AG-164, 1972.
- [48] S. Dhawan and R. Narasimha, "Some Properties of Boundary Layer Flow During Transition from Laminar to Turbulent Motion," Journal of Fluid Mechanics, Vol. 3, 1958, pp. 418-436.
- [49] E. R. Van Driest and C. B. Blumer, "Boundary Layer Transition: Free-Stream Turbulence and Pressure Gradient Effects," AIAA Journal, Vol. 1 , 1963, pp. 1303-1306.
- [50] A. W. Goldstein and A. Mager, "Attainable Circulation about Aerofoils in Cascades," NACA Report 953, 1950.
- [51] L. F. Crabtree, "Prediction of Natural Transition in the Boundary Layer on An Aerofoil," Journal of the Royal Aeronautical Society, Vol. 62, 1958, pp. 525-528.
- [52] B. J. Abu-Ghannam and R. Shaw, "Natural Transition of Boundary Layers: The Effects of Turbulence, Pressure Gradient, and Flow History," Journal of Mechanical Engineering Science, Vol. 22, No. 5, 1980, pp. 213- 228.

- [53] D. J. Hall and J. C. Gibbings, "Influence of Stream Turbulence and Pressure Gradient Upon Boundary Layer Transition," *Journal of Mechanical Engineering Science*, Vol. 14, No. 2, 1972, pp. 134-146.
- [54] L. L. Debruge, "A Theoretical Determination of Convection Heat Transfer Coefficients During Transition on the Suction Side of Turbine Airfoils," AFAPL-TR-69-95, 1970.
- [55] B. W. Martin, A. Brown and S. E. Garrett, "Heat Transfer to a PVD Rotor Blade at High-Subsonic Passage Throat Mach Number," *Proc. Instn. Mech. Engrs.*, Vol. 192, 1978, pp. 225-235.
- [56] D. B. Spalding, "Applications of Boundary Layer Theory," Imperial College, Mechanical Engineering Department, Report BL/TN/A/8, 1969 .
- [57] M. C. Smith and A. M. Kuethe, "Effects of Turbulence on Laminar Skin Friction and Heat Transfer," *Physics of Fluids*, Vol. 9, 1966, pp. 2337 -2344.
- [58] L. D. Hylton, M. S. Mihelc, E. R. Turner, D. A. Nealy and R. E. York, "Analytical and Experimental Evaluation of the Heat Transfer Distribution Over the Surfaces of Turbine Vans," NASA CR 168015, May 1983.
- [59] P. M. Gerhart and L. C. Thomas, "Prediction of Heat Transfer for Turbulent Boundary Layer with Pressure Gradient," *AIAA Journal*, Vol. 11, No. 4, April 1973, pp. 552-554.



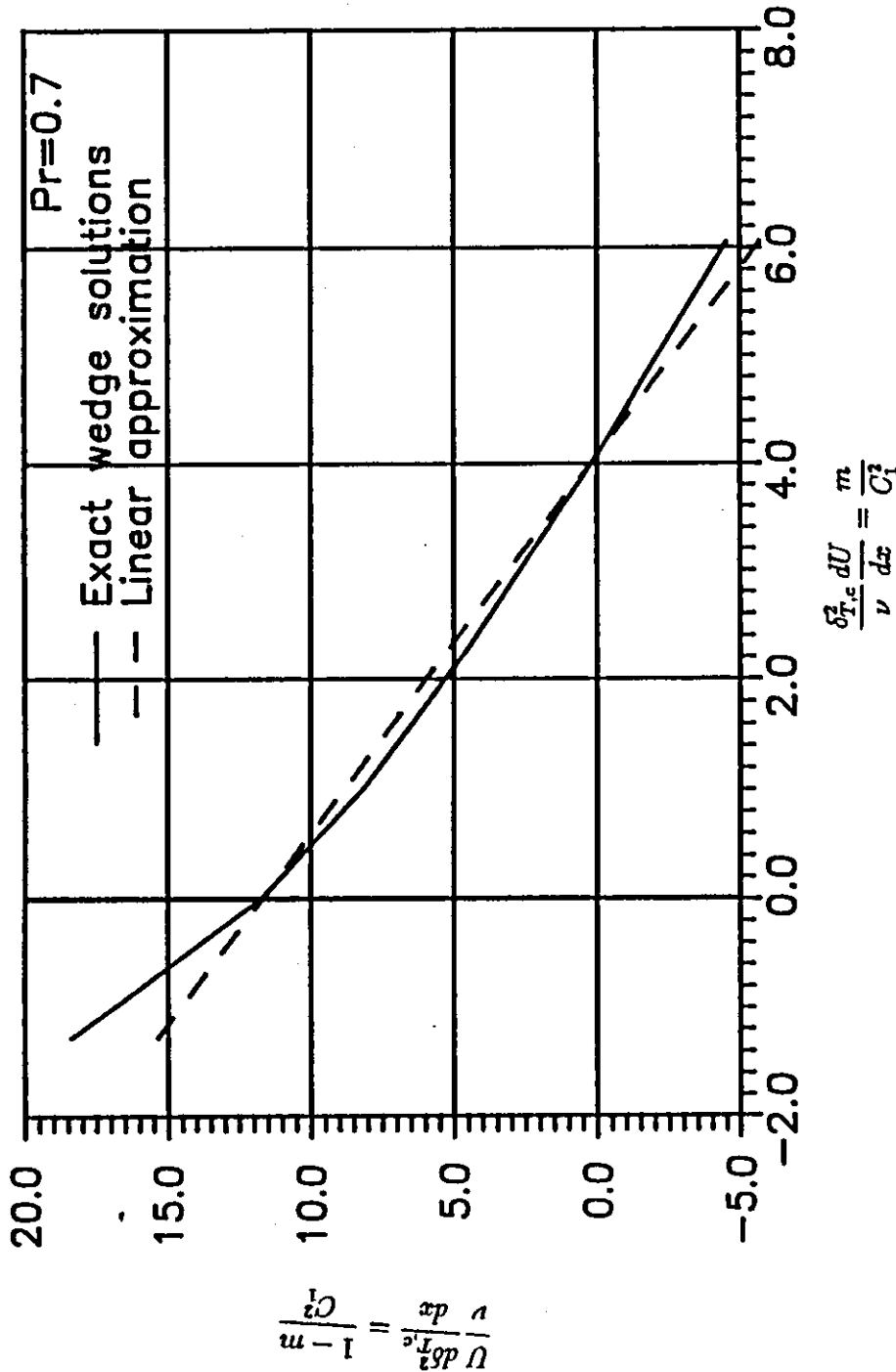


Figure (2.1) Plot of equation (2.10).

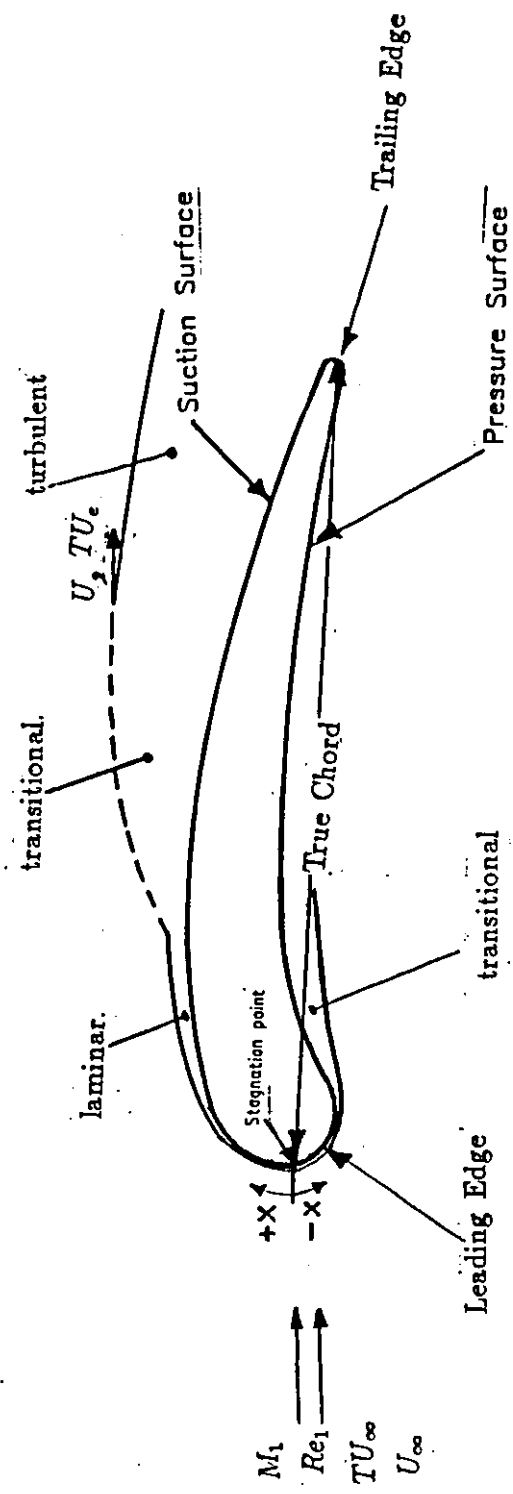


Figure (3.1) Blade geometry and boundary layer development.

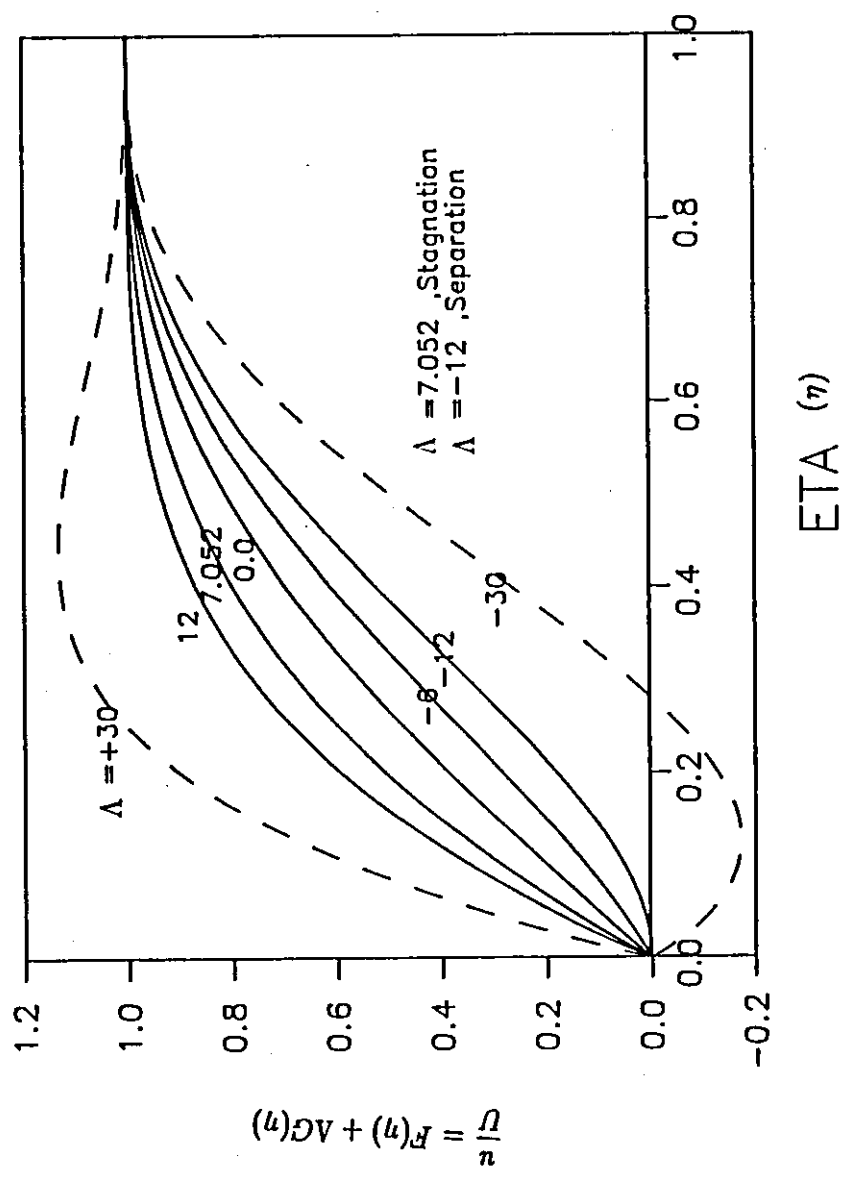


Figure (3.2) The one-parameter family of velocity profiles from equation (3.10).

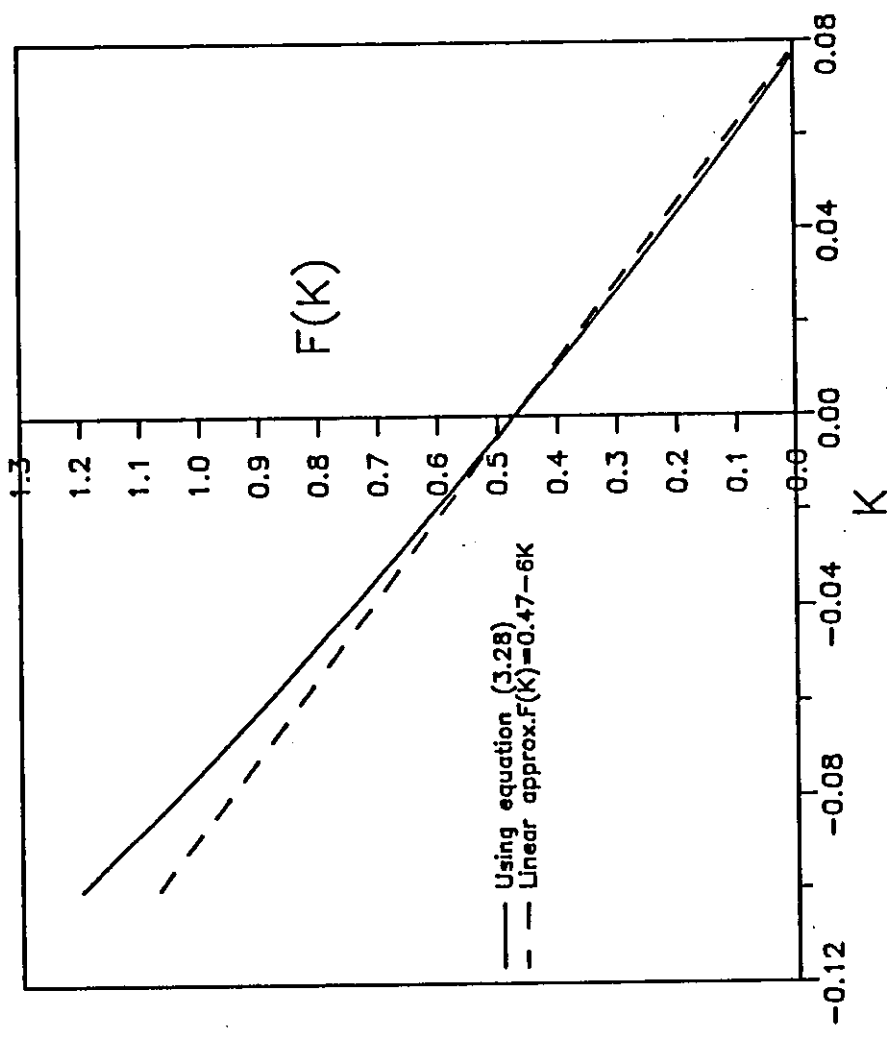


Figure (3.3) The auxiliary function  $F(K)$  for the calculation of laminar boundary layer by the method of section (3.2).

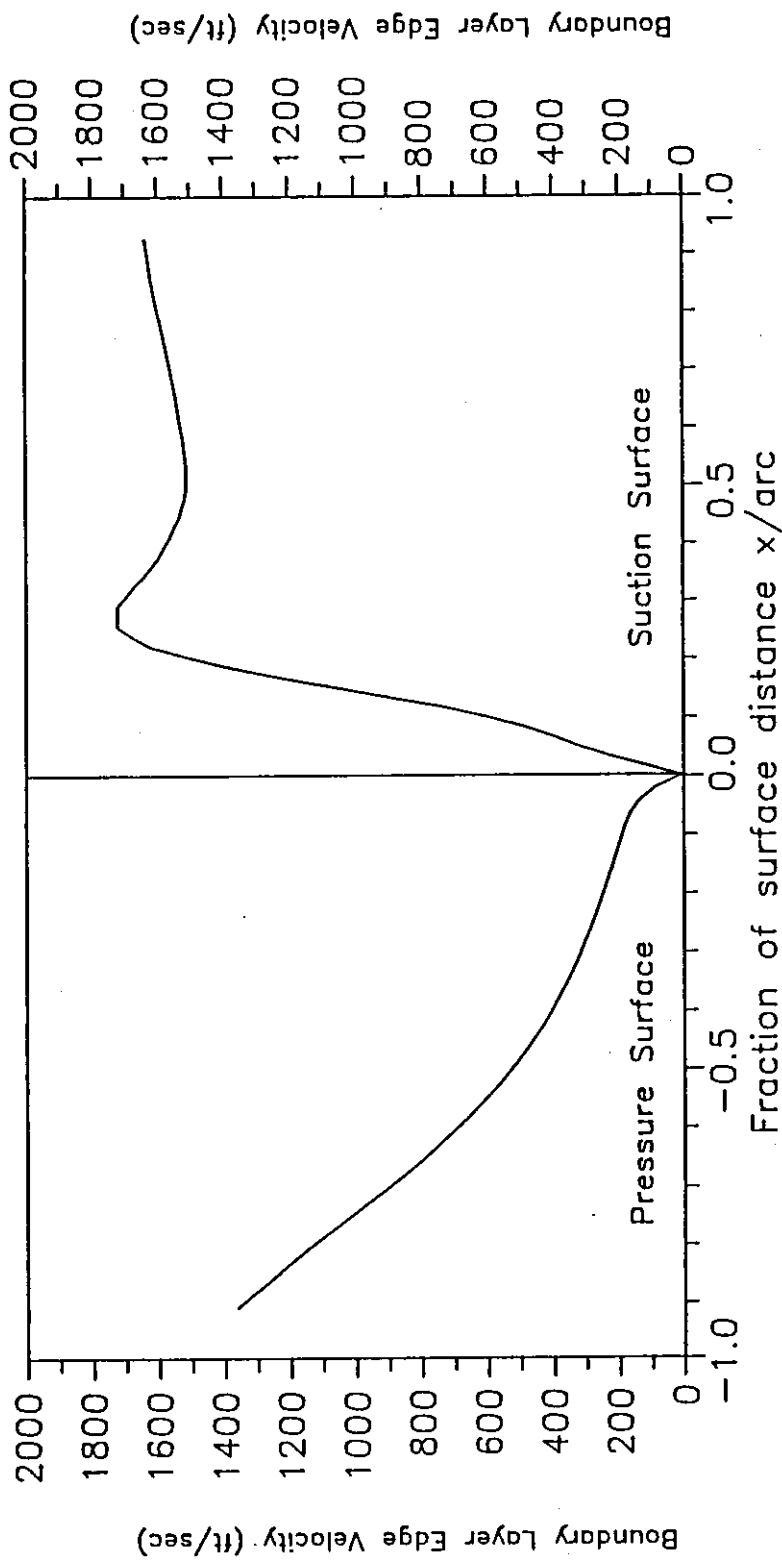


Figure (5.1) Blade surface velocity distribution.

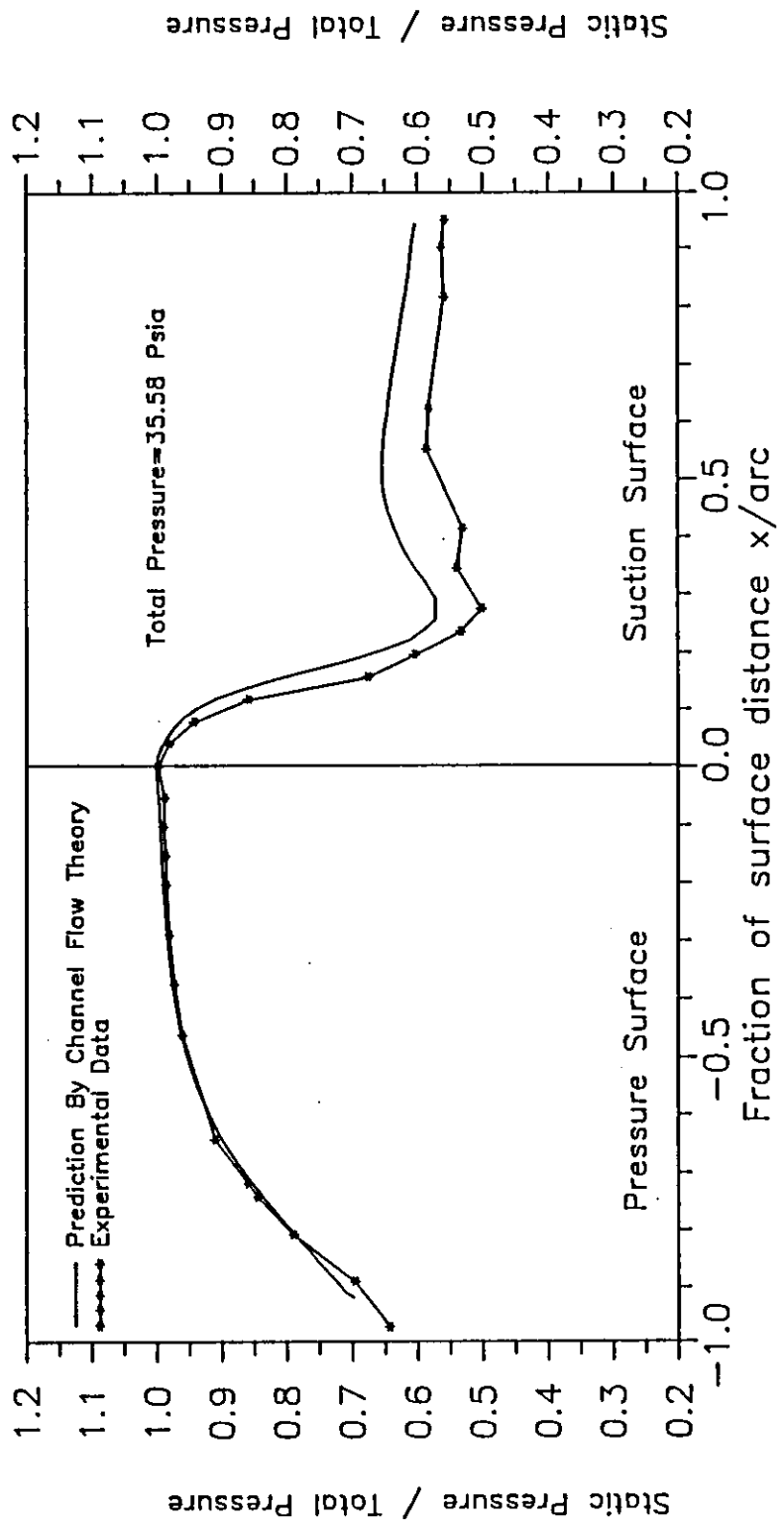


Figure (5.2) Blade surface static pressure/total pressure distribution.

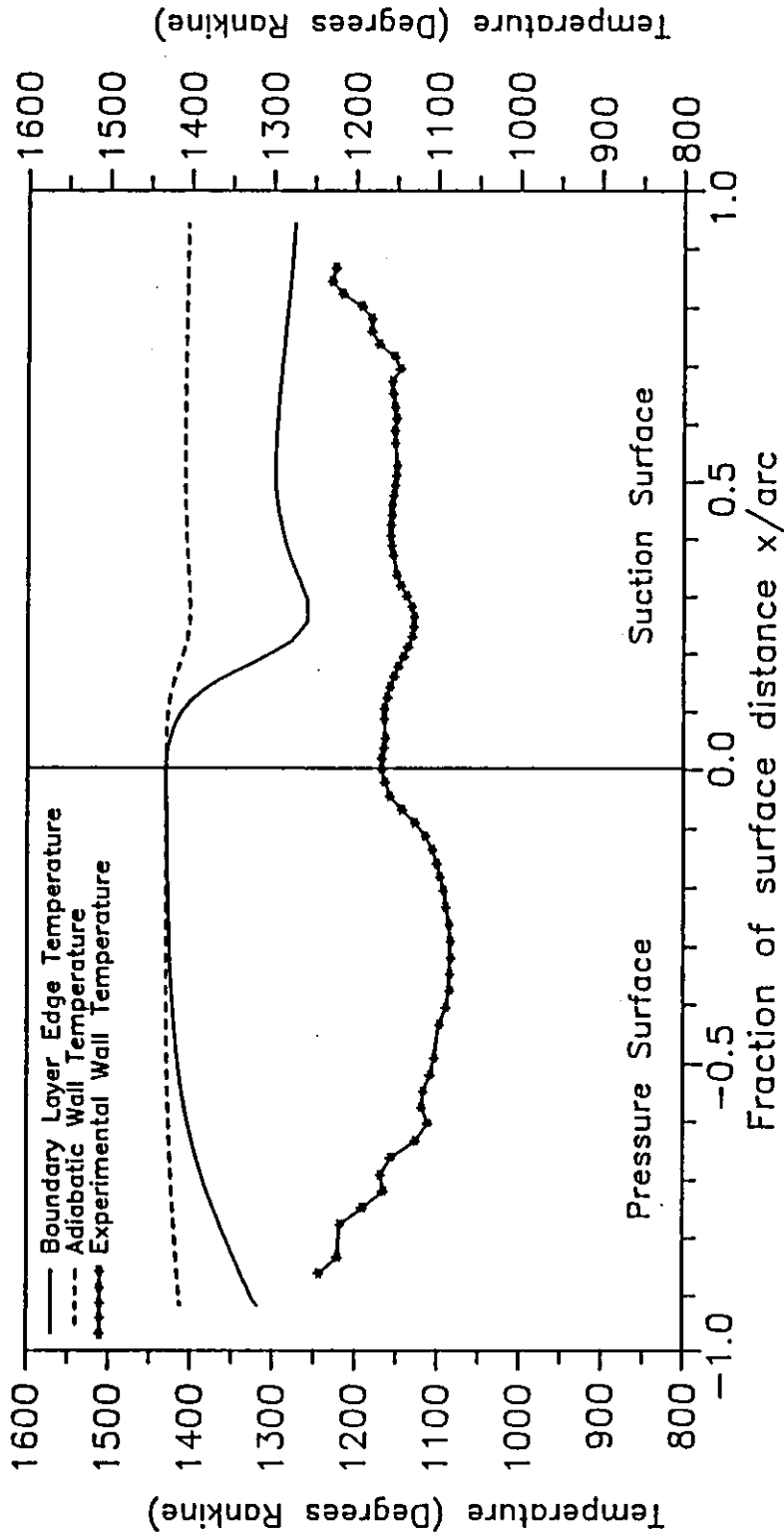


Figure (5.3) Blade surface and air temperatures distributions.

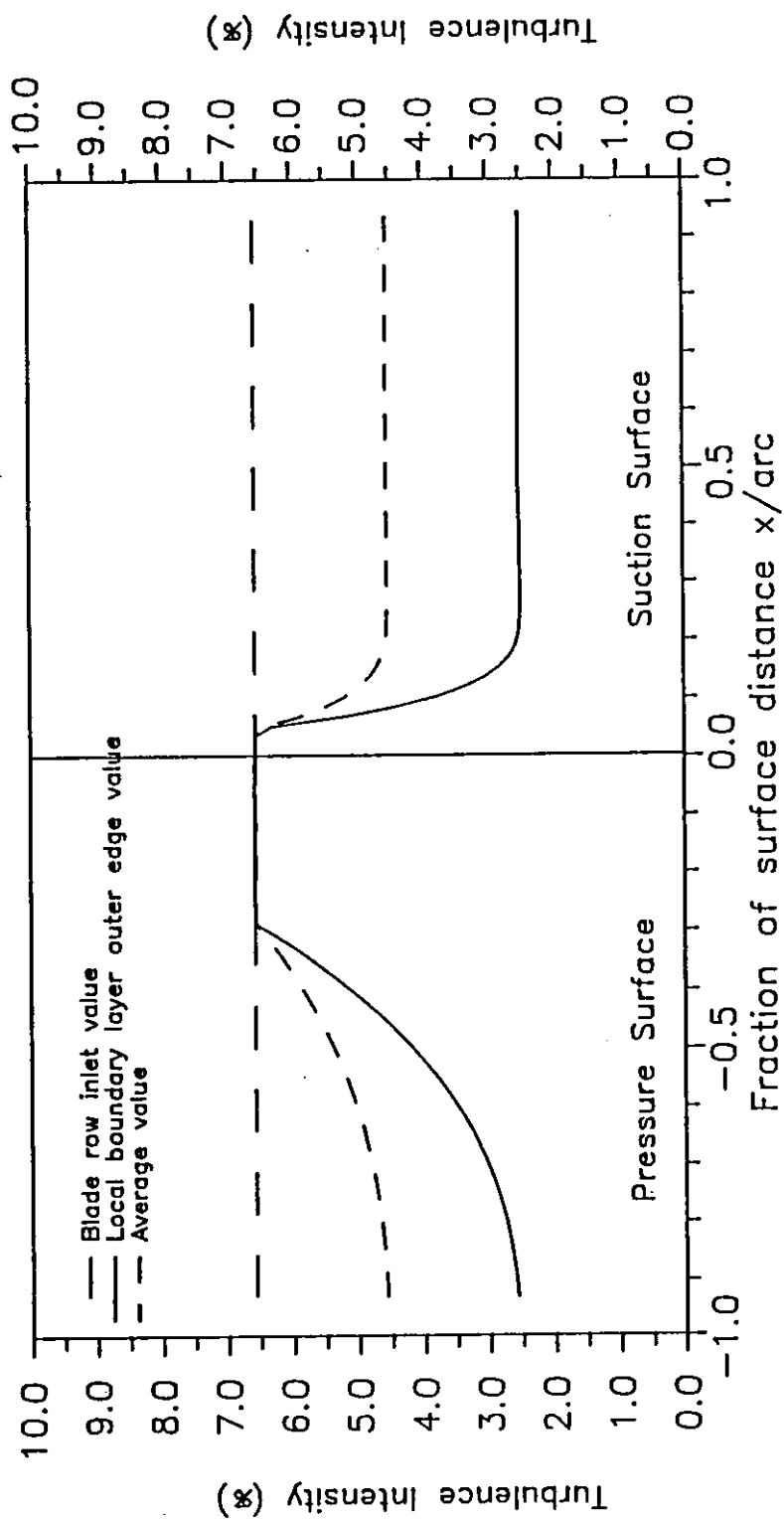


Figure (5.4) Turbulence intensity distribution along blade surfaces.



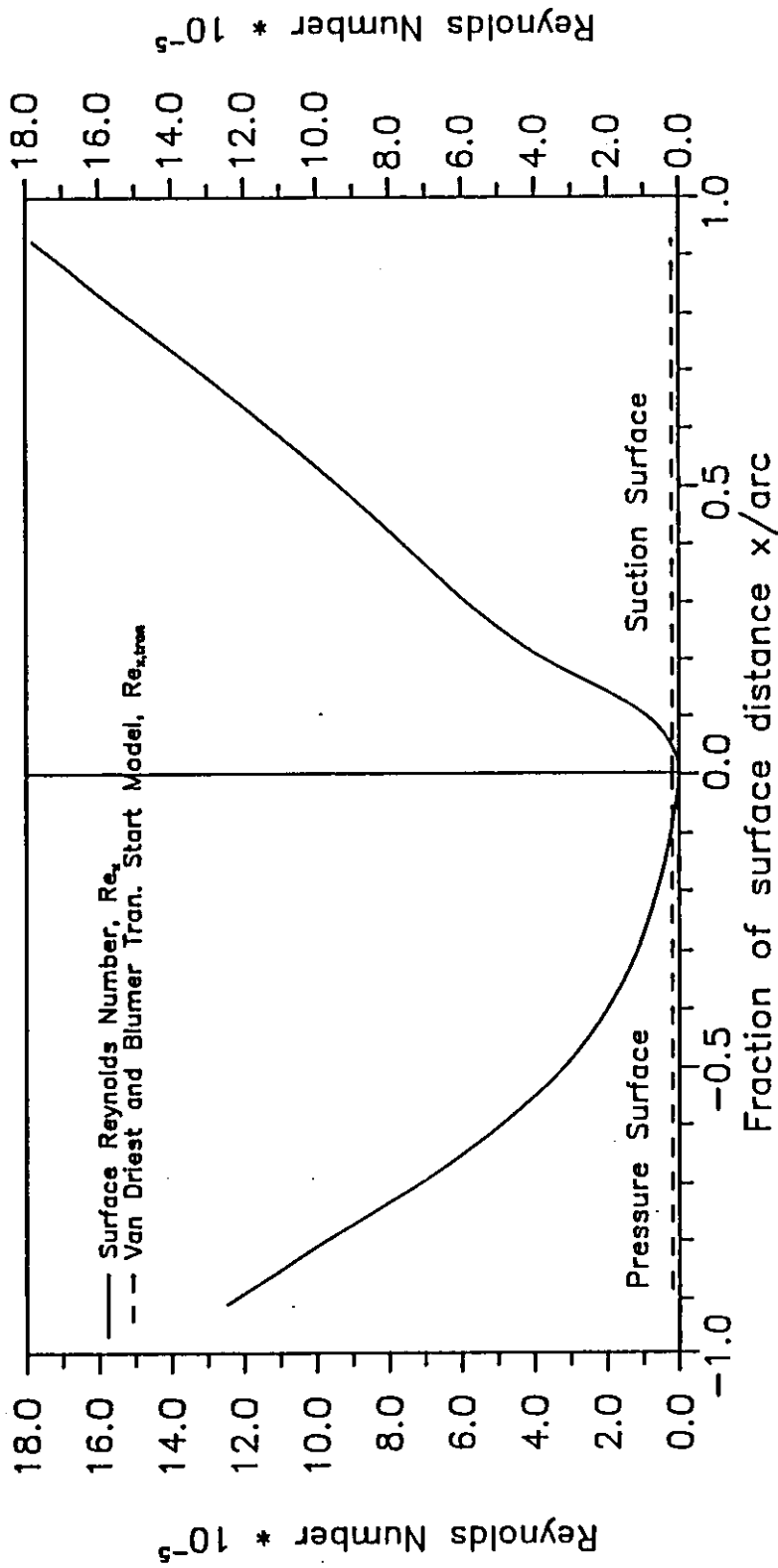


Figure (5.5) Surface Reynolds number ( $Re_x$ ) distribution.

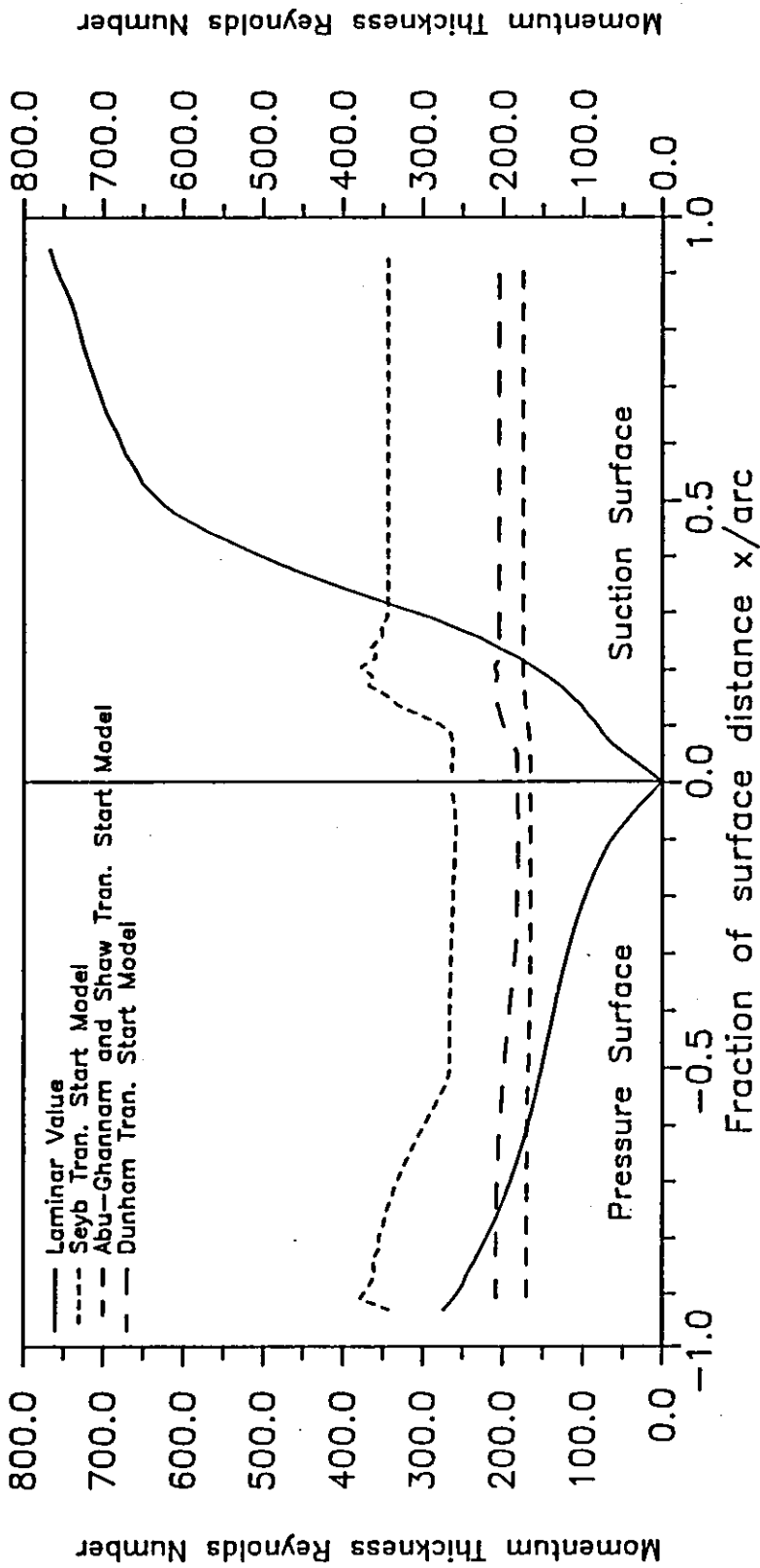


Figure (5.6) Transition start models solutions.

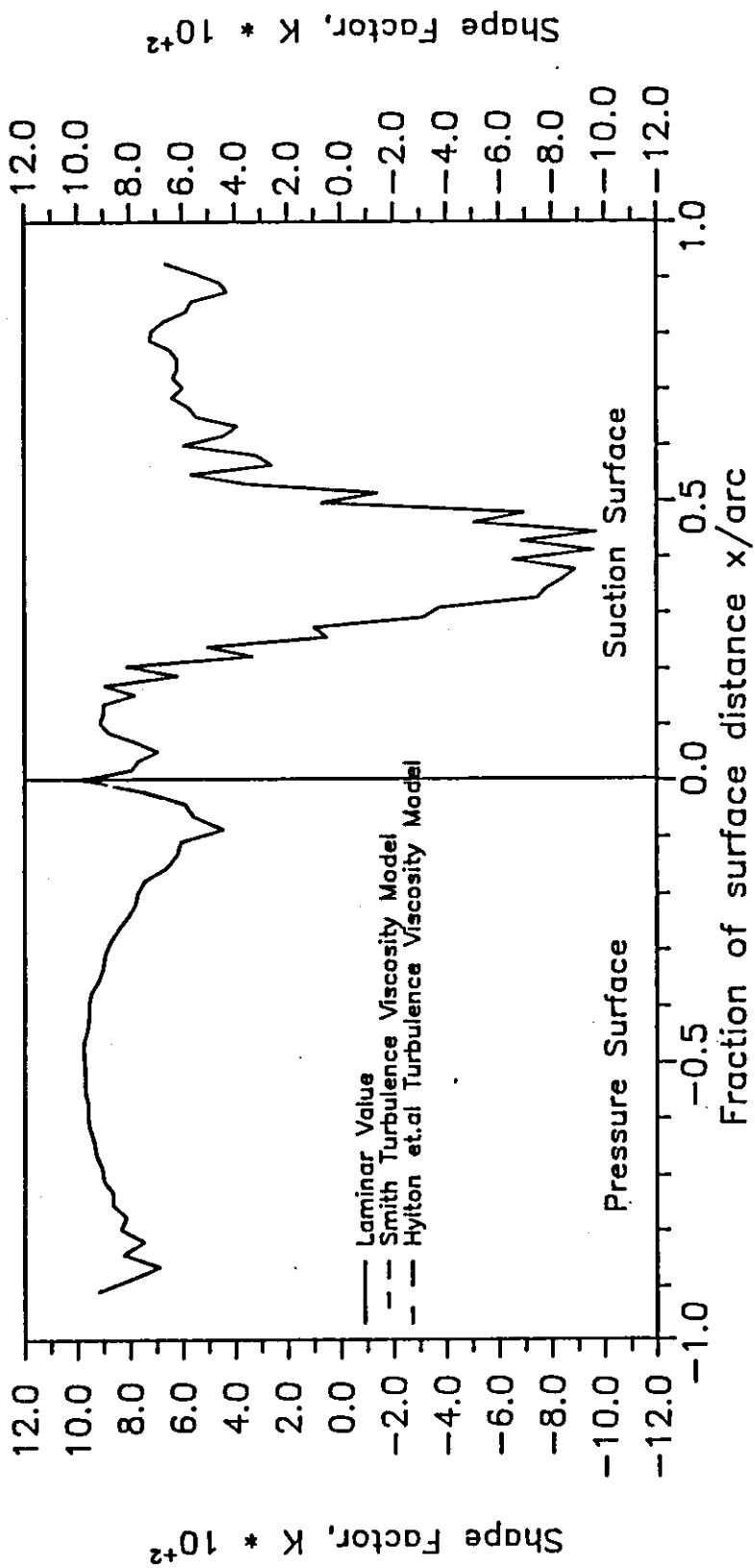


Figure (5.7) Shape factor (K) distribution.

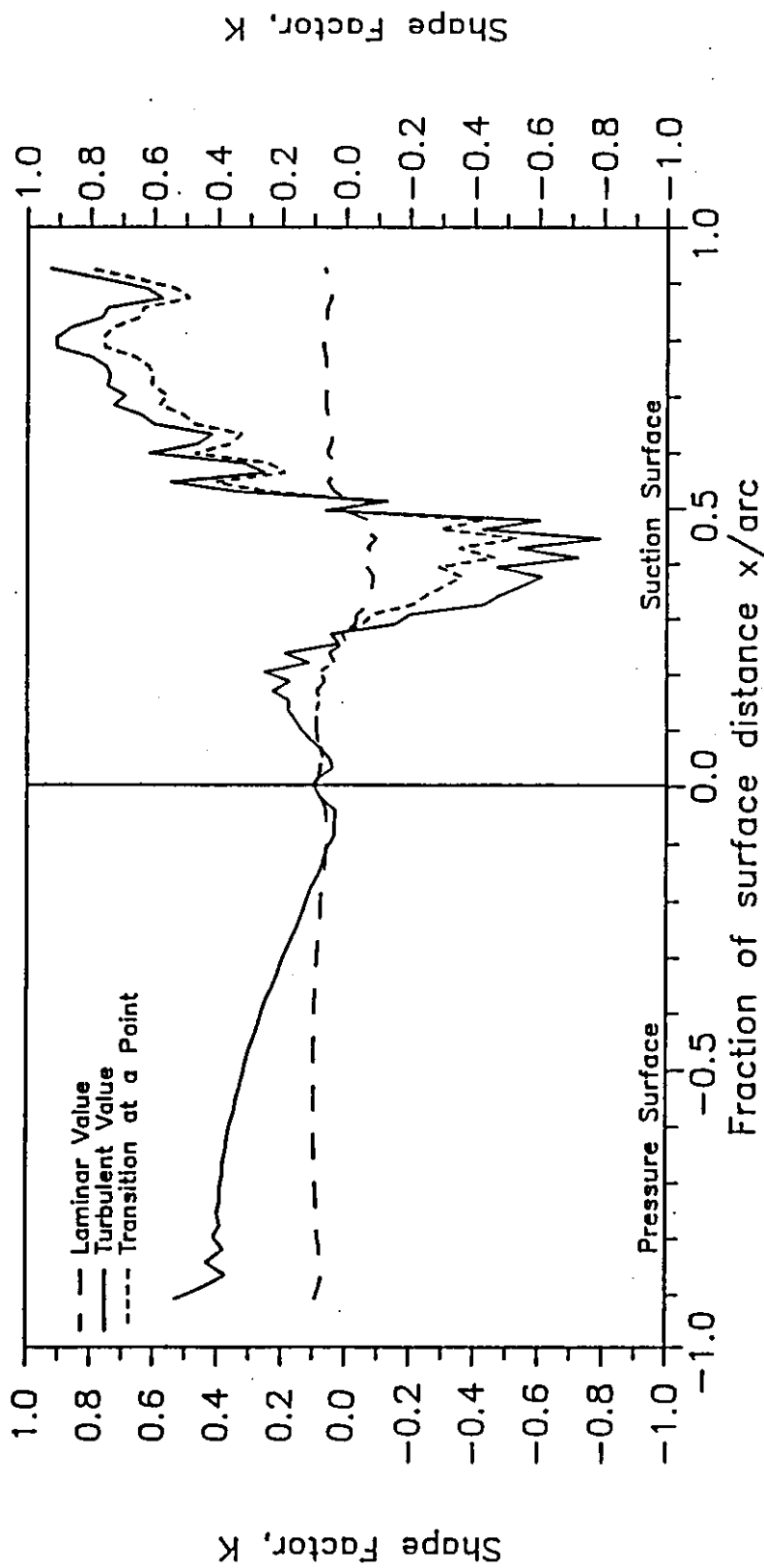


Figure (5.8 ) Shape factor (K) distribution.

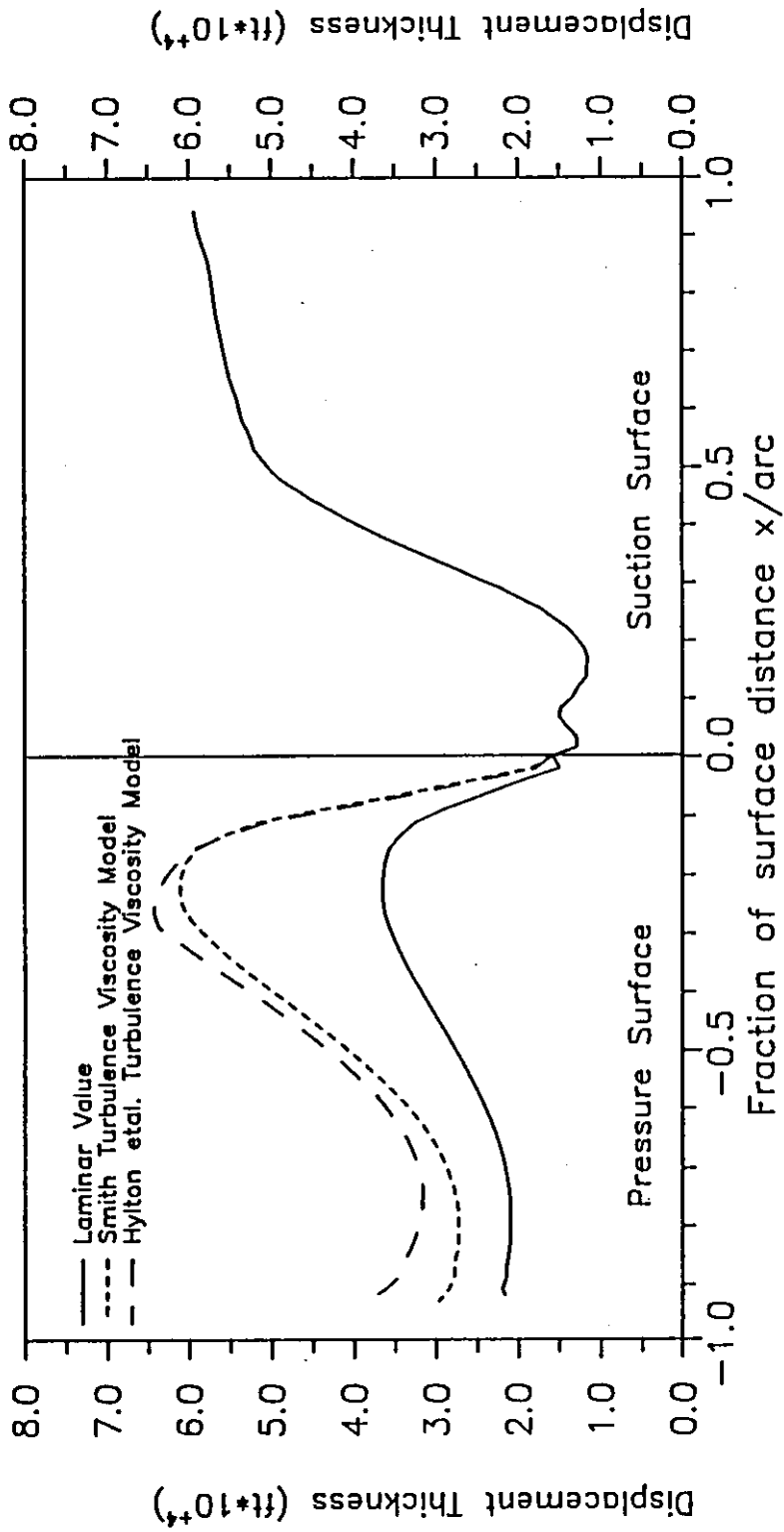


Figure (5.9) Boundary layer displacement thickness distribution.

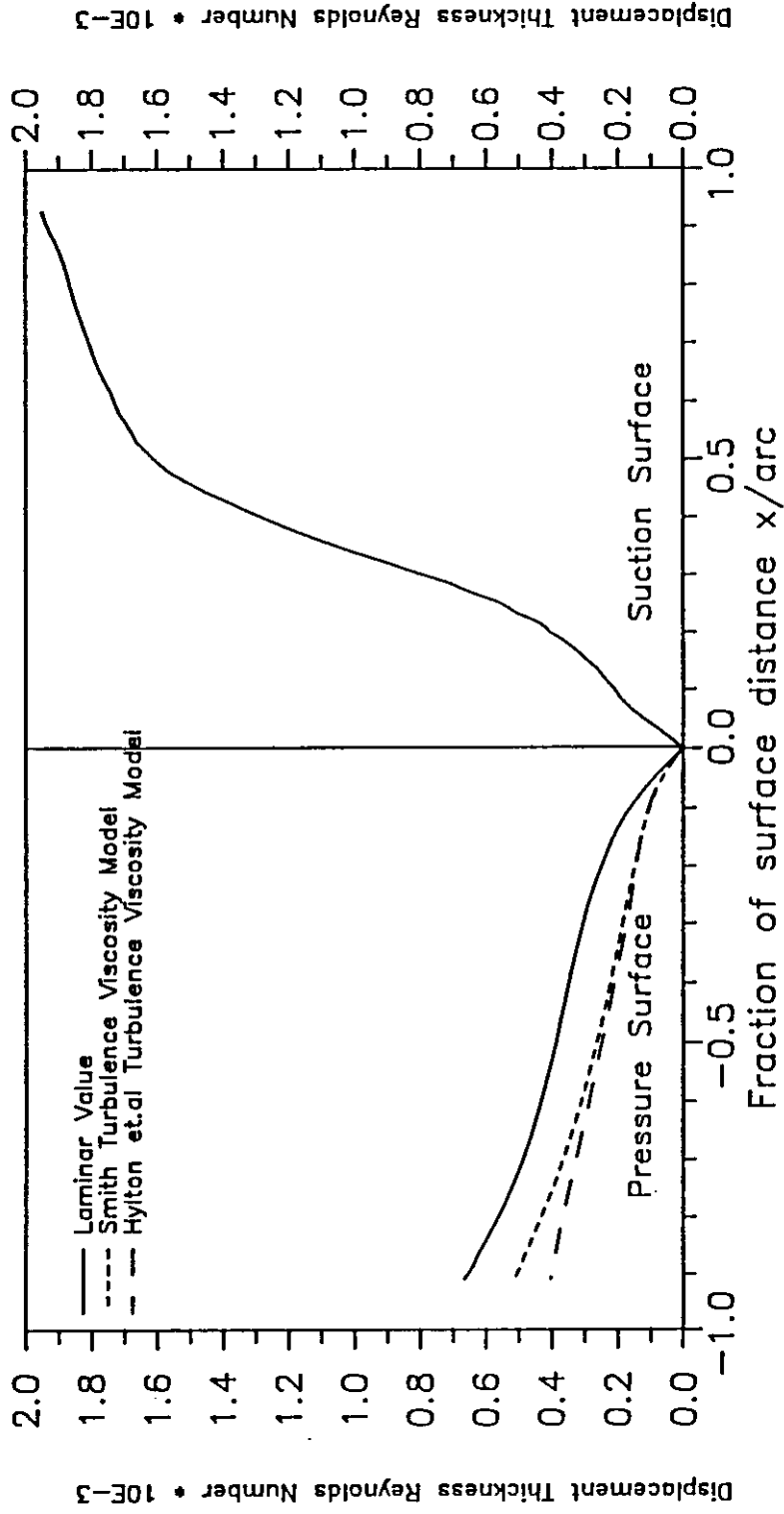


Figure (5.10) Displacement thickness Reynolds number distribution.

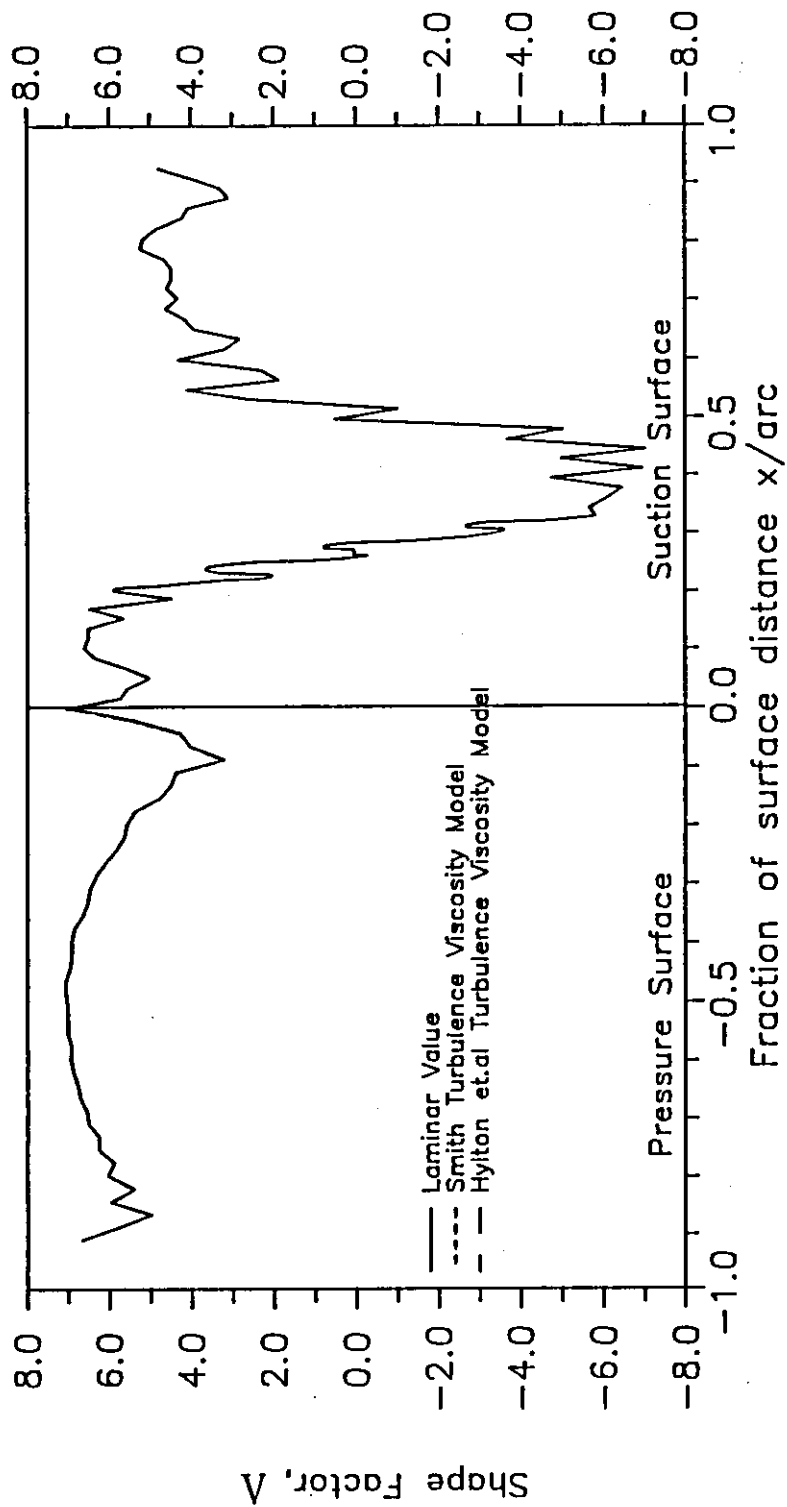


Figure (5.11) Shape factor ( $\Delta$ ) distribution.

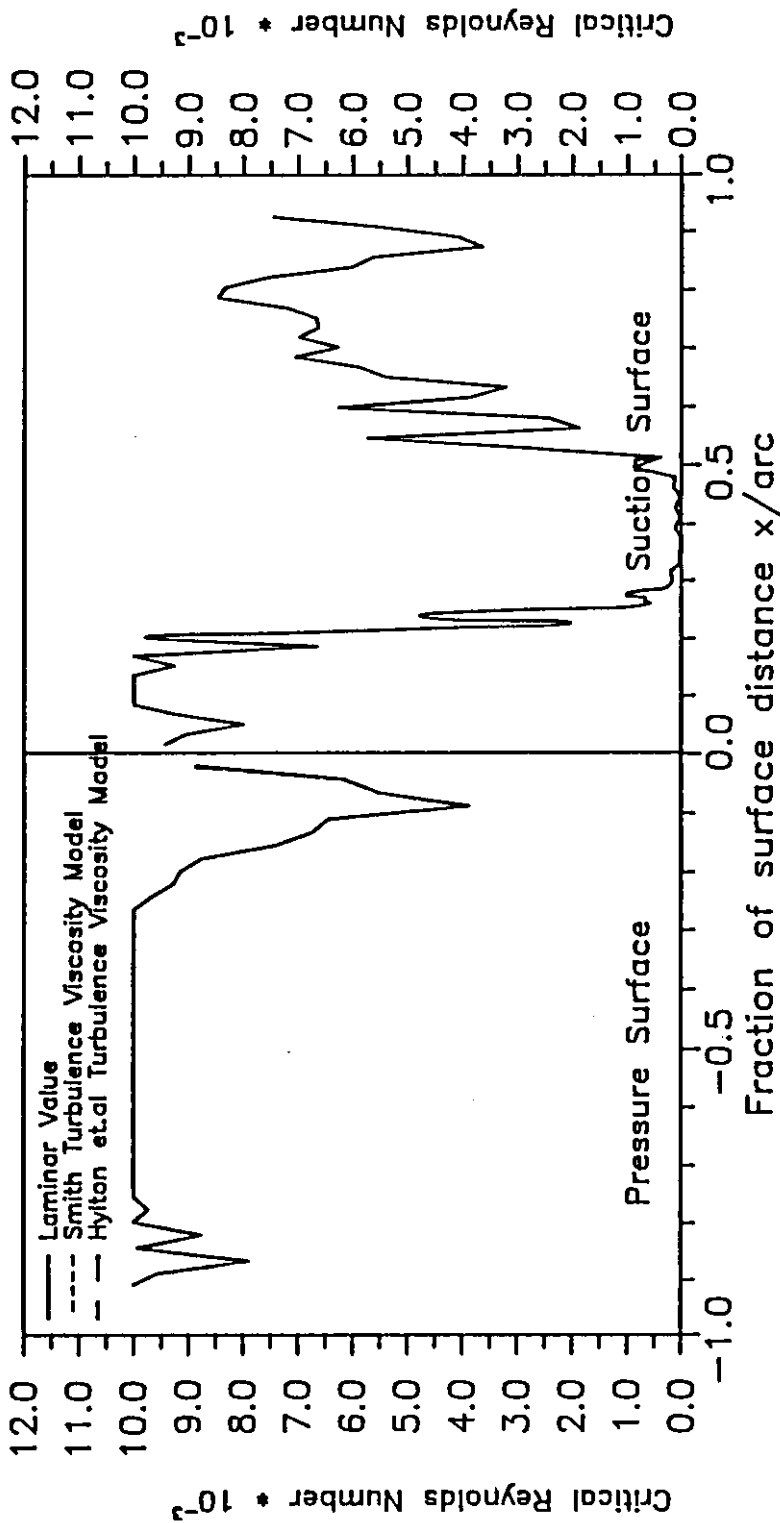


Figure (5.12) Critical displacement thickness Reynolds number distribution.



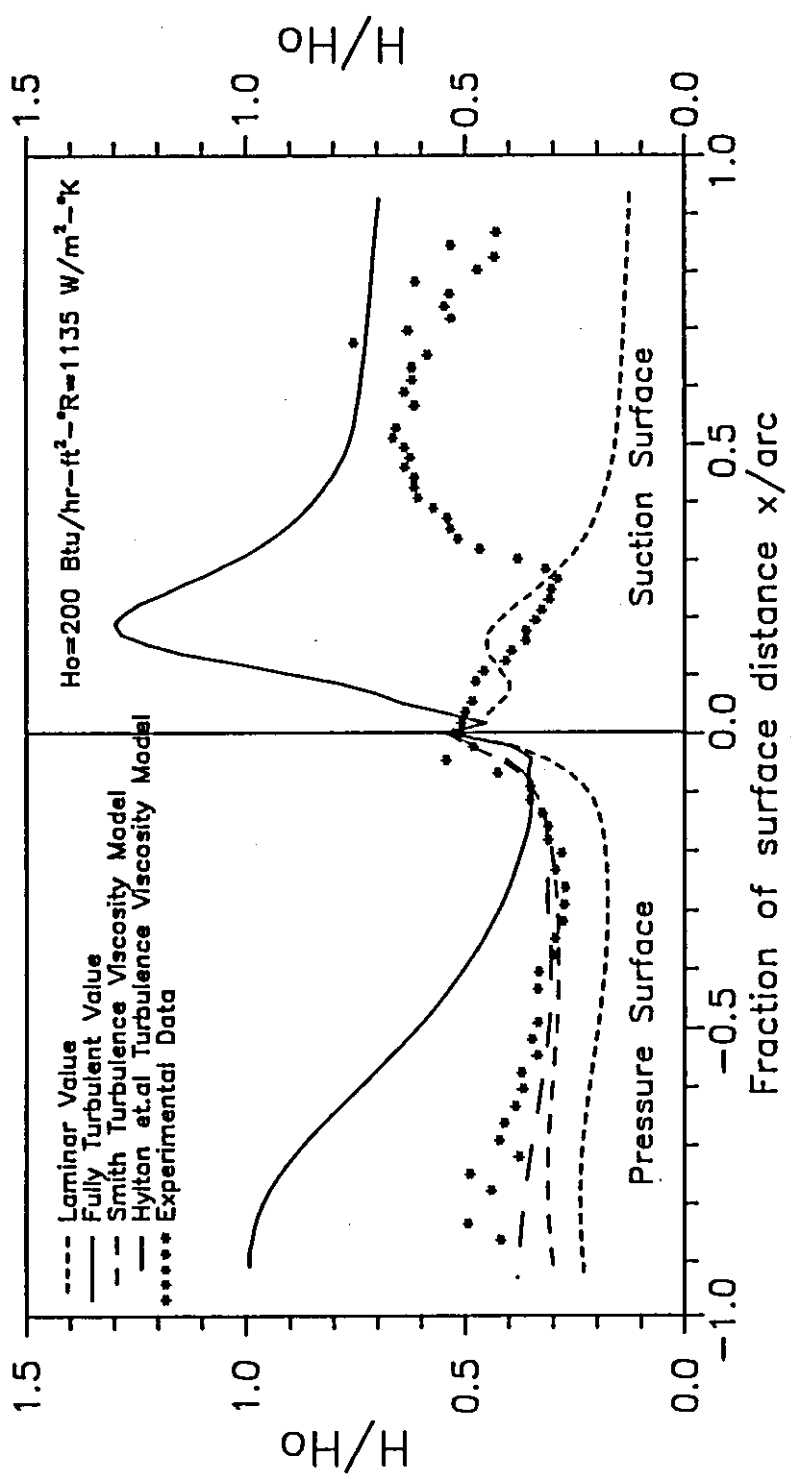


Figure (5.13) Heat transfer coefficient distribution. Base line unmodified solution results obtained for modified method evaluation process (Step No. 1). Modified solution results obtained for determination of best turbulence viscosity model (Pressure surface Step No. 2).

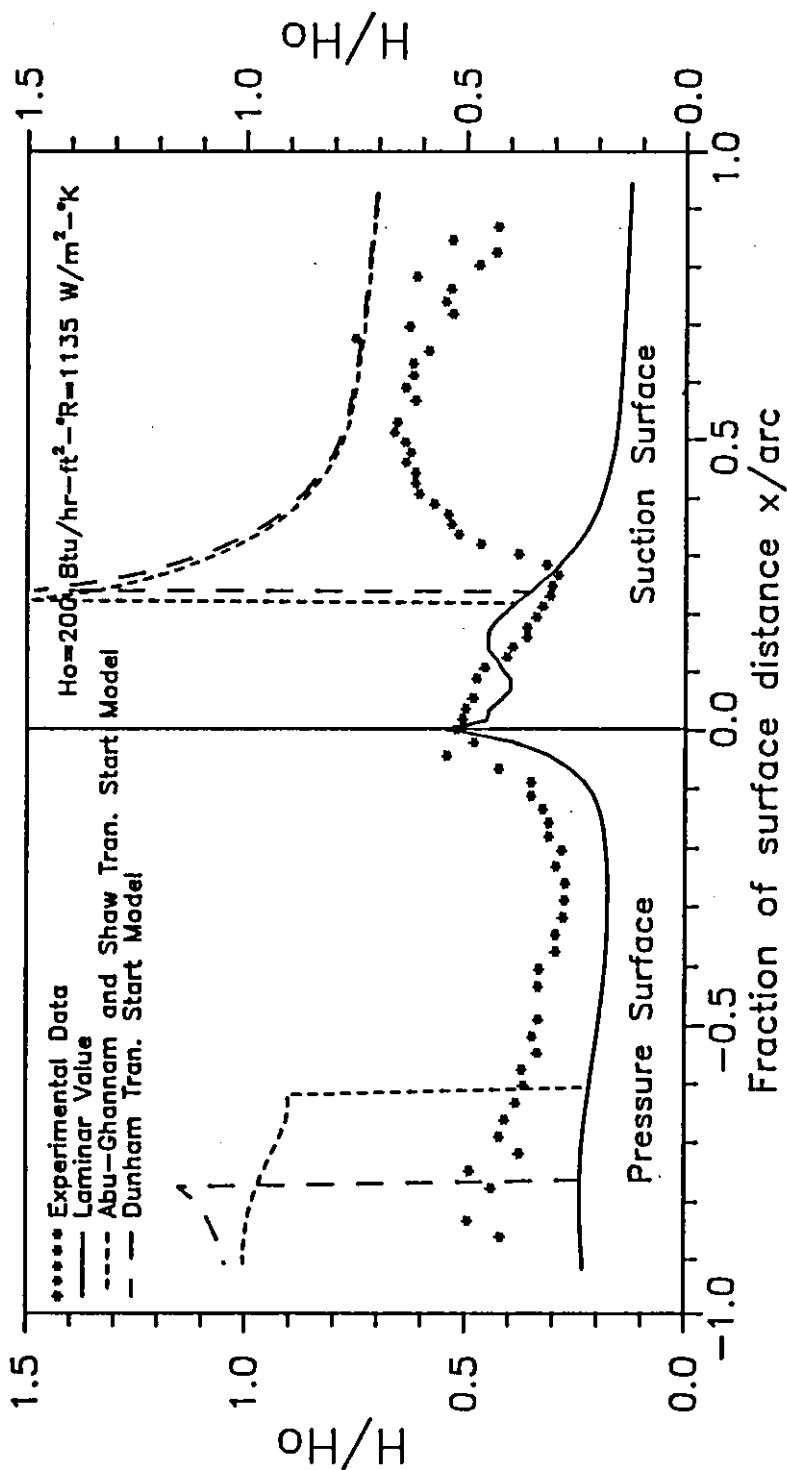


Figure (5.14) Heat transfer coefficient distribution. Modified solution results obtained for determination of best transition start model (Step No. 2).

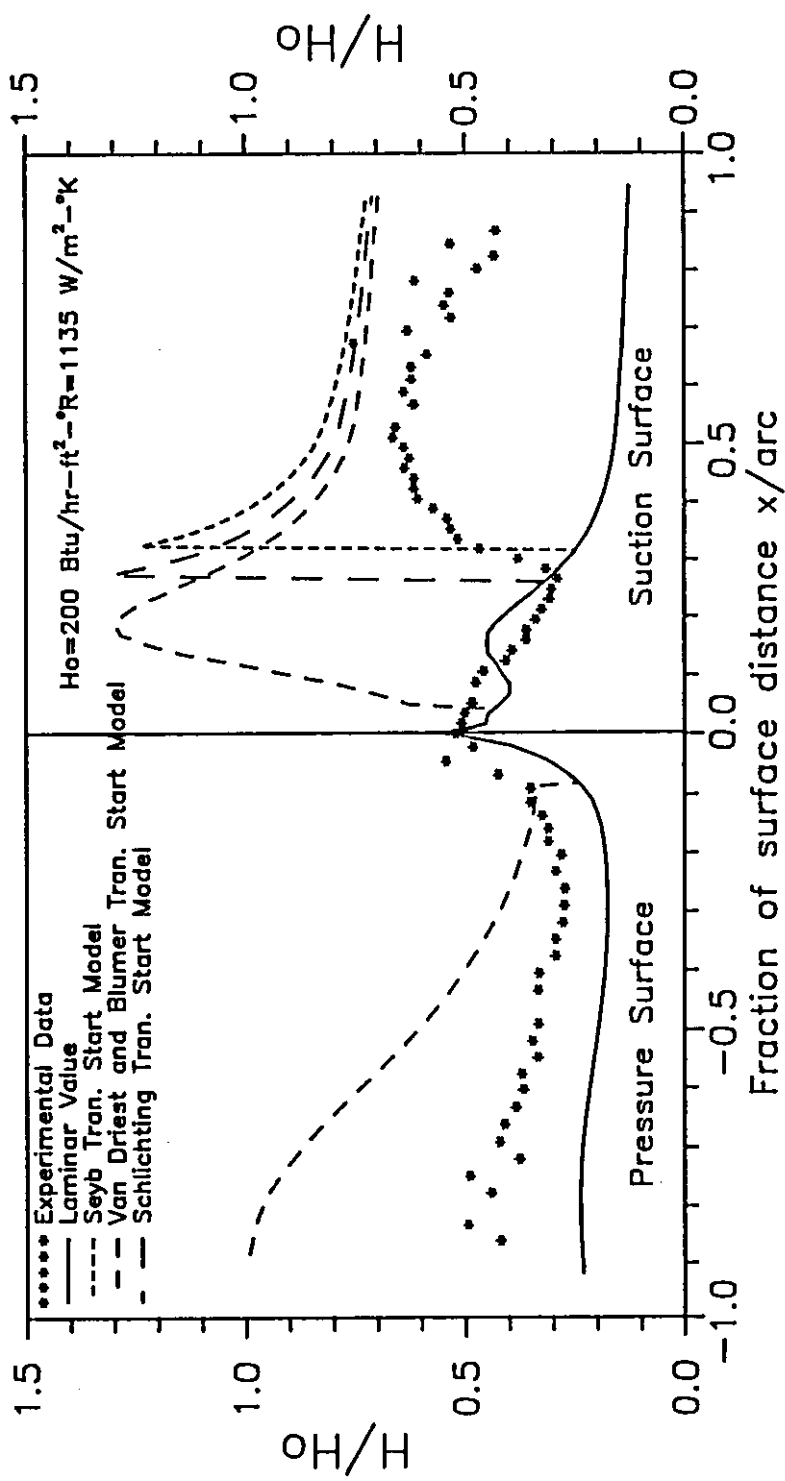


Figure (5.15) Heat transfer coefficient distribution. Modified solution results obtained for determination of best transition start model (Step No. 2).

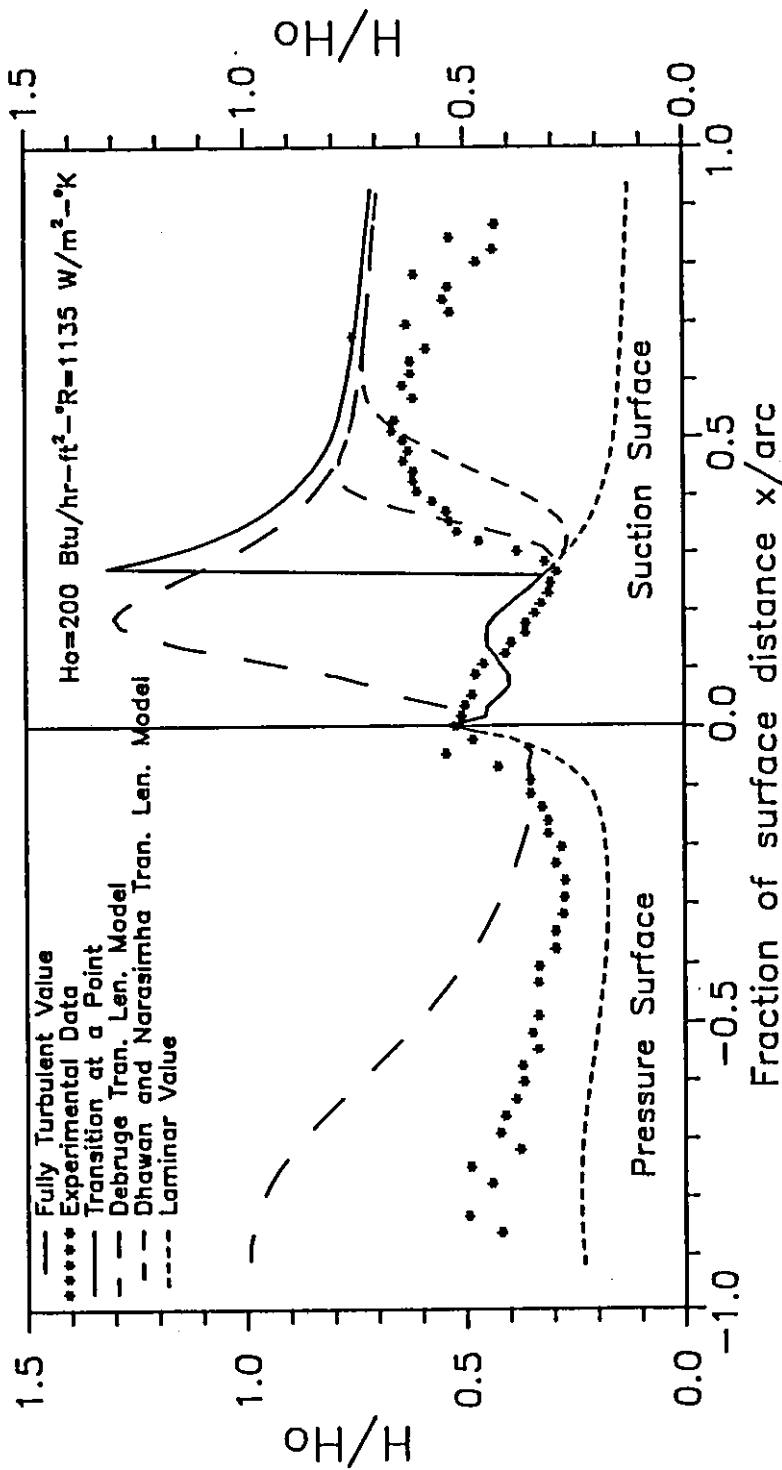


Figure (5.16) Heat transfer coefficient distribution. Modified solution results obtained for determination of best transition length model (Step No. 3).

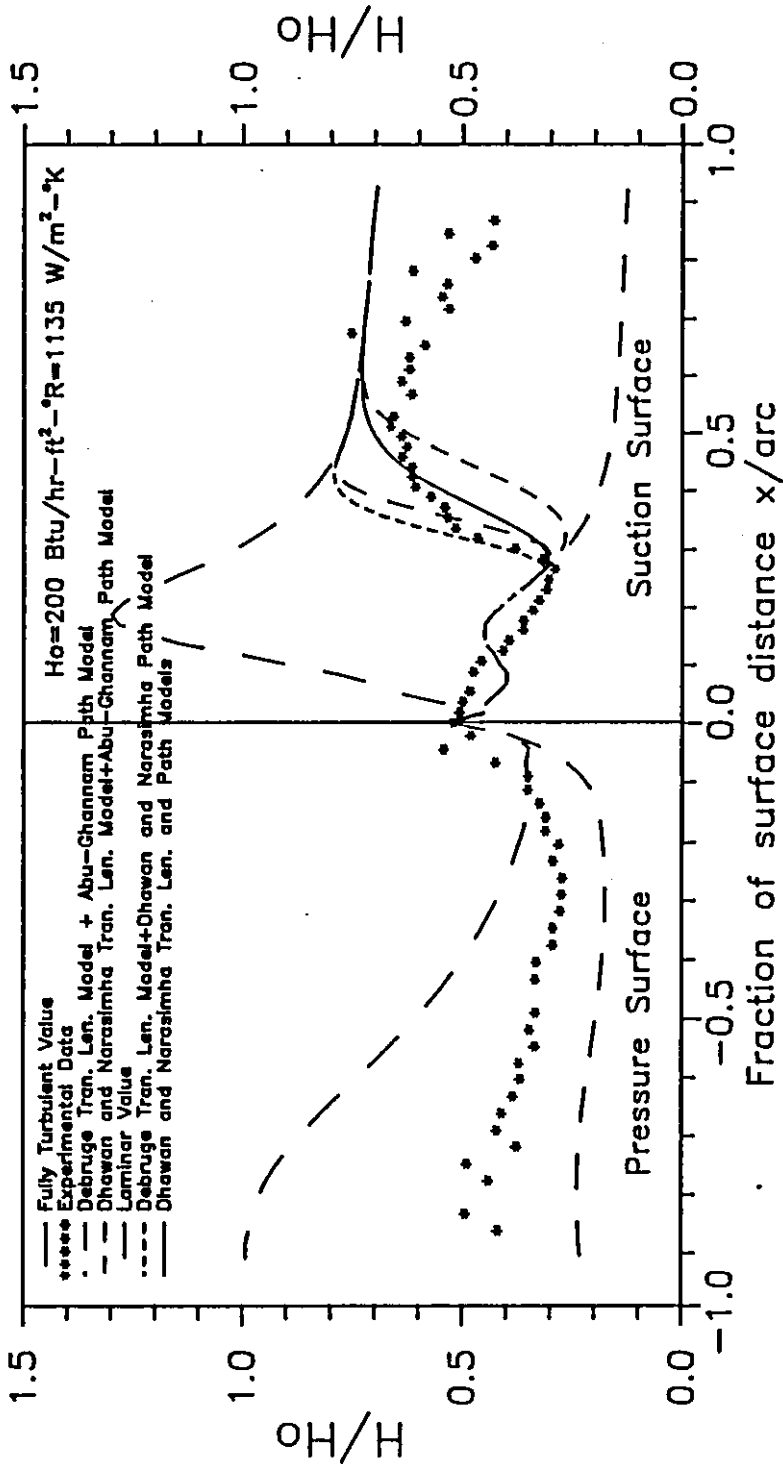


Figure (5.17) Heat transfer coefficient distribution. Modified solution results obtained for determination of best transition path (intermittency) model (Step No. 4).

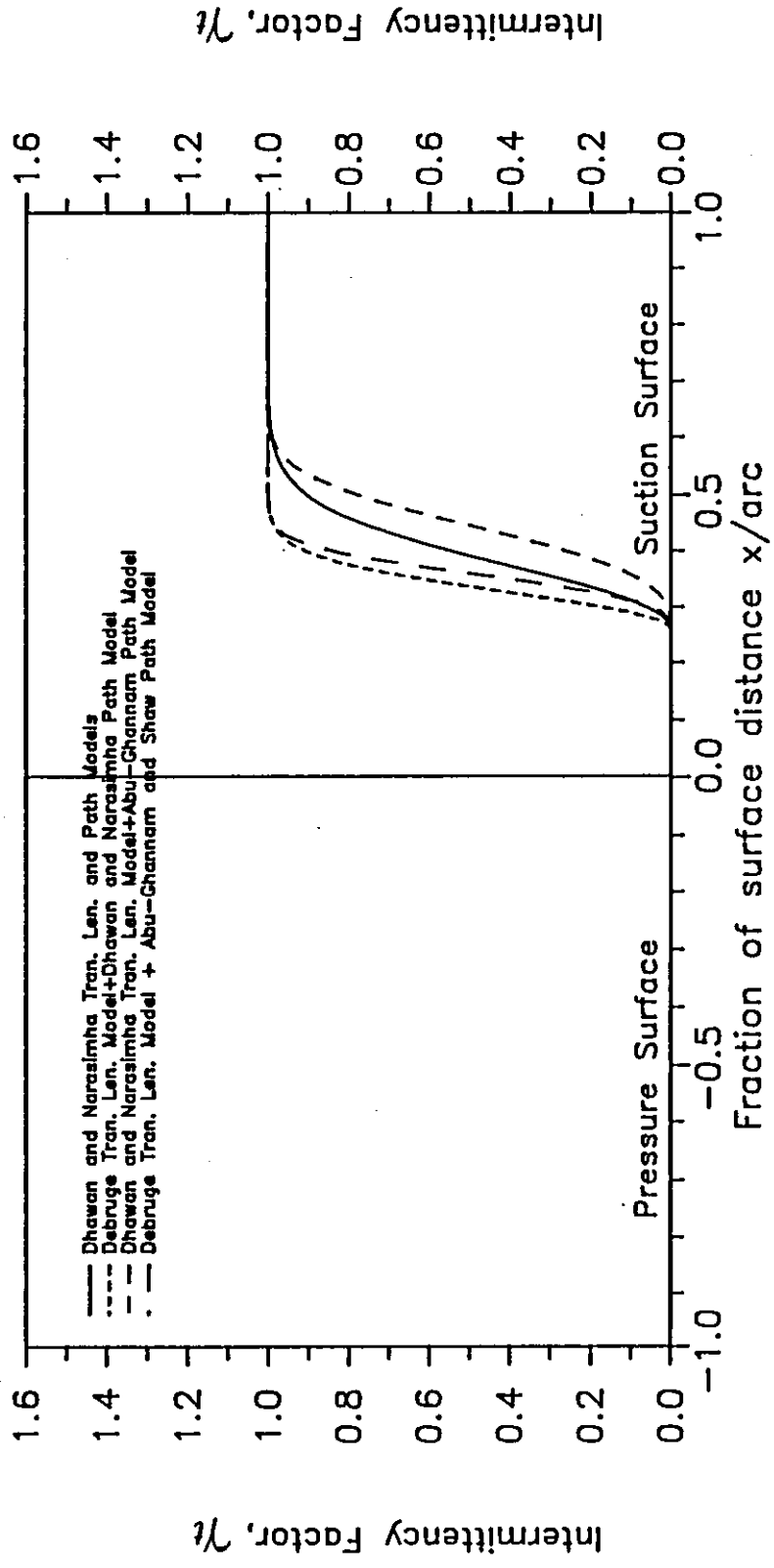


Figure (5.18) Intermittency factor ( $\gamma_t$ ) distribution.

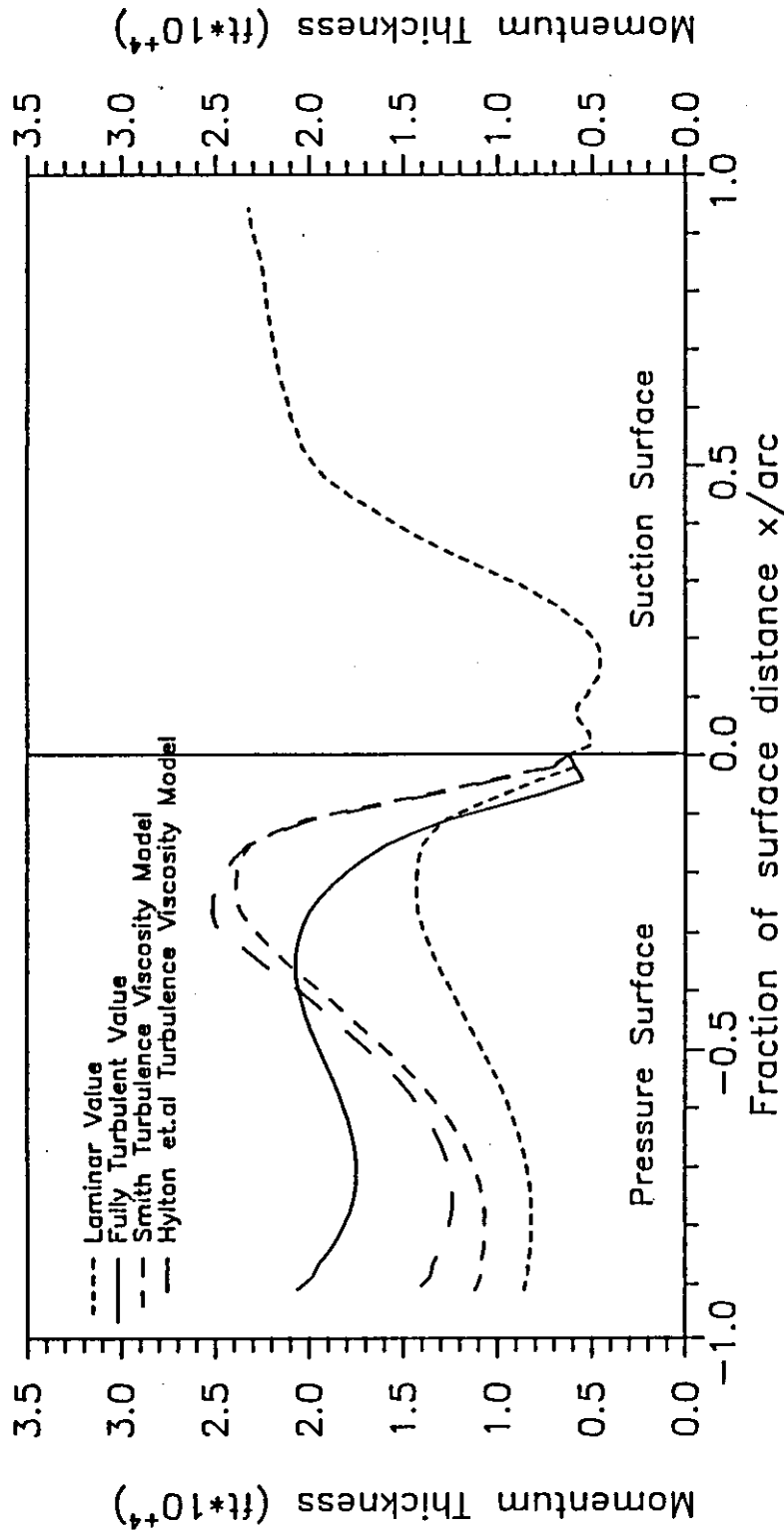


Figure (5.19) Momentum thickness distribution. Pressure surface computational process step No. 1 and 2.

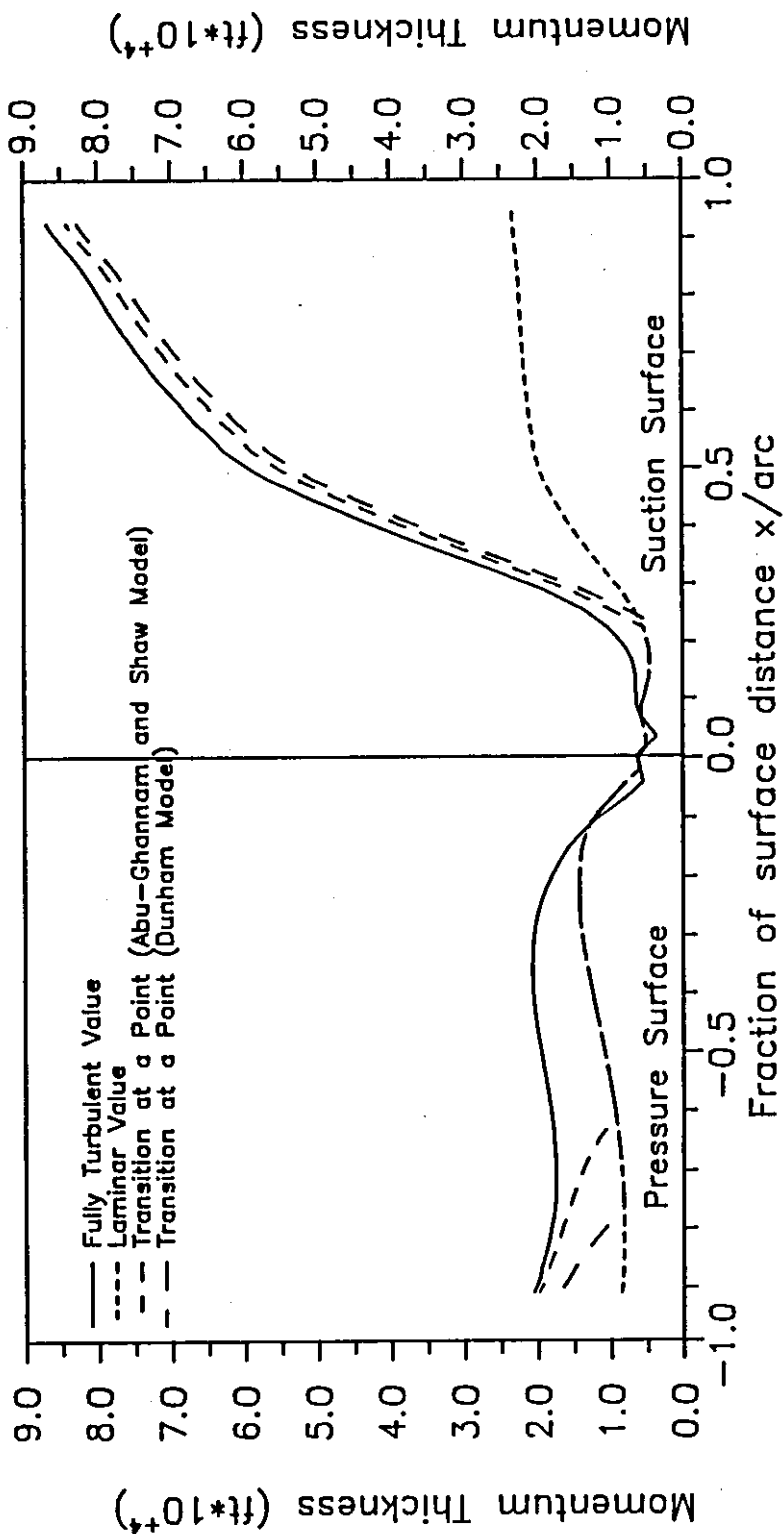


Figure (5.20) Momentum thickness distribution. Suction surface computational process step No. 1 and 2.



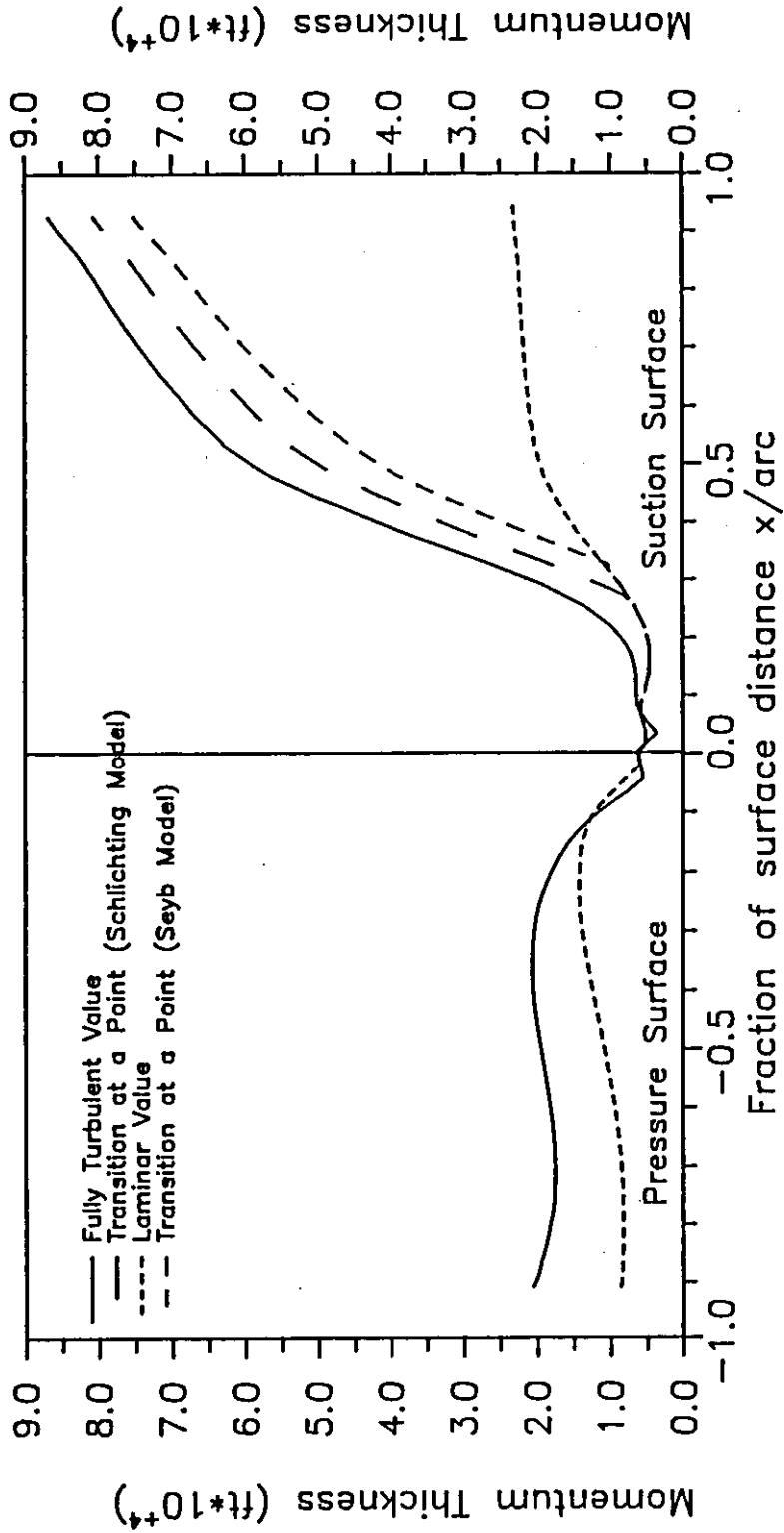


Figure (5.21) Momentum thickness distribution. Suction surface computational process step No. 1 and 2.

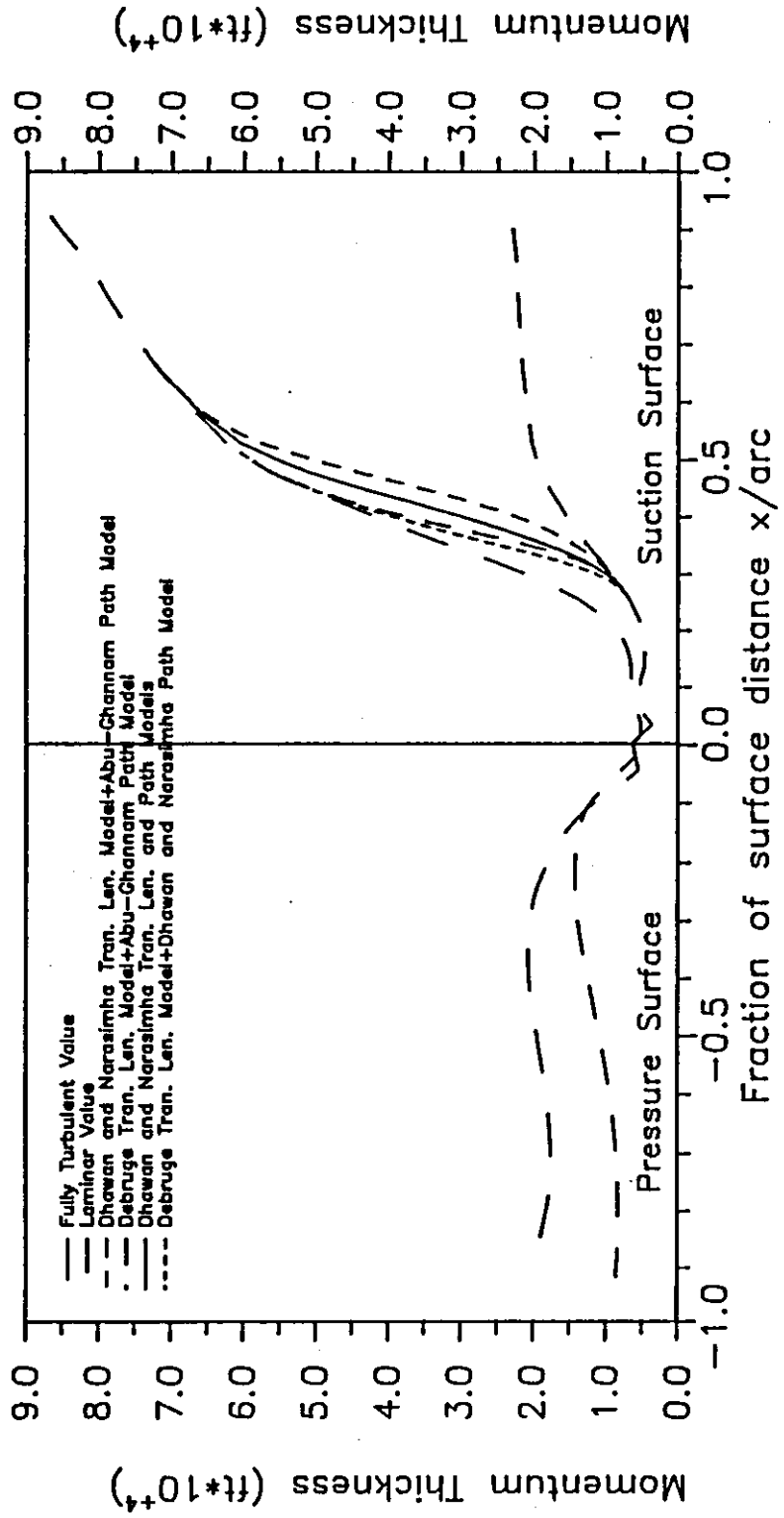


Figure (5.22) Momentum thickness distribution. Suction surface computational process step No. 3 and 4.

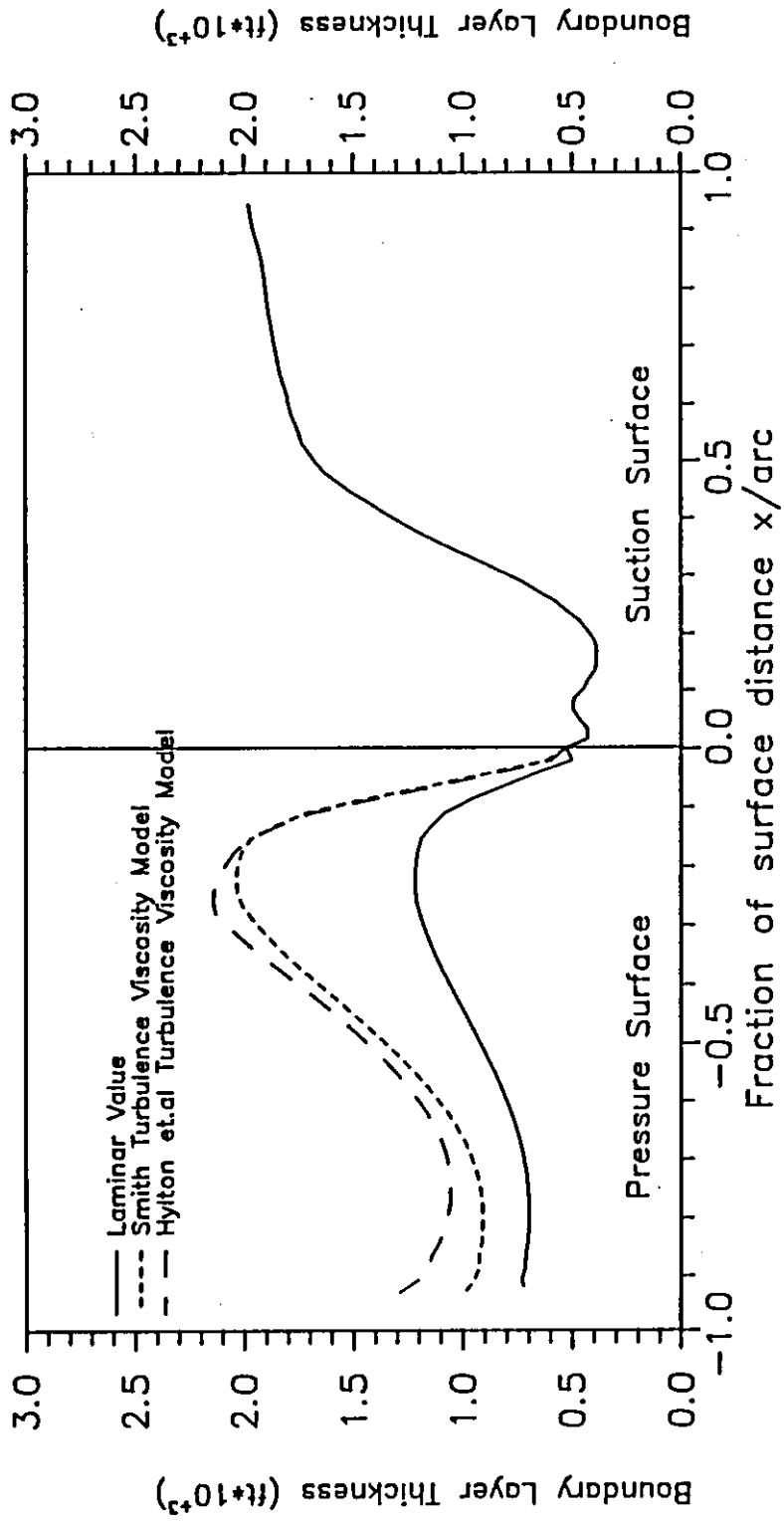


Figure (5.23) Boundary layer thickness distribution.

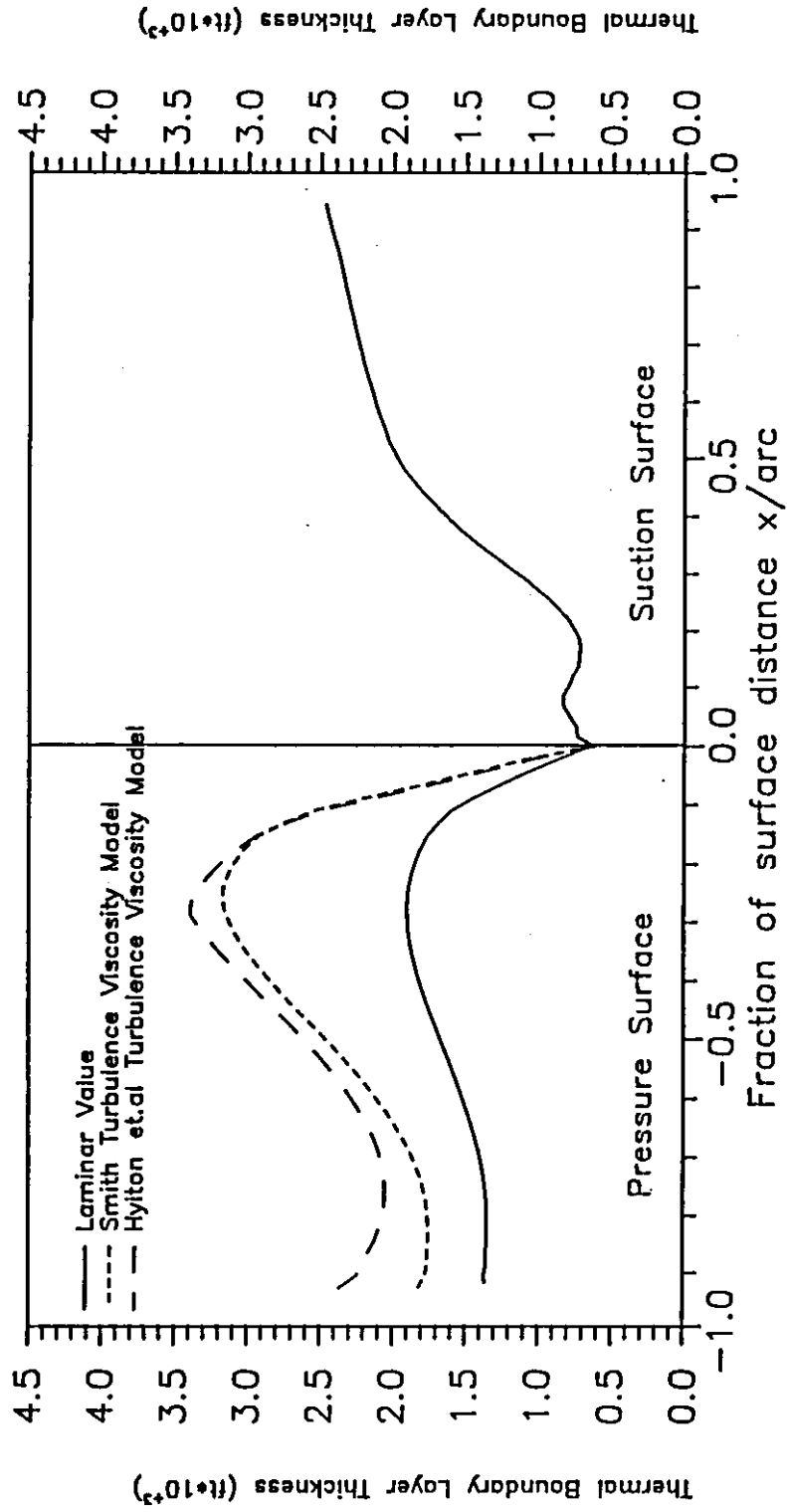


Figure (5.24) Thermal boundary layer thickness distribution.

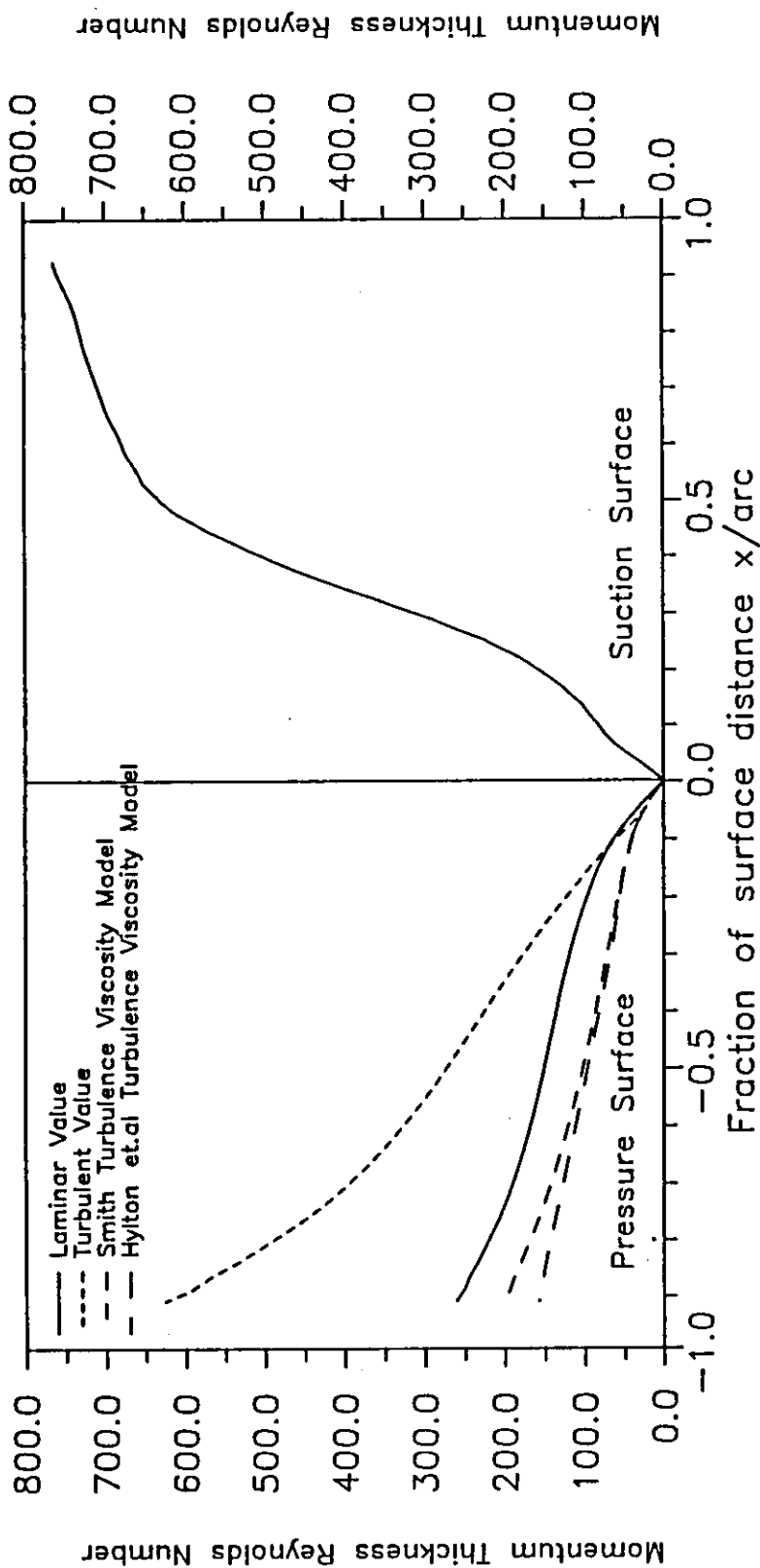


Figure (5.25) Momentum thickness Reynolds number distribution. Pressure surface computational process step No. 1 and 2.

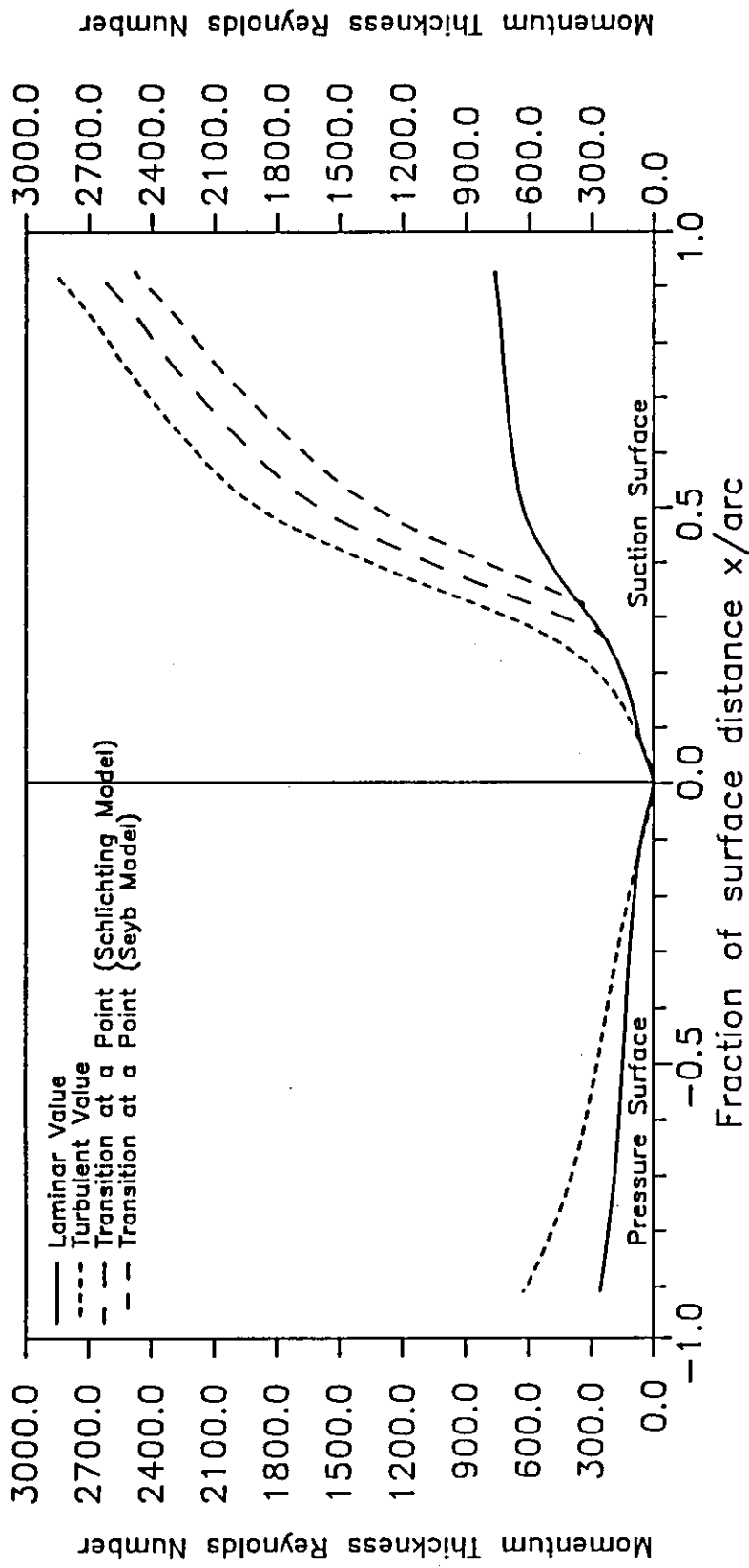


Figure (5.26) Momentum thickness Reynolds number distribution. Suction surface computational process step No. 1 and 2.

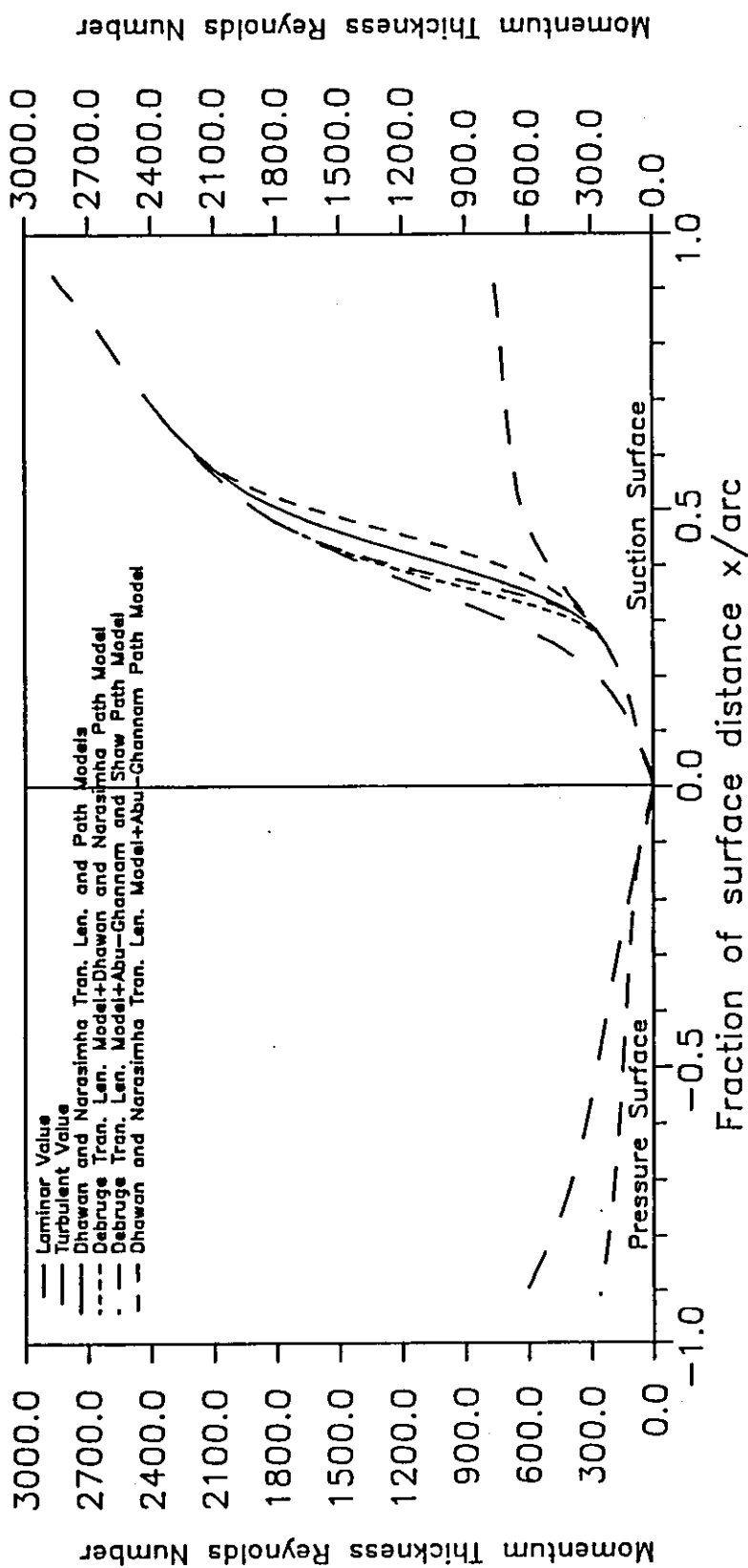


Figure (5.27) Momentum thickness Reynolds number distribution. Suction surface computational process step No. 3 and 4.

# APPENDIX A

## Derivation of the momentum and energy integral equations for the boundary layer

For steady, two-dimensional, and incompressible boundary layer flow, the equations of motion for the boundary layer simplifies to:

$$u \frac{\partial u}{\partial x} + v \frac{\partial u}{\partial y} = -\frac{1}{\rho} \frac{dP}{dx} + \nu \frac{\partial^2 u}{\partial y^2} - \frac{\partial}{\partial y}(\overline{u'v'}) \quad (\text{A.1})$$

$$\frac{\partial u}{\partial x} + \frac{\partial v}{\partial y} = 0 \quad (\text{A.2})$$

with the boundary conditions :

$$y = 0 ; u = 0 ; v = 0$$

$$y = \infty ; u = U(x)$$

Upon integrating the equation of motion (A.1) with respect to  $y$ , from  $y = 0$  (wall) to  $y = h$ , such that  $y = h$  is every where outside the boundary layer, the following is obtained :

$$\int_{y=0}^h \left( u \frac{\partial u}{\partial x} + v \frac{\partial u}{\partial y} - U \frac{dU}{dx} \right) dy = \frac{-\tau_o}{\rho} \quad (\text{A.3})$$

The shearing stress at the wall  $\tau_o$ , has been substituted for  $\mu \left( \frac{\partial u}{\partial y} \right)_o$ , so that equation (A.3) is seen to be valid both for laminar and turbulent flows, on condition that in the



later case  $u$  and  $v$  denote the time averages of the respective velocity components.

The normal velocity component  $v$ , can be replaced by  $v = -\int_0^y \left(\frac{\partial u}{\partial x}\right) dy$ , as seen from the equation of continuity (A.2), and, consequently, the following is obtained :

$$\int_{y=0}^h \left( u \frac{\partial u}{\partial x} - \frac{\partial u}{\partial y} \int_0^y \frac{\partial u}{\partial x} dy - U \frac{dU}{dx} \right) dy = \frac{-\tau_o}{\rho}$$

Integrating by parts, the second term in the above equation may be written as,

$$\int_{y=0}^h \left( \frac{\partial u}{\partial y} \int_0^y \frac{\partial u}{\partial x} dy \right) dy = U \int_0^h \frac{\partial u}{\partial x} dy - \int_0^h u \frac{\partial u}{\partial x} dy$$

so that,

$$\int_0^h \left( 2u \frac{\partial u}{\partial x} - U \frac{\partial u}{\partial x} - U \frac{dU}{dx} \right) dy = \frac{-\tau_o}{\rho}$$

which can be written in the following form :

$$\int_0^h \frac{\partial}{\partial x} [u(U-u)] dy + \frac{dU}{dx} \int_0^h (U-u) dy = \frac{\tau_o}{\rho} \quad (A.4)$$

Since in both integrals the integrand vanishes outside the boundary layer, it is permissible to put  $h \rightarrow \infty$ .

The displacement thickness  $\delta_1$  and the momentum thickness  $\delta_2$  are defined by :

$$\delta_1 U = \int_{y=0}^{\infty} (U-u) dy \quad (A.5)$$

and,

$$\delta_2 U^2 = \int_{y=0}^{\infty} u(U-u) dy \quad (A.6)$$

Thus  $\delta_1$  is a measure of the displacement of the main stream resulting from the presence of the body (blade) and its boundary layer. Similarly  $\delta_2$  is a measure of the momentum flux decrement caused by the boundary layer, which according to the momentum theorem, is proportional to the drag of the body.

It should be noted that in the first term of equation (A.4), differentiation with respect to  $x$ , and integration with respect to  $y$ , may be interchanged as the upper limit  $h$  is independent of  $x$ .

Substituting equation (A.5) and equation (A.6) into equation (A.4), then

$$\frac{\tau_o}{\rho} = \frac{d}{dx} (U^2 \delta_2) + \delta_1 U \frac{dU}{dx} \quad (\text{A.7})$$

or using the shape factor  $H_{12} = \frac{\delta_1}{\delta_2}$ ,

$$\frac{\tau_o}{\rho U^2} = \frac{d\delta_2}{dx} + (H_{12} + 2) \frac{\delta_2}{U} \frac{dU}{dx} \quad (\text{A.8})$$

This is the momentum-integral equation for two-dimensional, incompressible boundary layers. As long as no statement is made concerning  $\tau_o$ , equations (A.7) or (A.8) applies to laminar and turbulent boundary layers alike.

Using similar approach, the energy-integral equation is obtained by multiplying the equation of motion (A.1) by  $u$  and then integrating from  $y = 0$  to  $y = h > \delta(x)$ .

Substituting, again,  $v$  from the equation of continuity (A.2), the following is obtained :

$$\rho \int_0^h \left[ u^2 \frac{\partial u}{\partial x} - u \frac{\partial u}{\partial y} \left( \int_0^y \frac{\partial u}{\partial x} dy \right) - uU \frac{dU}{dx} \right] dy = \mu \int_0^h u \frac{\partial^2 u}{\partial y^2} dy$$

The second term can be transformed by integration by parts :

$$\int_0^h \left[ u \frac{\partial u}{\partial y} \left( \int_0^y \frac{\partial u}{\partial x} dy \right) \right] dy = \frac{1}{2} \int_0^h (U^2 - u^2) \frac{\partial u}{\partial x} dy$$

Furthermore, by combining the first term with the third term, the following is obtained,

$$\int_0^h \left[ u^2 \frac{\partial u}{\partial x} - uU \frac{dU}{dx} \right] dy = \frac{1}{2} \int_0^h u \frac{d}{dx} [u^2 - U^2] dy$$

Finally, upon integrating the right-hand side by parts, the following is obtained :

$$\frac{1}{2} \rho \frac{d}{dx} \int_0^\infty u (U^2 - u^2) dy = \mu \int_0^\infty \left( \frac{\partial u}{\partial y} \right)^2 dy \quad (\text{A.9})$$

Again, the upper limit of integration may be replaced by  $y = \infty$ , because the integrands become equal to zero outside the boundary layer. The quantity  $\mu \left( \frac{\partial u}{\partial y} \right)^2$  represents the energy, per unit volume and time, which is transformed into heat by friction (dissipation). The term  $\frac{1}{2}\rho(U^2 - u^2)$  on the left-hand side represents the loss in mechanical energy (kinetic and pressure energy) taking place in the boundary layer as compared with the potential flow. Hence the term  $\frac{1}{2}\rho \int_0^\infty u(U^2 - u^2) dy$  represents the flux of dissipated energy, and the left-hand side of equation (A.9) represents the rate of change of the flux of dissipated energy per unit length in the x-direction.

Introducing the dissipation-energy thickness,  $\delta_3$ , from the definition :

$$U^3 \delta_3 = \int_0^\infty u (U^2 - u^2) dy \quad (\text{A.10})$$

Rewriting the energy-integral equation (A.9) using the definition of  $\delta_3$ , then,

$$\frac{d}{dx} (U^3 \delta_3) = 2\nu \int_0^\infty \left( \frac{\partial u}{\partial y} \right)^2 dy \quad (\text{A.11})$$

or,

$$\frac{d}{dx} (U^3 \delta_3) = 2 \int_0^\infty \frac{\tau}{\rho} \left( \frac{\partial u}{\partial y} \right) dy \quad (\text{A.12})$$

which represents the energy-integral equation for two-dimensional, incompressible boundary layer flow.

# APPENDIX B

## Literature figures

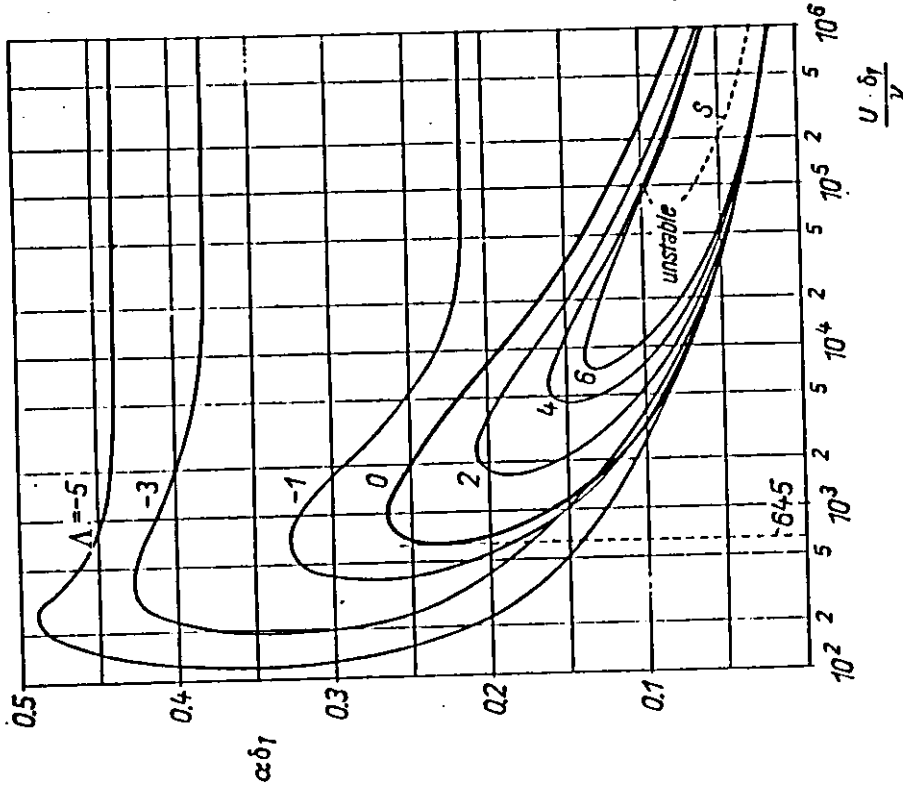


Figure (3.4) Curves of neutral stability for laminar boundary layer profiles with pressure decrease ( $\Lambda > 0.0$ ) and pressure increase ( $\Lambda < 0.0$ ). [24]

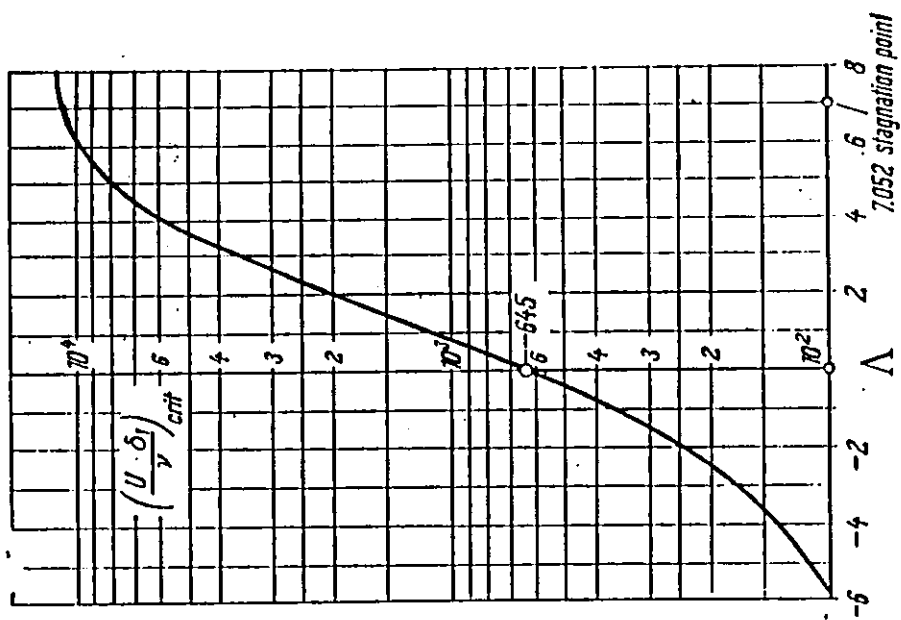


Figure (3.5) Critical displacement thickness Reynolds number of boundary layer velocity profiles with pressure gradient as a function of the shape factor ( $\Lambda$ ). [24]

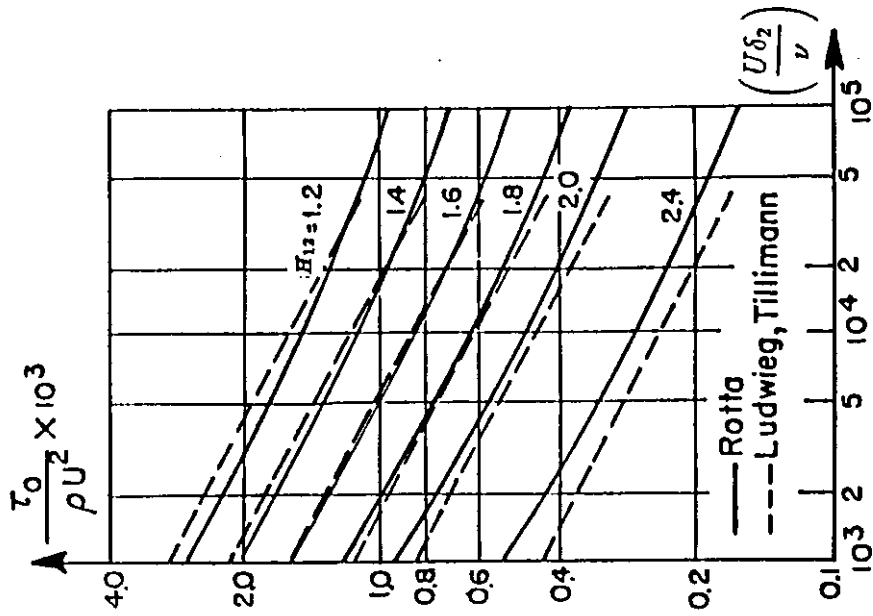


Figure (3.6) Turbulent wall-shear stress (according to H. Ludwig, W. Tillmann, and J. Rotta). [26]

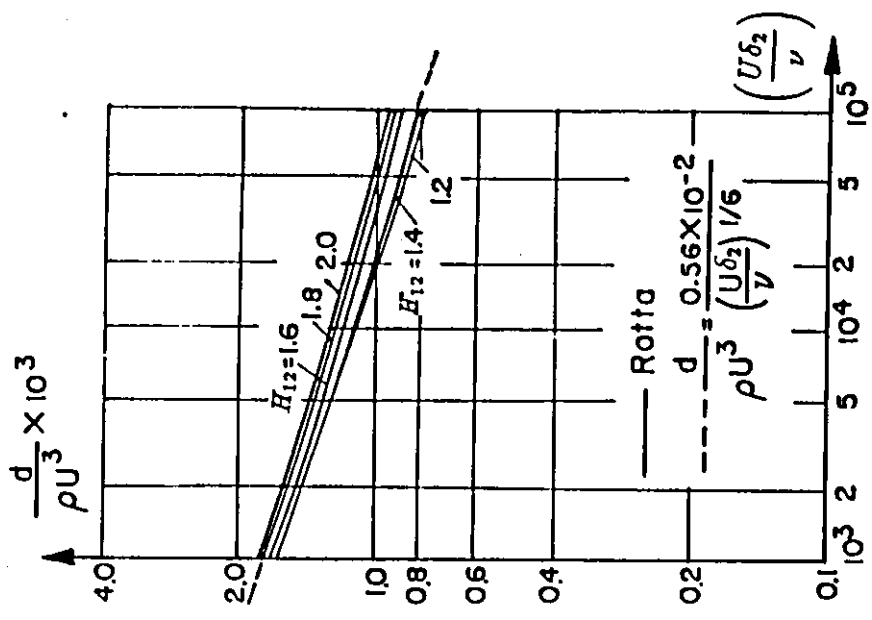


Figure (3.7) Turbulent dissipation (according to J. Rotta). [26]



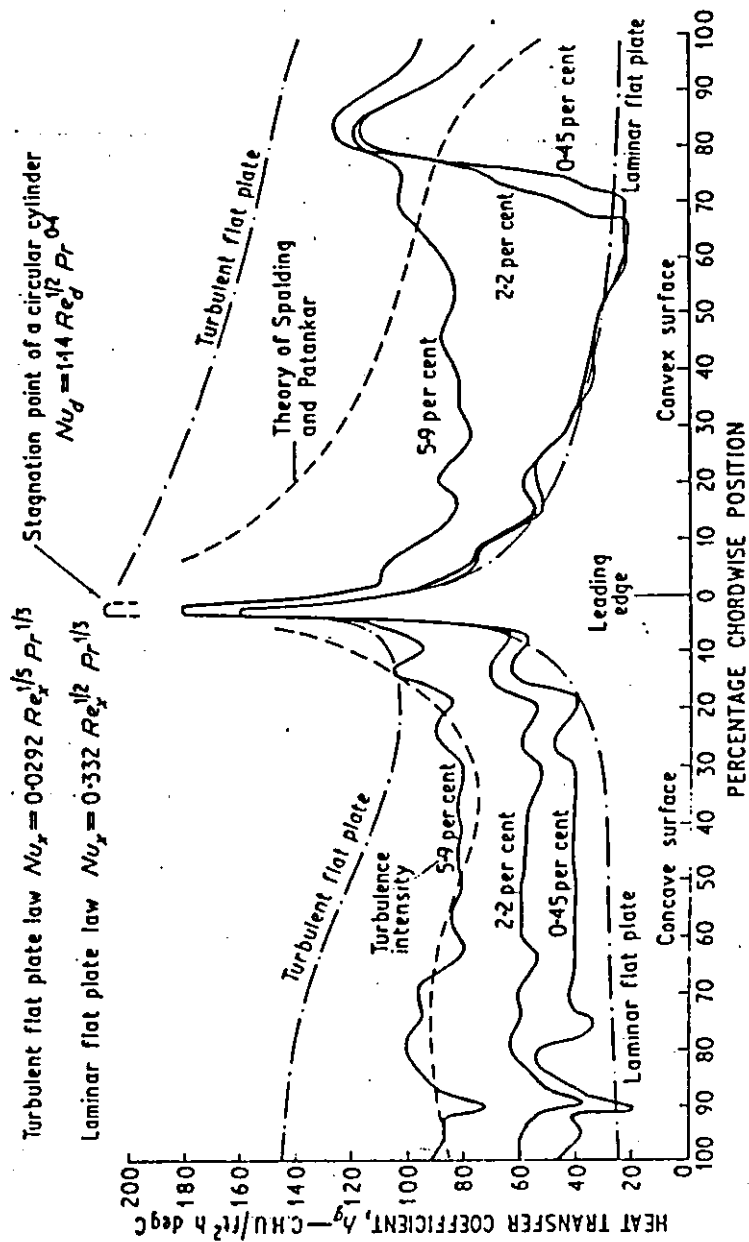


Figure (4.1) Experimental distribution of heat transfer coefficient for an exit Mach number of 0.75 (according to Turner [19]).

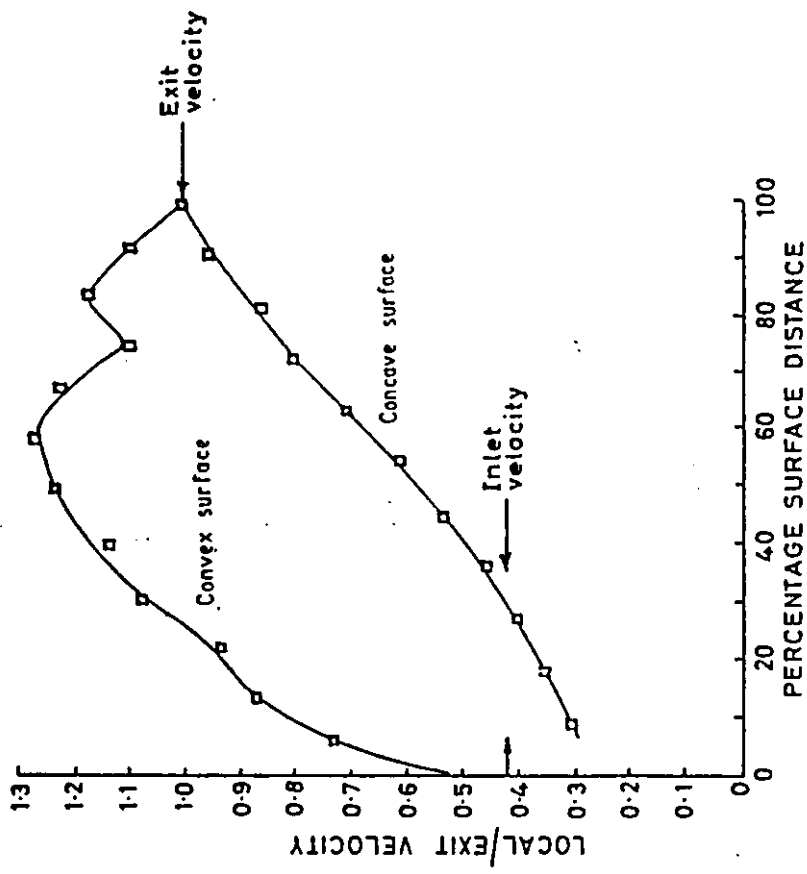


Figure (4.2) Turner blade experimental velocity distribution (Mach number 0.77) [19].

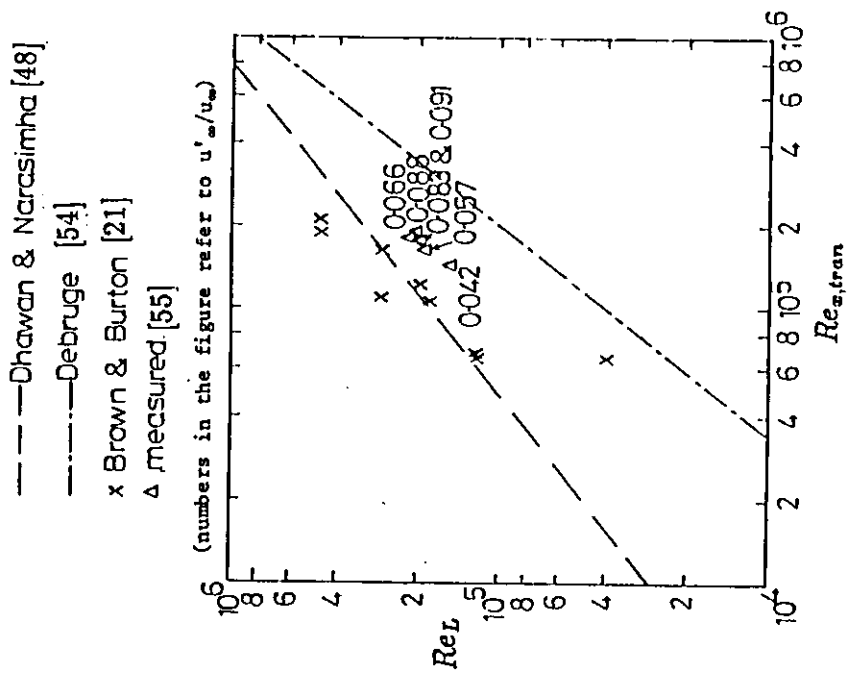


Figure (4.3) Variation of length of transition with the position of start of transition. [55]

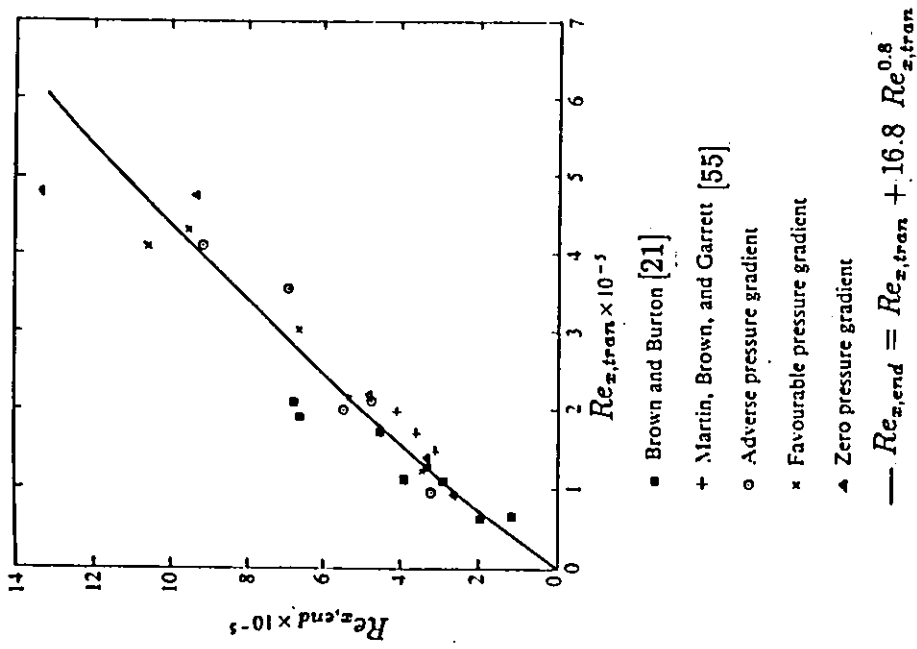
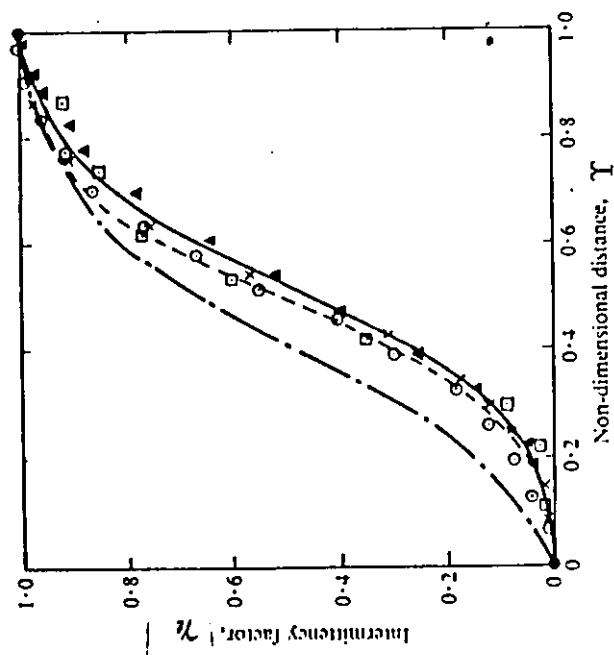


Figure (4.4) Relation between the end and start of transition Reynolds numbers. [52]



- Fixed tunnel velocity,  $U_R = 20$  m/s } Zero pressure
- × Fixed chordwise station,  $X = 29$  in } gradient
- Adverse pressure gradient,  $X = 20$  in
- ▲ Favourable pressure gradient,  $X = 29$  in
- $\gamma_i = 1 - \exp(-4.65 \Upsilon^3)$
- - - Schubauer and Klebanoff curve
- · - Dhawan and Narasimha curve  $\gamma_i = 1 - \exp[-4.65 \Upsilon^2]$

Figure (4.5) Development of the intermittency factor during transition. [52]

# APPENDIX C

Integral method Fortran program

```

C $$$$$$$$$$$$$$$$$$
C $$ MAIN PROGRAM $$
C $$$$$$$$$$$$$$$$$$
C This is the main program. It is divided into two basic parts :laminar
C boundary layer and turbulent boundary layer. Initially the program
C reads in the input data,calculates the initial conditions of the
C laminar boundary layer,iterates through the laminar calculations
C until transition is reached,then proceeds into the turbulent section
C and iterates until the end of the blade is reached. All integrations
C are performed in the program and are basically trapezoidal.
C
C *****
C *****
C $$$$$$$$$$$$$$$$$$
C $$ VLOCT(alternate entry CURVE) $$
C $$$$$$$$$$$$$$$$$$
C This routine reads in the velocity profile versus surface distance.
C It uses the alternate entry to find the velocity and the first and
C second derivatives for a given surface distance .It should be noted
C that the first and second derivatives are somewhat inaccurate since
C they are based upon a finite length rather than a point .
C Uses subroutine TLOOK
C
C *****
C *****
C $$$$$$$$$$$$$$
C $$ DTFRMX $$
C $$$$$$$$$$$$$$
C This routine solves the universal function of DELTA for DELTA greater
C than 1.0 .It iteratively solves for the unknown DELTA given H(DELTA).
C Uses subroutine AFQUIR.
C
C *****
C *****
C $$$$$$$$$$$$$$
C $$ PRANX $$
C $$$$$$$$$$$$$$
C This routine looks up in a table the constant used in the heat-
C transfer equation near the stagnation point as a function of the
C prandtl number .
C Uses subroutine SRCHX
C
C *****
C *****
C $$$$$$$$$$$$$$
C $$ PROPEX $$
C $$$$$$$$$$$$$$
C This routine calculates the viscosity,density,prandtl number,and
C specific heat of air as a function of temperature and pressure .
C Uses subroutine PROCOM and TLOOK .
C
C *****
C *****
C $$$$$$$$$$$$$$
C $$ TLOOKX $$
C $$$$$$$$$$$$$$
C The function subprogram TLOOK is a general purpose routine to perform
C a table look-up in a two-dimensional table (dependent variable versus
C independent variable).It first locates the input independent variable

```

```

C in its table,then takes the nearest 'N'pairs of points and calls sub-
C routine LAGRNG. This program uses an interpolating polynomial of
C degree 'N-1',in the Lagrangian form,to evaluate the dependent variable.
C TLOOK also has the capability of remembering where it found the inde-
C pendent variable in the table . Thus,search time is saved when the
C next time it is called the independent variable has changed only
C slightly.
C Uses subroutine LAGRNG.
C
C *****
C *****
C $$$$$$$$$$$$
C $$ LAGRNG $$
C $$$$$$$$$$$$
C See description of TLOOK
C
C *****
C *****
C $$$$$$$$$$$$
C $$ SRCHXX $$
C $$$$$$$$$$$$
C This subprogram is a table lookup routine using linear interpolation.
C
C *****
C *****
C $$$$$$$$$$$$
C $$ PROCOM $$
C $$$$$$$$$$$$
C This routine calculates the thermodynamic properties of air or air-
C JP4 mixtures.Given temperature and fuel-air ratio,it calculates speed
C of sound,ratio of specific heats,specific heat of constant pressure,
C gas constant,and nonpressure biased entropy and enthalpy.
C
C *****
C *****
C $$$$$$$$$$$$
C $$ AFQUIR $$
C $$$$$$$$$$$$
C This program is a quadratic convergence routine.It is a routine having
C general application and is used to converge practically any function .
C
C *****
C *****
C $$$$$$$$$$$$
C $$ CRITXX $$
C $$$$$$$$$$$$
C This routine takes an input shape factor(ALAM)and looks up on a curve
C the critical Reynolds number.
C Uses subroutine SRCHX.
C
C *****
C *****
C $$$$$$$$$$$$$$$$$$$$
C $$ INPUT VARIABLES $$
C $$$$$$$$$$$$$$$$$$$$
C NUMB : number of points in velocity profile curve(velocity versus
C surface distance curve).
C XS, X : surface distance.
C VS, UX : surface velocity.

```





```

OPEN(6,FILE='O.OUT',STATUS='NEW')
CALL READIN(XMAX)
ALENTH=0.4755
TTZERO=1431
PTZERO=35.58
UCRIT=1666.22
AK=1.3
UIN=303.
ARC=.583417
DIA=0.0767
DX=1.E-5
PRINT=1.E-2
R=DIA/2.
AINT=0.0
BINT=0.0
VISKI=0.0
URATI1=0.0
URATI2=0.0
X=0.0
UX5=0.0
I=0
IBIN=1
ALAMO=7.053

```

```

C *****
C *****
C ***** START OF LAMINAR *****
C *****
C *****
C *****
C *****
C *****
C *****

```

X=ZERO CALCULATIONS

```

DXB=DX
ALAM=7.0529
X=0.0
CALL CURVE(X,DXB,UX,UPX,UPPX)
T=TTZERO
P=PTZERO
CALL PROPER(T,P,AMU,RHO,PN,CP)
VISK=AMU/RHO
VISK0=VISK
CFL=1.328/SQRT(UIN*ALENTH/VISK0)
DEL=SQRT(ALAM*VISK/UPX)
THETA=0.11746*DEL
DELSTR=(2.554-0.0709*ALAM)*THETA
CALL PRAN(PN,CONST1)
AND=2.*CONST1*SQRT(UIN*DIA/VISK)
DELT=2.*DIA/AND
RAT=DEL/DELT
H=0.3-0.3*RAT+0.13333*(RAT**2.)-0.0214286*(RAT**4.)
&+0.005555*(RAT**5.)
HL=(2.*CP*AMU/(PN*DELT))*4.6275)
TAD=T
H0=H
DELO=DEL

```

END OF X=ZERO CALCULATIONS

```

XARC=X/ARC
IPS=PRINT/DX+DX
UX5S=UX**5.

```

```

WRITE(6,100)X,UX,T
WRITE(6,101)P,VISK,THETA
WRITE(6,102)DEL,DELSTR,UDQVIS
WRITE(6,103)TRMCRT,ALAM,PN
PRINT*,X,HL,DEL,THETA,DELT
WRITE(6,104)DELTA,DELT,HL
WRITE(6,105)TAD
100 FORMAT(8H      X=,E15.7,5X,7H      UX=,E15.7,5X,7H      T=,E15.7)
101 FORMAT(8H      P=,E15.7,5X,7H      VISK=,E15.7,5X,7H      THETA=,E15.7)
102 FORMAT(8H      DEL=,E15.7,5X,7HDELSTR=,E15.7,5X,7HUDQVIS=,E15.7)
103 FORMAT(8H      TRMCRT=,E15.7,5X,7H      ALAM=,E15.7,5X,7H      PN=,E15.7)
104 FORMAT(8H      DELTA=,E15.7,5X,7H      DELT=,E15.7,5X,7H      HL=,E15.7)
105 FORMAT(8H      TAD=,E15.7)
      IP=0
      UX5=UX**5.
11      I=I+1
      AI=I
      X=AI*DX
      IP=IP+1
14      CALL CURVE(X,DX,UX,UPX,UPPX)
      IF(UX.LT.6.0)GO TO 11
      UX5=UX**5.
      T=TTZERO*(1.-((AK-1.)/(AK+1.))*(UX/UCRIT)**2.)
      P=PTZERO*((T/TTZERO)**(AK/(AK-1.)))
      CALL PROPER(T,P,AMU,RHO,PN,CP)
      VISK=AMU/RHO
      CALL PRAN(PN,CONST1)
      AND=2.*CONST1*SQRT(UIN*DIA/VISK)
      DELT0=2.*DIA/AND
      IH=1
      DEL02=ALAM0*VISK/UPX
      TERM1=DEL02*UX**6./(34.*VISK)
      UEINT1=0.0
      DTUH2=0.0
      DELAS=DELO
      DEL2AS=DELAS*DELAS
      GO TO 2
1      I=I+1
      AI=I
      X=AI*DX
      IP=IP+1
2      CONTINUE
      UX5S=UX5
      UXS=UX
      CALL CURVE(X,DX,UX,UPX,UPPX)
      UX5=UX**5.
      T=TTZERO*(1.-((AK-1.)/(AK+1.))*(UX/UCRIT)**2.)
      P=PTZERO*((T/TTZERO)**(AK/(AK-1.)))
      CALL PROPER(T,P,AMU,RHO,PN,CP)
      VISK=AMU/RHO
      VISKI=VISKI+VISK*DX
      TERM1=TERM1+((UX5+UX5S)/2.)*DX
      C=34.*VISK/((UX5*UX+UX5S*UXS)/2.)
      DEL2A=DEL2AS+C*((UX5+UX5S)/2.)*DX
      DELA=SQRT(DEL2A)
      DEL2E=C*TERM1
      DELE=SQRT(DEL2E)
      DEL=DELE
      DEL2=DEL2E
      THETA=0.11746*DEL

```

```

ALAM=DEL2*UPX/VISK
DELSTR=(2.554-0.0709*ALAM)*THETA
UDQVIS=UX*DELSTR/VISK
CALL CRITCL (ALAM,TRMCRT)
IF(UDQVIS.GE.TRMCRT)GO TO 190
GO TO (50,99),IH
C
C   USED FIRST TIME ONLY
C
50  IH-2
    X1=X
    CALL CURVE(X1,DX,UX1,UPX1,UPPX1)
    Z1=PN*(DELO*UX1*H0)**2./(4.*VISK)
    Z2=Z1+(H0*(UX1+UX)/2.)*DX
    ZZ1=DELO**2.*UX1**6./(34.*VISK)
    ZZ2=ZZ1+((UX1**5.+UX**5.)/2.)*DX
    HD2=0.11765*UX**4.*Z2/(PN*ZZ2)
    CALL DTFRM(HD2,DELTA2)
    HG=HD2/(DELTA2**2.)
    AQB=HD2/((0.11765/PN)*UX**4.)
    CQD=(HD2/((0.11765/PN)*UX**4.))*HG
    TERMC=UX*HG*DX
    TERMD=C/CQD
    TERMB=TERMD
    TERMA=B/AQB
    GO TO 108
C
C   USED ALL BUT FIRST TIME
C
99  CONTINUE
    TERMA=TERMA+((UX+UXS)/2.)*DX
    TERMB=TERMB+((UX**5.+UXS**5.)/2.)*DX
    D2HG=(0.11765/PN)*UX**4.*TERMA/TERMB
    CALL DTFRM(D2HG,DELTA1)
    HG=D2HG/(DELTA1**2.)
    TERMC=TERMC+((UX+UXS)/2.)*((HG+HS)/2.)*DX
    TERMD=TERMB
    D2HG1=(0.11765/PN)*UX**4.*TERMC/(TERMD*HG)
    CALL DTFRM(D2HG1,DELTA2)
108 H=HG
    DELTA=DELTA2
    DELT=DELTA*DEL
    HL=(2.*CP*AMU/(PN*DELT))*4.62725)
    TAD=T+(TTZERO-T)*SQRT(PN)
    DXL=DX/ALENTH
    AINT=AINT+(((UX/UIIN)**5.+(UXS/UIIN)**5.)/2.)*DXL
    C1STR=((CFL/2.)*SQRT(AINT))**1.25
    UXS=UX
    HS=H
    IF(IP.NE.IPS)GO TO 1
500 IP=0
C   XARC=X/ARC
    WRITE(6,100)X,UX,T
    WRITE(6,101)P,VISK,THETA
    WRITE(6,102)DEL,DELSTR,UDQVIS
    WRITE(6,103)TRMCRT,ALAM,PN
    WRITE(6,104)DELTA,DELT,HL
    PRINT*,X,HL,DEL,THETA,DELT
    WRITE(6,105)TAD
    GO TO 1

```

```

C *****
C *****
C ***** END OF LAMINAR *****
C *****
C *****
190 WRITE(6,211)X
    XARC=X/ARC
211 FORMAT(1H 16HTRANSITION AT X=,E15.7)
    WRITE(6,100)X,UX,T
    WRITE(6,101)P,VISK,THETA
    WRITE(6,102)DEL,DELSTR,UDQVIS
    WRITE(6,103)TRMCRT,ALAM,PN
    WRITE(6,104)DELTA,DELT,HL
    PRINT*, 'TRANSITION'
    PRINT*,X,HL,DEL,THETA,DELT
    WRITE(6,105)TAD
    XT=X
    VISKA=VISKI/XT
    C1STRS=C1STR
C *****
C *****
C ***** START OF TURBULENT *****
C *****
C *****
800 IF(IP.EQ.IPS)IP=0
    I=I+1
    AI=I
    UXS=UX
    X=AI*DX
    IP=IP+1
    CALL CURVE(X,DX,UX,UPX,UPPX)
    T=TTZERO*(1.-((AK-1.)/(AK+1.))*(UX/UCRIT)**2.)
    P=PTZERO*((T/TTZERO)**(AK/(AK-1.)))
    CALL PROPER(T,P,AMU,RHO,PN,CP)
    VISK=AMU/RHO
    TAD=T+(TTZERO-T)*(PN**(1./3.))
    BINT=BINT+(((UX/UIN)**3.5+(UXS/UIN)**3.5)/2.)*DXL
    CF2=0.016/((UIN*ALENTH/VISK)**0.25)
    THQL=(UX/UIN)**(-3.)*((C1STRS+CF2*BINT)**0.8)
    THETA=THQL*ALENTH
    TUQV=THETA*UX/VISK
    TAUQDU=0.0128/(TUQV**0.25)
    HX=(TAUQDU*RHO*CP*UX*(3600./778.)/
    1(1.+5.*SQRT(TAUQDU)*((PN-1.)
    2+ALOG(1.+(5./6.)*(PN-1.))))
    IF(IP.EQ.IPS) GO TO 900
825 IF(X.LT.XMAX) GO TO 800
1111 STOP
900 IP=0
    XARC=X/ARC
    WRITE(6,100)X,UX,T
    WRITE(6,101)P,VISK,THETA
    WRITE(6,901)CF2,RHO,TUQV
    PRINT*,X,HX,CF2,THETA,TUQV
    WRITE(6,902)PN,TAD,HX
901 FORMAT(8H      CF2=,E15.7,5X,7H      RHO=,E15.7,5X,7H      TUQV=,E15.7)
902 FORMAT(8H      PN=,E15.7,5X,7H      TAD=,E15.7,5X,7H      HX=,E15.7)
    GO TO 825
C *****
C *****

```

```

C ***** END OF TURBULENT *****
C *****
C *****
C     END
C *****
C *****
C *****
C
C     SUBROUTINE READIN(XMAX)
C     DIMENSION XS(200),VS(200)
C     OPEN(3,FILE='N.OUT',STATUS='OLD')
C     READ(3,100)NUMB
C     OPEN(4,FILE='v1.OUT',STATUS='OLD')
C     READ(4,*)(XS(I),VS(I),I=1,NUMB)
100  FORMAT(I3)
C 101  FORMAT(2F20.0)
C     DO 1 I=1,NUMB
C     T=I
C     1  XS(T)=XS(I)/12.
C 1    XS(T)=XS(I)
C     XMAX=XS(T)
C     RETURN
C     ENTRY CURVE(X,DX,UE,UEP,UEPP)
C     X1=X+DX
C     X2=X1+DX
C     K=0
C     NPT=4
C     UE=TLOOK(X,XS,VS,NUMB,NPT,K,ILAST)
C     UE1=TLOOK(X1,XS,VS,NUMB,NPT,K,ILAST)
C     UE2=TLOOK(X2,XS,VS,NUMB,NPT,K,ILAST)
C     UEP=((UE1-UE)/(X1-X))
C     UEPX=((UE2-UE1)/(X2-X1))
C     UEPP=((UEPX-UEP)/(X1-X))
C     RETURN
C     END
C
C *****
C *****
C
C     SUBROUTINE DTFRM(ANS,DEL)
C     DIMENSION Q(9)
C     Q(2)=0.0
C     Q(3)=0.0
C     AJ=50.
C     TOL=0.0001
C     DIR=1.01
C     TRY=1.5
C     1  TRY2=TRY*TRY
C     TERM=0.3*TRY2-0.3*TRY+0.13333-(0.0214286/TRY2)+
C     &0.005555/(TRY2*TRY)
C     CALL AFQUIR(Q,TRY,TERM,ANS,AJ,TOL,DIR,ANEW,ICON)
C     IF(ICON.EQ.3)GO TO 5
C     IF(ICON.EQ.2)GO TO 10
C     TRY=ANEW
C     GO TO 1
C     5  WRITE(6,100)ANS
100  FORMAT(1H0,19HERROR IN DELTA,ANS=,E15.7)
C     10  DEL=TRY
C     RETURN
C     END

```

```

C
C *****
C *****
C
SUBROUTINE PRAN(P,C)
  DIMENSION PX(9),CX(9)
  DATA (PX(I),I=1,9)/0.6,0.7,0.8,0.9,1.0,1.1,7.,10.,15./
  DATA (CX(I),I=1,9)/0.466,0.495,0.521,0.546,0.570,
&0.592,1.18,1.34,1.54/
  CALL SRCHX(P,PX(1),9,0,IL,ATERM)
  C=CX(IL)+ATERM*(CX(IL+1)-CX(IL))
  RETURN
  END
C
C *****
C *****
C
SUBROUTINE PROPER(T,P,AMU,RHO,PN,CP)
  DIMENSION HT5(31),HT6(31)
C 5 TEMPERATURE (INDEPENDENT VARIABLE TABLE)
C NUMBER OF POINTS 31
  DATA (HT5(K),K=1,31)/450.,540.,630.,720.,810.,900.,990.,1080.,1170
&.,1260.,1350.,1440.,1530.,1620.,1710.,1800.,1980.,2160.,2340.,2520
&.,2700.,2880.,3060.,3240.,3420.,3600.,3780.,3960.,4140.,4320.,4620
&./
C 6 PRANDTLE NUMBER VERSUS TEMPERATURE
C
C INDEPENDENT VECTOR AT (5)
C LENGTH 31
C NPR FOR DRY AIR
  DATA (HT6(K),K=1,31)/.722,.708,.697,.689,.683,.68,.68,.68,.682,.68
&4,.686,.689,.692,.696,.699,.702,.706,.714,.722,.726,.734,.741,.749
&.,.759,.767,.783,.803,.831,.863,.916,.972/
  NP=4
  NT=31
  KL=0
C T=DEGREES RANKIN
C P=POUNDS/SQ. IN.
C AMU=POUNDS*SEC./SQ. FT.
C RHO=POUNDS*SEC. SQ./FT.**4
C CP=FT.SQ./(SEC. SQ. DEGREE RANKIN)
C TK=BTU/(HR FT DEGREE RANKIN)
C PN=UNITLESS
C VIS=POUNDS/HR FT
C T3=DEGREES KELVIN
C RX=BTU/(POUND DEGREE RANKIN)
C CPX=BTU/(POUND DEGREE RANKIN)
  CALL PROCOM(0.0,T,X1,X2,CPX,RX,X3,X4)
  T3=0.55556*T
  VIS=0.00353*T3**1.5/(T3+110.4)
  TK=0.6325*SQRT(T3)*0.00248/(1.+245.4*10.**(-12./T3)/T3)
  PN=TLOOK(T,HT5,HT6,NT,NP,KL,ILAST)
  CP=CPX*32.174049*778.26
  AMU=VIS/(3600.*32.174049)
  RHO=(P*144./((RX*778.26*T)))/32.174049
  RETURN
  END
C
C *****
C *****

```

```

C      FUNCTION TLOOK(P,PT,QT,NT,NP,K,ILAST)
C      PT IS TABLE OF INDEPENDENT VARIABLES
C      QT IS TABLE OF DEPENDENT VARIABLES
C      NT-SIZE OF ABOVE TABLES
C      NP-NUMBER OF POINTS FOR INTERPOLATION
C      K=0,LIMIT OUTPUT TO BOUNDARY OF TABLE
C      K=1,EXTRAPOLATE FOR VALUES OUTSIDE TABLE
      DIMENSION PT(1),QT(1),XT(10),YT(10)
      IF(ILAST.LE.0)ILAST=1
      I=ILAST+1
      IF(PT(1)-PT(NT))4,15,15
C      TABLE PT IS IN ASCENDING ORDER
4      IF(PT(I).GE.P.AND.PT(ILAST).LE.P)GO TO 8
      DO 5 I=1,NT
      IF(P.LE.PT(I))GO TO 8
5      CONTINUE
      ILAST=NT-1
6      IF(K.GE.1)GO TO 7
      TLOOK=QT(NT)
      RETURN
7      IL=NT-NP+1
      GO TO 20
8      IF(I.GT.1)GO TO 10
      ILAST=1
      IF(K.GE.1)GO TO 9
      TLOOK=QT(1)
      RETURN
9      IL=1
      GO TO 20
10     ILAST=I-1
      IL=I-NP/2
      GO TO 20
C      TABLE PT IS IN DESCENDING ORDER
15     IF(PT(I).LE.P.AND.PT(ILAST).GE.P)GO TO 8
      DO 16 I=1,NT
      IF(P.GE.PT(I))GO TO 8
16     CONTINUE
      GO TO 6
20     IF(IL.LT.1)IL=1
      IF(IL.GT.NT-NP+1)IL=NT-NP+1
      DO 21 J=1,NP
      L=IL+J-1
      XT(J)=PT(L)
21     YT(J)=QT(L)
      CALL LAGRNG(P,Y,XT,YT,NP)
      TLOOK=Y
      RETURN
      END
C
C *****
C *****
C
      SUBROUTINE LAGRNG(X,Y,XT,YT,N)
C
C      THIS ROUTINE USES A LAGRANGIAN POLYNOMIAL BASED ON N TABULAR
C      POINTS TO INTERPOLATE Y AS A FUNCTION OF X IN A TWO DIMENSIONAL
C      TABLE.
C
      DIMENSION XT(1),YT(1)

```



```

DO 1 I=1,N
IF(X.EQ.XT(I))GO TO 5
1 CONTINUE
L1=1
L2=N-1
S=(XT(N)-XT(1))/ABS(XT(N)-XT(1))
6 DO 7 I=L1,L2
IF(ABS(XT(I)-XT(I+1)).GT. .001*ABS(XT(I)))GO TO 7
IF((X-XT(I))*S.LE. 0.)GO TO 8
L1=I+1
GO TO 6
8 L2=I
GO TO 9
7 CONTINUE
L2=N
9 Y=0.
DO 3 I=L1,L2
Z=1.
DO 2 J=L1,L2
IF(J.EQ.I)GO TO 2
Z=Z*(X-XT(J))/(XT(I)-XT(J))
2 CONTINUE
3 Y=Y+Z*YT(I)
RETURN
5 Y=YT(I)
RETURN
END

C
C *****
C *****
C
C SUBROUTINE SRCHX(V,VT,N,KEX,IL,C)
C
C THIS ROUTINE LOCATES V IN TABLE VT
C IF KEX=0,LIMIT OUTPUT TO TABLE BOUNDARY
C IF KEX=1,EXTRAPOLATE IF V IS OUTSIDE TABLE
C DIMENSION VT(N)
C IF(VT(2).LT.VT(1))GO TO 6
C TABLE VT IS IN ASCENDING ORDER
DO 1 I=1,N
IF(V-VT(I)) 2,2,1
1 CONTINUE
15 IL=N-1
IF(KEX.EQ.1) GO TO 3
C=1.
RETURN
2 IL=I-1
IF(I.EQ.1) GO TO 4
3 C=(V-VT(IL))/(VT(IL+1)-VT(IL))
RETURN
4 IL=1
IF(KEX.EQ.1) GO TO 3
C=0.
RETURN
C TABLE VT IS IN DESCENDING ORDER
6 DO 7 I=1,N
IF(V-VT(I)) 7,2,2
7 CONTINUE
GO TO 15
END

```

```

C
C *****
C *****
C
      SUBROUTINE PROCOM(FARX,TEX,CSEX,AKEX,CPEX,REX,SEX,HEX)
      IF(TEX-300.)2,3,3
2      WRITE(1,102)
102     FORMAT(1H 35HPROCOM INPUT TEMPERATURE BELOW 300.)
      RETURN
3      IF(TEX-4500.)5,5,4
4      WRITE(1,103)
103     FORMAT(1H 36HPROCOM INPUT TEMPERATURE ABOVE 4500.)
      RETURN
5      IF(FARX)6,7,7
6      WRITE(1,104)
104     FORMAT(1H 38HPROCOM INPUT FUEL-AIR RATIO BELOW ZERO)
      FARX=0.0
C  AIR PATH
7      CPA((((((1.0115540E-25*TEX-1.4526770E-21)*TEX
&+7.6215767E-18)*TEX-1.5128259E-14)*TEX-6.7178376E-12)
&*TEX+6.5519486E-08)*TEX-5.1536879E-05)*TEX+2.5020051E-01
      HEA((((((1.2644425E-26*TEX-2.0752522E-22)*TEX
&+1.2702630E-18)*TEX-3.0256518E-15)*TEX-1.6794594E-12)*TEX
&+2.1839826E-08)*TEX-2.5768440E-05)*TEX+2.5020051E-01)*TEX
&-1.7558886E+00
      SEA++2.5020051E-01*ALOG(TEX)+((((((1.4450767E-26*TEX
&-2.4211288E-22)*TEX+1.5243153E-18)*TEX-3.7820648E-15)*TEX
&-2.2392790E-12)*TEX+3.2759743E-08)*TEX-5.1576879E-05)*TEX
&+4.5432300E-02
      IF(FARX)200,200,8
C  FUEL/AIR PATH
8      IF(FARX-.067623)10,10,9
9      WRITE(1,101)
101     FORMAT(1H 63HINPUT FUEL-AIR RATIO ABOVE LIMITS, IT HAS BEEN RESET
&TO 0.067623)
      FARX=0.067623
10      CPF((((((7.2678710E-25*TEX-1.3335668E-20)*TEX
&+1.0212913E-16)*TEX-4.2051104E-13)*TEX+9.9686793E-10)*TEX
&-1.3771901E-06)*TEX+1.2258630E-03)*TEX+7.3816638E-02
      HEF((((((9.0848388E-26*TEX-1.9050949E-21)*TEX
&+1.7021525E-17)*TEX-8.4102208E-14)*TEX+2.4921698E-10)*TEX
&-4.5906332E-07)*TEX+6.1293150E-04)*TEX+7.3816638E-02)
&*TEX+3.0581530E+01
      SEF++7.3816638E-02*ALOG(TEX)+((((((1.0382670E-25*TEX
&-2.2226118E-21)*TEX+2.0425826E-17)*TEX-1.0512776E-13)*TEX
&+3.3228928E-10)*TEX-6.8859505E-07)*TEX+1.2258630E-03)*TEX
&+6.483398E-01
200     CPEX=(CPA+FARX*CPF)/(1.+FARX)
      HEX=(HEA+FARX*HEF)/(1.+FARX)
      SEX=(SEA+FARX*SEF)/(1.+FARX)
      AMW=28.97-.946186*FARX
      REX=1.986375/AMW
      AKEX=CPEX/(CPEX-REX)
      CSEX=SQRT(AKEX*REX*TEX*25031.37)
      RETURN
      END
C
C *****
C *****
C

```

```

SUBROUTINE AFQUIR(X,AIND,DEPEND,ANS,AJ,TOL,DIR,ANEW,ICON)
DIMENSION X(9)
C
C X(1)=NAME OF ARRAY TO USE
C AIND-INDEPENDANT VARIABLE
C DEPEND-DEPENDANT VARIABLE
C ANS=ANSWER UPON WHICH TO CONVERGE
C AJ=MAX NUMBER OF TRYs
C TOL=PERCENT TOLERANCE FOR CONVERGENCE
C DIR=DIRECTION AND PERCENTAGE FOR FIRST GUESS
C ANEW-CALCULATED VALUE OF NEXT TRY AT INDEPENDANT VARIABLE
C ICON-CONTROL -1 GO THRU LOOP AGAIN
C -2 YOU HAVE REACHED THE ANSWER
C -3 COUNTER HAS HIT LIMITS
C X(2)=COUNTER STORAGE
C X(3)=CHOOSES METHOD OF CONVERGENCE
C X(4)-THIRD DEPENDANT VARIABLE
C X(5)-THIRD INDEPENDANT VARIABLE
C X(6)-SECOND DEPENDANT VARIABLE
C X(7)-SECOND INDEPENDANT VARIABLE
C X(8)-FIRST DEPENDANT VARIABLE
C X(9)-FIRST INDEPENDANT VARIABLE
C X(3) MUST BE ZERO UPON FIRST ENTRY TO ROUTINE
C
      Y=0.
      IF(ANS)1,2,1
1     DEP=DEPEND-ANS
      TOLANS=TOL*ANS
      GO TO 3
2     DEP=DEPEND
      TOLANS=TOL
3     IF(ABS(DEP)-TOLANS)5,5,4
4     IF(X(2)-AJ)8,8,7
5     ANEW=AIND
      X(2)=0.
      ICON=2
      RETURN
6     ANEW=Y
      X(2)=X(2)+1.
      ICON=1
      RETURN
7     ANEW=Y
      X(2)=0.
      ICON=3
      RETURN
8     IF(X(3))9,9,12
C ****FIRST GUESS USING DIR
9     X(3)=1.
      X(8)=DEP
      X(9)=AIND
      IF(AIND)10,11,10
10    Y=DIR*AIND
      GO TO 6
11    Y=DIR
      GO TO 6
12    IF(X(3)-1.)13,13,16
C ****LINEAR GUESS
13    X(3)=2.
      X(6)=DEP
      X(7)=AIND

```

```

      IF(X(8)-X(6))14,9,14
14    IF(X(9)-X(7))15,9,15
15    A=(X(9)-X(7))/(X(8)-X(6))
      Y=X(9)-A*X(8)
      IF(ABS(10.*X(9))-ABS(Y))9,9,6
C ***QUADRATIC GUESS
16    X(4)=DEP
      X(5)=AIND
      IF(X(7)-X(5))18,17,18
17    IF(X(6)-X(4))13,9,13
18    IF(X(6)-X(4))19,13,19
19    IF(X(9)-X(5))23,20,23
20    IF(X(8)-X(4))21,22,21
21    X(9)=X(7)
      X(8)=X(6)
      GO TO 13
22    X(9)=X(7)
      X(8)=X(6)
      X(3)=1.
      IF(X(9))10,11,10
23    IF(X(8)-X(4))24,21,24
24    F=(X(6)-X(4))/(X(7)-X(5))
      A=(X(8)-X(4)-F*(X(9)-X(5)))/((X(9)-X(7))*(X(9)-X(5)))
      B=F-A*(X(5)+X(7))
      C=X(4)+X(5)*(A*X(7)-F)
      IF(A)242,240,242
240   IF(B)241,7,241
241   Y=-C/B
      GO TO 37
242   IF(B)247,243,247
243   IF(C)245,244,245
244   Y=0.
      GO TO 37
245   G=-C/A
      IF(G)7,7,246
246   Y=SQRT(G)
      YY=-SQRT(G)
      GO TO 270
247   IF(C)249,248,249
248   Y=-B/A
      YY=0.
      GO TO 270
249   D=4.*A*C/B**2
      IF(1.-D)13,25,26
25    Y=-B/(2.*A)
      GO TO 37
26    E=SQRT(1.-D)
27    Y=(-B/(2.*A))*(1.+E)
      YY=(-B/(2.*A))*(1.-E)
270   J=4
      DEPMIN=ABS(X(4))
      DO 29 I=6,8,2
      IF(DEPMIN-ABS(X(I)))29,29,28
28    J=I
      DEPMIN=ABS(X(I))
29    CONTINUE
      K=J+1
      IF((X(K)-Y)*(X(K)-YY))32,32,30
30    IF(ABS(X(K)-Y)-ABS(X(K)-YY))37,37,31
31    Y=YY

```

```

GO TO 37
32 IF(J-6)33,34,34
33 JJ=J+2
   KK=K+2
   GO TO 35
34 JJ=J-2
   KK=K-2
35 SLOPE=(X(KK)-X(K))/(X(JJ)-X(J))
   IF(SLOPE*X(J)*(X(K)-Y))36,36,37
36 Y=YY
37 X(9)=X(7)
   X(8)=X(6)
   X(7)=X(5)
   X(6)=X(4)
   GO TO 6
END

```

```

C
C
C
C

```

```

SUBROUTINE CRITCL(ALAM,TERM)
DIMENSION ALMTAB(13),TRMTAB(13)
DATA(ALMTAB(I),I=1,13)/-6.,-5.,-4.,-3.,-2.,-1.,0.,
&1.,2.,3.,4.,5.,6./
DATA(TRMTAB(I),I=1,13)/0.,120.,138.,175.,250.,375.,
&645.,1125.,2000.,3500.,5500.,8000.,10000./
CALL SRCHX(ALAM,ALMTAB(1),13,0,IL,C)
TERM=TRMTAB(IL)+C*(TRMTAB(IL+1)-TRMTAB(IL))
RETURN
END

```

# APPENDIX D

**Experimental data base**

# Static pressure distribution

	Surface distance over arc length	Axial distance over axial chord	static pressure /total pressure  PS/PT
PRESSURE SURFACE			
	.0001	.0	.9980
	.0525	.0276	.9875
	.1027	.0937	.9896
	.1527	.1632	.9860
	.2029	.2302	.9854
	.2894	.3384	.9811
	.3751	.4369	.9728
	.4603	.5265	.9603
	.6422	.6949	.9099
	.7179	.7570	.8587
	.7414	.7755	.8443
	.8073	.8255	.7895
	.8894	.8843	.6955
	.9745	.9416	.6425
SUCTION SURFACE			
	.0393	.0246	.9799
	.0781	.0697	.9409
	.1176	.1342	.8571
	.1569	.2181	.6747
	.1962	.3058	.6025
	.2358	.3816	.5321
	.2750	.4409	.5001
	.3147	.5200	.5388
	.3545	.5844	.5294
	.3934	.6963	.5859
	.4333	.7485	.5819
	.4766	.8863	.5579
	.5020	.9427	.5627
	.5505	.9723	.5575

414003

# Heat transfer coefficient distribution

	Surface distance over arc length x/arc	Axial distance over axial chord	Normalized temperature (Tw/811 K)	Normalized heat transfer coefficient H/Ho
	.8627	.8656	.8511	.4176
	.8341	.8451	.8354	.4032
	.7777	.8034	.8334	.4333
	.7485	.7810	.8147	.4888
	.7194	.7582	.7974	.5749
	.6918	.7360	.8001	.6207
	.6627	.7121	.7912	.6611
	.6337	.6876	.7705	.6833
	.6037	.6616	.7602	.6666
	.5765	.6374	.7659	.6701
	.5476	.6110	.7644	.6888
	.5194	.5845	.7583	.7000
	.4906	.5567	.7552	.6600
	.4343	.5000	.7509	.6333
	.4055	.4697	.7454	.6133
	.3766	.4385	.7425	.6444
	.3479	.4066	.7425	.6300
	.3193	.3738	.7418	.6666
	.2902	.3394	.7419	.6444
	.2617	.3047	.7433	.7200
	.2327	.2685	.7461	.6993
	.2045	.2323	.7480	.6993
	.1912	.2016	.7510	.6993
	.1585	.1711	.7538	.6993
	.1361	.1405	.7577	.6993
	.1135	.1090	.7635	.6993
	.0900	.0757	.7721	.6993
	.0681	.0454	.7831	.6993
	.0457	.0211	.7933	.6993
	.0222	.0051	.7973	.6993
	.0001	.0	.8001	.6993
	.0184	.0059	.7998	.6993
	.0360	.0213	.7979	.6993
	.0534	.0395	.7968	.6993
	.0978	.0835	.7979	.6993
	.1055	.1125	.7977	.6993
	.1237	.1463	.7953	.6993
	.1412	.1831	.7930	.6993
	.1592	.2233	.7894	.6993
	.1765	.2626	.7858	.6993
	.1939	.3010	.7814	.6993
	.2116	.3372	.7776	.6993
	.2299	.3714	.7743	.6993
	.2477	.4012	.7729	.6993
	.2652	.4274	.7727	.6993
	.2829	.4512	.7752	.6993
	.3009	.4732	.7796	.6993
	.3184	.4928	.7845	.6993
	.3356	.5109	.7879	.6993
	.3533	.5284	.7899	.6993
	.3709	.5452	.7910	.6993
	.3884	.5613	.7923	.6993
	.4058	.5769	.7930	.6993
	.4236	.5923	.7926	.6993
	.4412	.6072	.7918	.6993
	.4585	.6216	.7918	.6993
	.4758	.6357	.7903	.6993
	.4936	.6500	.7890	.6993
	.5109	.6636	.7881	.6993
	.5285	.6772	.7873	.6993
	.5473	.7068	.7894	.6993
	.5891	.7232	.7894	.6993
	.6099	.7287	.7880	.6993
	.6310	.7542	.7897	.6993
	.6527	.7701	.7913	.6993
	.6736	.7853	.7919	.6993
	.6949	.8006	.7847	.6993
	.7169	.8164	.7900	.6993
	.7380	.8315	.8029	.6993
	.7598	.8468	.8091	.6993
	.7810	.8617	.8090	.6993
	.8016	.8760	.8173	.6993
	.8231	.8907	.8333	.6993
	.8440	.9049	.8420	.6993
	.8662	.9195	.8388	.6993

